INCLUSION CONTROL MODEL IN THE LADLE METALLURGY FURNACE

INCLUSION CONTROL MODEL IN THE LADLE METALLURGY FURNACE

By

JORGELINA PÉREZ, Chemical Eng.

A Thesis

Submitted to the School of Graduate Studies

in Partial Fulfillment of the Requirements

for the Degree

Master of Science

McMaster University

MASTER OF SCIENCE (2011) McMaster University

(Materials Science and Engineering) Hamilton, Ontario, Canada

TITLE: Inclusion Control Model in Ladle Metallurgy Furnace

AUTHOR: Jorgelina Pérez (Chemical Engineer, Universidad Nacional de Córdoba, Argentina)

SUPERVISOR: Dr Gordon A. Irons

NUMBER OF PAGES: xix, 131

ABSTRACT

In Secondary Steelmaking Processes, one of the most used technologies is the Ladle Metallurgy Furnace (LMF). This unit operation enables the adjustment of the chemical composition by ferroalloy addition, electrical reheating to the aim temperature, desulphurization and float out of the inclusions produced during steel deoxidation.

The inclusions are harmful to the steel cleanliness. Process parameters such as stirring and steel and slag oxidation must be controlled to obtain a final number of inclusions in the steel whose size is smaller than the critical size for each steel product.

This thesis concerns the development of a mathematical model to predict inclusion control during the ladle metallurgy process. Three parameters are evaluated, the initial steel oxidation level, the impact of the slag oxidation level on the reoxidation, and the stirring power with a double effect: to float out inclusions and produce reoxidation. The results of the model were validated with 20 samples taken in 4 heats in the Ternium Siderar plant. The model results were consistent with experimental data.

Several alternatives were evaluated to illustrate the effect of the main parameters on the steel cleanliness control in a ladle metallurgy process.

ACKNOWLEDGMENTS

These projects gave me the possibility of enriching my technical knowledge and strengthen the personal ties with other companies and a different culture.

The results of this thesis could not have been achieved without the financial support of my company, my supervisor's guidance and the unconditional support of my family.

I want to thank Ternium Siderar and mainly my bosses Alfredo Rabasedas and Marcelo Chara for giving me the support to start as a visiting researcher in McMaster University and then approving my master program.

My collegues from Ternium, specially Walter Balante and Roberto Donayo who helped me during the thesis facilitating me to take samples from the industrial trials, the laboratory work and replacing me during my absences to study or travel to Canada.

Special thanks are owed to Dr Ken Coley and Dr Gordon Irons for allowing me to do the master program as a part-time student from another country. Sincere and grateful acknowledgment to Dr Irons for its patience, supervising support and inspiring discussion.

My husband, Pablo, deserves my deepest gratitude for motivating me to achieve this project agreeing to move to Canada and supporting me in every moment. To my daughter Bernardita who lived the cultural change and to my

little daughter Mercedes who was born during this project, both understanding my absences in several moments so as to complete this thesis.

TABLE OF CONTENTS

LIST OF FIGURES

Chapter 1

Chapter 2

Chapter 3

Chapter 4

Chapter 5

Appendix

LIST OF TABLES

LIST OF VARIABLES

a_{FeO}	--------	FeO activity in the slag
a_{MnO}	--------	MnO activity in the slag
%Al	--------	Aluminium content in the steel (%)
$\%Al_2O_3$	--------	Alumina content in slag (%)
A_{13B}	--------	Hamaker constant of Al_2O_3- liq steel-bubble system (J)
A_{Eye}	--------	Eye area without slag (m^2)
A_{Ladle}	--------	Ladle area (m^2)
A_{Ref}	--------	Refractory area (m^2)
A_{Slag}	--------	Slag area (m^2)
%CaO	--------	CaO content in slag (%)
D_B	--------	Diameter of the bubble (m)
D_I	--------	Diameter of the inclusion (m)
Do	--------	Diffusion coeficient of oxygen in steel (m^2/ s)
E_1	--------	Energy barrier for the bubble-particle adhesion to calculate P_A
E_k	--------	Kinetic energy of collision to calculate P_A
%FeO	--------	FeO content in slag (%)
g	--------	Gravity acceleration (m/ s^2)
G	--------	Dimensionless constant
H	--------	Height of ladle (steel height) (m)
H_{Cr}	--------	Critical film thickness (m)
I	--------	Number of alumina molecules included into an inclusion of R_I
K_{FeO}	--------	FeO equilibrum constant
K_{MnO}	--------	MnO equilibrum constant
%Mn	--------	Manganese content in the steel (%)
%MgO	--------	MgO content in slag (%)
%MnO	--------	MnO content in slag (%)
M_O	--------	Molar weight of oxygen (kg)
M_P	--------	Molar weight of particle, Al_2O_3 (kg)
N	--------	Total number of molecules function of total oxygen ($1/m^3$)
N_A	--------	Avogadro's Number (1/ mol)

NR_{BI}	--------	Total number of "effective adhesions" bubble- inclusion for inclusion of radius *i* (1/ m^3)
NR_{FinI}	--------	Number of total inclusions at the end of treatment (1/ m^3)
NR_I	--------	Total number of radius *I* (1/ m^3)
NR_{OI}	--------	Initial number of total inclusions for inclusion of radius *i* (1/m^3)
NR_{Ref}	--------	Number of inclusion of Ri removal to refractory (1/ m^3)
NR_{ReO}	--------	Number of particles produced by reoxidation (1/ m^3)
NR_{Slag}	--------	Number of particles removal to slag of radius *i* (1/m^3)
O_{Atm}	--------	Oxygen in atmosphere for reoxidation (%)
O_{Eq}	--------	Oxygen in equilibrium with aluminum content (ppm)
O_{Ini}	--------	Total oxygen before tapping (ppm)
O_{Slag}	--------	Oxygen content in the slag (ppm)
O_{Tot}	--------	Total Oxygen for reoxidation, it's dissolve oxygen (%)
O_{Total}	--------	Total oxygen in the steel (%)
P	--------	Standard atmosphere pressure (Pa)
P_A	--------	Adhesion Probability
P_C	--------	Collision probability
PM_{Al2O3}	--------	Molar weight of Al_2O_3 (kg)
PM_{CaO}	--------	Molar weight of CaO (kg)
PM_{FeO}	--------	Molar weight of FeO (kg)
PM_{MgO}	--------	Molar weight of MgO (kg)
PM_{MnO}	--------	Molar weight of MnO (kg)
PM_O	--------	Molar weight of Oxygen (kg)
PM_{SiO2}	--------	Molar weight of SiO_2 (kg)
Q	--------	Flow rate per Tn of steel (Nm^3/ s * Tn steel)
Q_1	--------	Number of molecules per unit volume, to calculate A_{13B}
R	--------	Ideal gas constant (J/ mol K)
R_B	--------	Bubble radius produced by gas injection (m)
Re	--------	Reynolds number
R_I	--------	Radius of an inclusion *i* (m)
R_{Ladle}	--------	Ladle radius (m)
R_M	--------	Al_2O_3 molecular radius (m)

R_{OC}	--------	It is the distance resulting of the addition of R_B and R_I during attachment of inclusion and bubble (m)
$\sum$ Oxides	--------	Total moles of oxides in the slag
$\%SiO_2$	--------	Silica content in slag (%)
T	--------	Temperature (K)
T_F	--------	Film drainage and rupture time (s)
TO	--------	Temperature of the gas before porous plugs (K)
V	--------	Volume of the steel (m^3)
V_B	--------	Velocity of the bubble (m/ s)
V_M	--------	Molecular volume of an alumina particle (m^3/ mol)
V_R	--------	Relative velocity of the particle respect to bubble (m/ s)
V_Z	--------	Velocity of particle in z direction (m/ s)
W_{Steel}	--------	Weight of steel (kg)
X_{FeO}	--------	FeO molar fraction
X_{MnO}	--------	MnO molar fraction
Z	--------	Portion of inclusion of each size at the beginning of treatment
α	--------	Semiangle of contact between inclusion and bubble
β_1	--------	London's constant for interaction between two atoms to calculate A_{13B}.
E	--------	Turbulent energy dissipation (m^2/ s^3)
ρ_{Fe}	--------	Steel density (kg/ m^3)
ρ_G	--------	Gas density (kg/ m^3)
ρ_P	--------	Particle density, Al_2O_3 is consider (kg/ m^3)
$\kappa_{O,I}$	--------	Mass transfer coefficient (depends of stirring intensity for slag) (m/s)
$\kappa_{O,1}$	--------	Mass transfer coefficient (depends of stirring intensity for eye) (m/s)
η_{Fe}	--------	Kinematic viscosity (m^2/ s)
η_O	--------	Effect oxygen in molar ratio
η_P	--------	Effect particle in molar ratio
σ	--------	Surface tension (N/m)

θ	--------	Contact angle between particle and bubble
μ_{Fe}	--------	Steel viscosity (kg/ m.s)
μ_G	--------	Gas viscosity (kg/ m.s)
γ	--------	Activity coefficient for each oxide

Chapter 1

INTRODUCTION

1.1 Modern Iron and Steelmaking

At the present time steel is produced by two main processes throughout the world: the blast furnace (integrated steelmaking) or electric arc furnace (from direct reduction iron (DRI) or from scrap in the minimills). The metallurgical route is chosen according to the investment level, capacity of the plant, energy costs and raw materials availability.

The integrated steelmaking route is used in plants with high production (highest investment). This process is presented in Figure 1-1, where the blast furnace produces molten iron (hot metal) starting from iron ore, lime, coke (produced by cokemaking) and sinter. Hot metal which is rich in carbon (4- 4.8 wt%C), steel scrap, solid pig iron (from the blast furnace too) and fluxes (lime, dolomite, recycled slag, etc) are charged in the steelmaking converter to lower carbon by oxidation with pure oxygen injection at supersonic velocity. At the end of converter process, the steel has a very high oxygen concentration in equilibrium with low carbon content (0.02- 0.10 %C). It must be refined with deoxidizing agents and it is adjusted chemically and thermally in a secondary metallurgy or ladle metallurgy process. The steel with the aim composition at process temperature is sent to the continuous casting machine where solidification occurs; slabs or billets are produced.

When the steel is produced by the electric arc furnace (Figure 1-1), DRI produced by direct reduction with scrap and fluxes are charged into the electric arc furnace to produce steel with high oxidation potential. After this point both routes are the same. A common use of the electric arc furnace is in the minimill, where the steel is produced starting from scrap only.

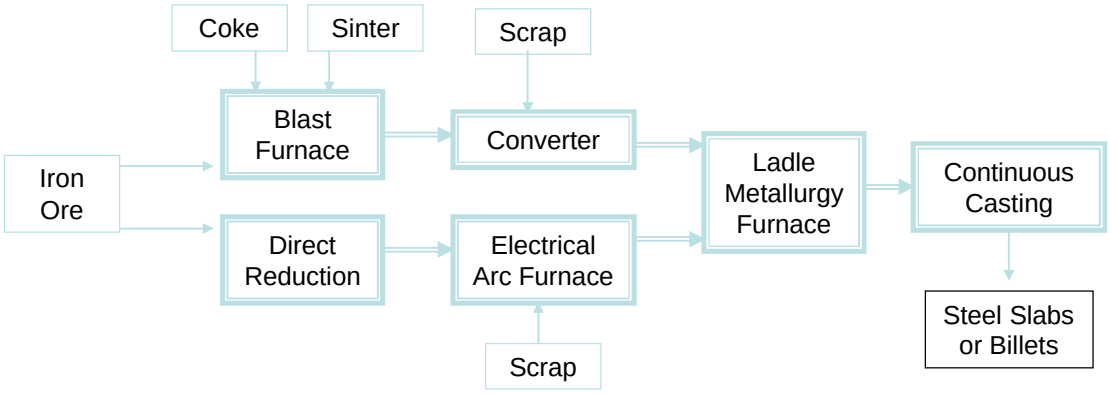

Figure 1-1. Schematic flowsheet of steelmaking production by blast furnace- converter route and electric arc furnace.

1.2 Secondary Metallurgy Process

Converters (BOFs) and electric arc furnaces (EAFs) produce steel by oxidation. At the end of blowing (in converters) or melting (in EAFs), the steel has high dissolved oxygen content, low phosphorous and low carbon content. The steel is tapped from each one of these reactors to a ladle (refractory vessel with metal shell), where the secondary metallurgy is performed.

The secondary metallurgy begins with deoxidation during tapping by aluminum, manganese, silicon and carbon depending of the level of deoxidation or “killing” required.

The oxides produced during deoxidation must be removed from the steel by floating out. The oxides which remain in the steel form solid particles with different melting points and mechanical properties than the steel, and they are called non-metallic inclusions. The inclusion liquidus temperature is very important during casting, because those oxides with higher liquidus temperature than the steel can attach in the small size casting channels (such as the ladle nozzle or tundish nozzle) and clog them. Regarding the mechanical properties, inclusions have low formability and during rolling they may produce cracks in the steel.

In ladle metallurgy the steel is adjusted to the chemical composition required in the final product, by refining processes such as desulphurization, alloying, heating, non-metallic inclusions removal and degassing in some occasions.

The main refining processes are:

1- Desulphurization: the sulfur dissolved in the steel can be removed from this by interactions between steel and slag, according to Equation 1-1 (ΔG° defined by Elliot & Gleiser 1960):

$$\underline{S} + CaO \;\text{à}\; \underline{O} + CaS \qquad K = \frac{a_{[CaS]}}{a_{[CaO]}}\frac{a_{[O]}}{a_{[S]}} \qquad \Delta G^\circ(J) = 104700 - 25.8T \qquad (1\text{-}1)$$

Desulphurization is a function of the interaction between steel and slag, because CaO is necessary to fix the sulphur in the slag, together with other thermodynamic conditions such as temperature and sulphur capacity.

2- Alloying: The chemical composition is adjusted with ferroalloys, by lumps added from chutes or injected as fine powder clad in metal tubes, known in

the industry as wires. The content of phosphorus cannot decrease during this process; this can be done only during oxidation (BOF and EAF process).

3- Degassing: Achieved under vacuum condition with specific equipment. It removes carbon and makes steel with very low carbon which cannot be produced in the BOF or EAF. Degassing is used also to obtain low dissolved nitrogen and hydrogen contents.

4- Inclusion removal: During the process coagulation and flotation of inclusions removes them from steel; the conditions and mechanisms to obtain clean steel (without inclusions) will be described in Section 2.6.

5- Calcium inclusion modification: The non-metallic inclusions cannot be removed completely; the remaining ones may be modified with calcium. The calcium aluminate formed has two advantages, it is liquid at casting temperature (it avoids casting problems due to nozzle clogging) and the inclusions present in solid steel are deformable during rolling.

Secondary metallurgy processes include different methods, where the vessel is a ladle. Some processes cannot reheat and in other ones electrical or chemical reheating are used.

Four different types of equipment for secondary metallurgy (without vacuum) are described below:

(a) LMF (Ladle Metallurgical Furnace). In this equipment the steel is heated by electric arcs; the furnace has three graphite electrodes which make an electrical arc with the liquid steel which transfers the thermal energy from the steel surface to the rest of the steel. It is possible to adjust the chemical

composition by ferroalloy addition. Bubbling is made by inert gas injection through porous plugs in the bottom of the ladle, to homogenize and achieve a good slag- steel interaction. It is excellent for desulphurization.

(b) CAS-OB (Composition Adjustment by Sealed argon bubbling with Oxygen Blowing). In this method the bell goes down to the steel to produce an inert area over the “slag eye” (area without slag because the bubbling plume pushed it aside). The alloy addition and chemical reheating by oxygen and aluminum injection are produced underneath this bell. It produces more Al_2O_3 than a LMF, and they must float out to obtain clean steel.

(c) IR-UT (Injection- Refining Up- Temperature). A vessel with aluminum and oxygen injection for alumino-thermic heating, argon is bubbling by a top lance for steel refining. It is a cheap, quick and low cost process. Low quality steel is obtained because it cannot achieve good inclusion cleanliness.

(d) Mannesmann Process. In this equipment the lime powder is injected with a top lance and argon is injected through the porous plugs placed in the bottom of the ladle. This process achieves very good slag-steel interaction for desulphurization and other refining process, but heating is not possible in this case.

The most common vacuum equipment used in the secondary metallurgy is summarized below:

(e) VD or VTD (Vacuum Tank Degassing). It is a hermetic tank where the steel ladle is placed. It is a non-recirculating system (as are VOD and VAD). The tank is connected to vacuum equipment. This process has high thermal losses and needs a large free board in the ladle (decreasing productivity).

(f) VOD (Vacuum Oxygen Degassing). It is a VD with oxygen injection. The decarburization reaction is favored by oxygen injection over the steel bath surface. It is predominantly used to produce stainless steel, because the oxygen reacts with carbon before chromium.

(g) VAD (Vacuum Arc Degassing). It is a VD with electrodes to heat by electrical arc.

(h) RH (Ruhrstahl - Heraeus). It is a recirculating system; it is a vessel under vacuum with 2 legs which immerse into steel. In one leg, argon is injected and produces the steel flow. In the vessel the decaburization is made; this equipment is faster than VD and has higher productivity.

A process under vacuum is mandatory when the final product requires very low carbon content (around 30 ppm). Under vacuum the partial pressure of CO decreases and carbon deoxidation by reaction of C and O dissolved in the steel is favored near stoichiometry, according to equation 1-2. With oxygen injection the final carbon content can be even lower.

$$\underline{C} + \underline{O} \quad \text{à} \quad CO_g \qquad K = a_{[C]}\, a_{[O]} / P_{CO} \qquad \text{Log } K = 1.16/T - 2.003 \qquad (1\text{-}2)$$

Figure 1-2 shows plant data obtained by carbon content before and after a vacuum treatment (by RH) reported by Turkdogan (1996) at 0.07 atm of CO pressure. The carbon content in equilibrium with dissolved oxygen before vacuum treatment is plotted in open symbols, under vacuum the CO partial pressure decreases and the carbon content lower a new equilibrium with the dissolved oxygen (filled symbols).

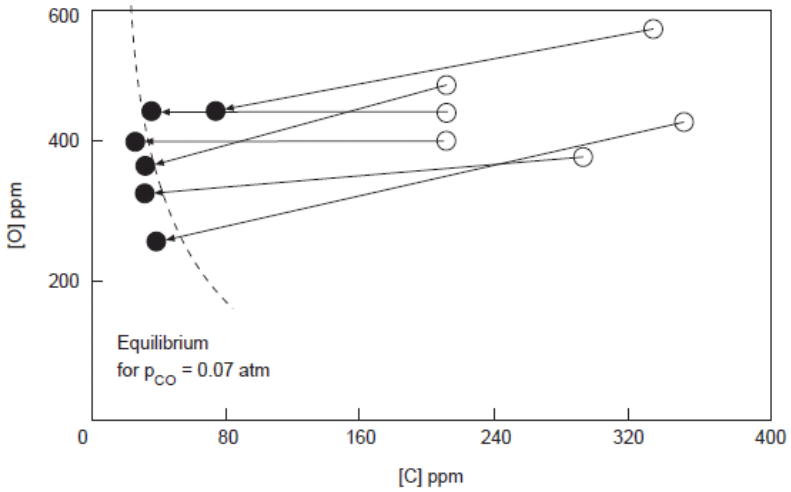

Figure 1-2. Carbon and oxygen contents of steel before (open symbol) and after (filled symbol) in a RH process. Turkdogan (1996).

There are two different types of degasser (Kor & Glaws, 1998): recirculating and non-recirculating systems; in both processes argon is used as lifting gas (to lower steel density to move the liquid from the ladle to the vacuum vessel) or stirring gas (to promote the removal of nitrogen and/ or hydrogen). Both methods achieve the same carbon, and gas content at the end of treatment. The difference is in the process time and investment cost; RH is quicker but more expensive.

The Ladle Metallurgy Furnace (LMF) is the process studied in the current work.

1.3 Ladle Metallurgy Furnace

The ladle metallurgy furnace is used in most steelmaking plants, where all the processes required for the secondary metallurgy can be made, except for degassing.

The LMF is shown in Figure 1-3:

(1) The transportation car is where the ladle containing liquid steel is placed. The ladle contains the steel and a top slag layer. Slag has the functions of protecting the steel from the atmosphere, thermal insulation and refining.

(2) Argon or nitrogen stirring can be made from one or more bottom plugs for homogenization, desulphurization and inclusion flotation.

(3) Water cooled lid to protect the steel and aspirate the fumes during the treatment.

(4) Current conducting arms.

(5) Chutes for alloy addition and injection machines to adjust the chemical composition. Wire feeding of powdered materials in steel shells is used when small quantities are required or when its vapor pressure is lower than liquid steel temperature (e.g., calcium); on the other hand bulk alloys are added by chutes for larger quantities.

(6) An automatic or manual lance is used to take steel samples and check the temperature.

(7) The furnace has three electrodes supported by current-conducting arms to reheat the steel to the aim value.

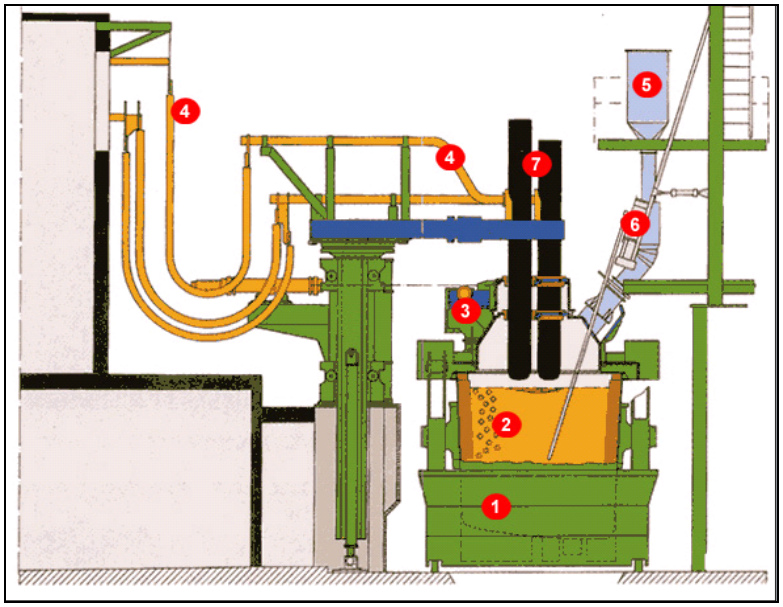

Figure 1-3. Schematic of Ladle Metallurgy Furnace. Website: //km.siderar.ot/mkm/siderar/mkm.asp

1.4 Current State of the Art

Iron and steelmaking industries are working continuously to develop cheaper and newer products to be able to compete in the market. High cost and shortage of some raw materials have caused engineers to redesign the processes. Furthermore, steel competes with other materials such as plastic and aluminum for some requirements, and thus better properties and improved quality are required continuously.

A competitive product in terms of quality and cost requires an optimized process. Models can be used as an easy, quick and cheap method to evaluate the results obtained when some variable of process is changed.

In steelmaking industry, mathematical, statistical and empirical models have been developed in order to improve process capacity and study changes in process or

products. In general these models are developed in laboratory scale and the validity in the industrial scale is very difficult to prove. In spite of this limitation, the usefulness of models to explain physico-chemical and thermodynamic aspects as regards of processes must be recognized.

In processes like secondary metallurgy, the variables are modified continuously and the different parameters vary heat-to-heat, with heating, stirring, alloying, and slag treatment. Process control is made from knowledge of the theoretical effect of each variable in the process and availability of sensors and samplers to make discreet measurements.

1.5 Objectives of the Research

The key work of this thesis is to develop an inclusion control model for the ladle furnace, which determines inclusion evolution during the process for different process variables, such as stirring variation, temperature, oxidation level and slag composition. In this way a mathematical model was developed and validated with steelmaking plant samples to achieve this research objective.

1.6 Organization of the Thesis

The present thesis is presented in 6 chapters. In Chapter 1 the subject and aspects which motivate the research and the goals are described. Chapter 2 presents the literature review of inclusion formation and characterization, and explains the clean steel concept and process engineering used to decrease the quantity of inclusions during secondary metallurgy. Chapter 3 is the key work of this thesis. A mathematical model has been developed to explain the inclusion evolution during the secondary metallurgy

process and its validation in Ternium Argentina. Chapter 4 is focused on the method of sampling and analysis and the results obtained from plant samples. Chapter 5 shows the information that the model can give and its correlation with the work of other authors. Conclusions regarding the industrial application of this work are presented in Chapter 6, and some proposals for future research are described.

Chapter 2

INCLUSION CHARACTERIZATION AND REMOVAL MECHANISMS

2.1 Deoxidation Practice and Inclusion Formation

At the end of the Converter or Electric Arc Furnace process the steel has high dissolved oxygen content (greater than 500 ppm) and it must be decreased to 2- 4 ppm dissolved oxygen to be able to cast as the final product. The secondary metallurgy process begins with deoxidation; the most common metals used to remove the oxygen dissolved (O) are summarized in the following reactions (Turkdogan, 1996), where Log means $\log_{10}$:

$\underline{C} + \underline{O}$	à $CO_{(g)}$	$K = a_{[C]}\, a_{[O]} / P_{CO}$	$\text{Log } K = 1.16/ T - 2.003$	(2-1)
$2\,\underline{Al} + 3\,\underline{O}$	à $Al_2O_{3(s)}$	$K = a_{[Al]}^2\, a_{[O]}^3$	$\text{Log } K = -62780/ T + 20.6$	(2-2)
$\underline{Mn} + \underline{O}$	à $MnO_{(s)}$	$K = a_{[Mn]}\, a_{[O]}$	$\text{Log } K = 15.05/ T + 6.75$	(2-3)
$\underline{Si} + 2\,\underline{O}$	à $SiO_{2(s)}$	$K = a_{[Si]}\, a_{[O]}^2$	$\text{Log } K = 30.11/ T + 10.4$	(2-4)
$\underline{Ca} + \underline{O}$	à $CaO_{(s)}$	$K = a_{[Ca]}\, a_{[O]}$	$\text{Log } K = -9.030$	(2-5)
$3\,\underline{Ti} + 5\,\underline{O}$	à $Ti_3O_{5(s)}$	$K = a_{[Ti]}^3\, a_{[O]}^5$	$\text{Log } K = 16.1$	(2-6)
$2\,\underline{Cr} + 3\,\underline{O}$	à $Cr_2O_{3(s)}$	$K = a_{[Cr]}^2\, a_{[O]}^3$	$\text{Log } K = 44.04/ T + 19.42$	(2-7)

The evolution of the different deoxidants as function of temperature summarized above is plotted in Figure 2-1.

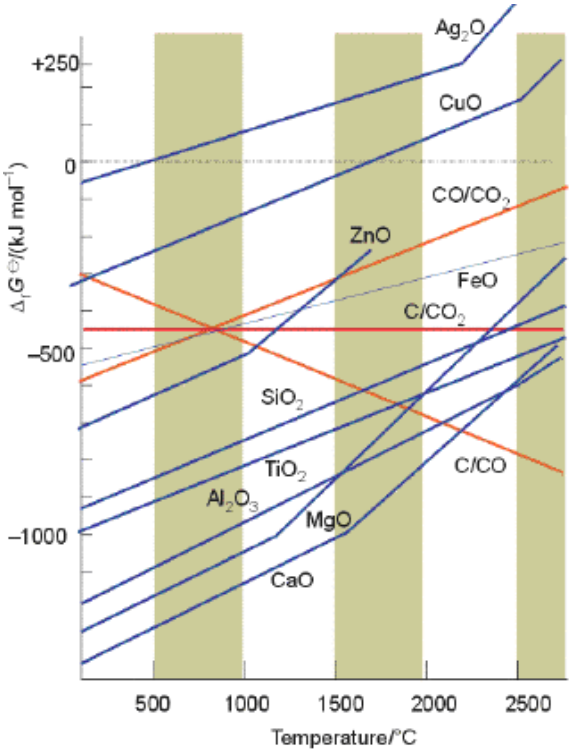

Figure 2-1. Ellingham diagrams for different deoxidants. website: www.metalurgia.uda.cl/apuntes/Jchamorro/termodinamica/DiagramasdeEllingham.pdf

In Equation 2-1, the oxygen reacts with the dissolved carbon to remove oxygen; the oxide produced is a gaseous compound which leaves the steel. Carbon is a weak deoxidant and reacts with oxygen only when it is in high concentration and no stronger deoxidants are present in the steel.

Aluminum is commonly used because it is a powerful deoxidant and is cheaper than other metals (eg. titanium). The oxide produced in the reaction 2-2 is solid and it must float up in the steel to reach the slag. In the absence of the quantity of aluminum necessary to kill the steel, manganese and silicon remove the oxygen according to reactions 2-3 and 2-4, where solid oxides are produced. Solid particles produced which do not float up during the process and remain in the solid steel are called inclusions.

When the quantity of metal added is greater than that necessary to kill the steel, aluminum, manganese and silicon are simply alloy additives.

In steel with high quantities of silicon or manganese added or without aluminum, reactions 2-3 and 2-4 are followed. If aluminum is added in the necessary quantity, reaction 2-2 displaces reactions 2-3 and 2-4.

The metals shown in equations 2-5, 2-6 and 2-7 are very reactive but with high cost. Their effect on the steel composition has a high impact on the mechanical properties.

When the steel is deoxided mainly by aluminum it is called aluminum killed steel and produces one kind of solid oxide (Al_2O_3). This is the kind of steel studied in the current work.

The inclusion chemistry in the solid steel depends of which deoxidizer has been used. Van der Eijk, Grong & Walmsley (2000) find in Al-Ca killed steels, Al, Ca and S are the main elements entering the inclusions and Ti-killed steels have Ti, Mn and S in their inclusions.

2.2 Clean Steel Concept

The steel has some elements and components which affect the properties of final product, such as: oxygen, nitrogen, sulphur, phosphorous, oxides and others. The term “clean steel” is commonly associated to low oxide content in the steel (called non-metallic inclusions); the presence of other elements is considered the “purity of the steel”. The non-metallic inclusions are created during deoxidation or by reoxidation during secondary metallurgy or casting processes. The cleanliness standard desired by

the customer has been increasing over time as a function of technological improvements.

The control of oxides is fundamental during steelmaking process, because lack of cleanliness affects the casting process and the final product. The inclusions can produce clogging during the casting in the submerged entry nozzle (Figure 2-2). The Al_2O_3 particles stick in the nozzle decreasing the casting velocity, and can even stop casting altogether (clogging).

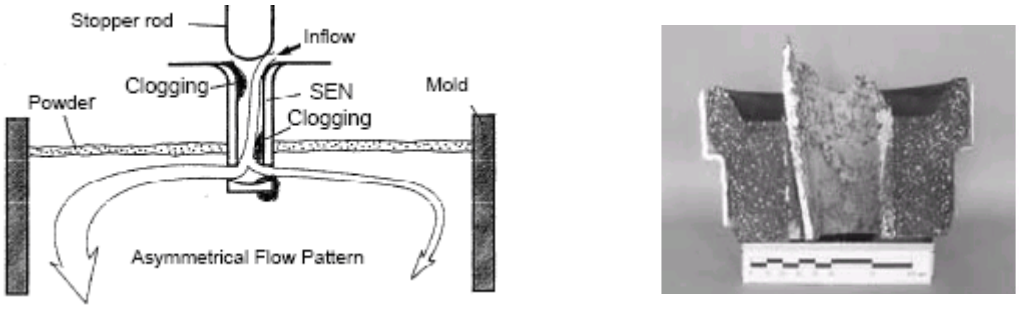

(a) (b)

Figure 2-2. (a) Schematic of steel flow pattern in a submerged entry nozzle (SEN) with cloggling (Zhang & Thomas, 2003). (b) Picture of a SEN with alumina clogging (Ternium Siderar internal report)

Inclusions may deform during rolling in detrimental ways. During hot rolling the inclusions are deformed in different way than steel, Wijk (1995) considered four kinds of inclusion deformation:

- Fragile inclusions; they are broken during rolling.
- Inclusions which cannot be deformed; they produce slivers in the rolling direction.
- Inclusions with a hard core, only the shell supports a low level of deformation.

- Ductile Inclusions, they present a similar deformation as the steel around them.

The inclusions can be exogenous or indigenous according to their source. In the first type all particles originating external to the steel and its refining reactions are considered, such as slag entrapment or oxides particles from the refractory. On the other hand, the second type is a product of deoxidation reactions (oxides) or precipitation reactions (nitrides, sulphides, etc). They are completely different according to composition and size; Zhang & Thomas (2003) showed the difference between these inclusion types shown here in Figures 2-3 and 2-4.

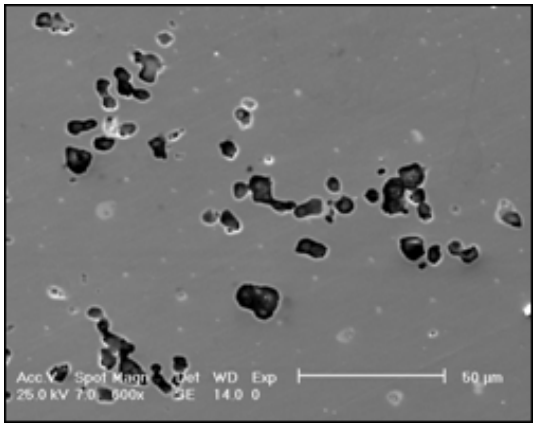

Figure 2-3. Indigenous inclusion: dendritic alumina inclusion (Zhang & Thomas, 2003)

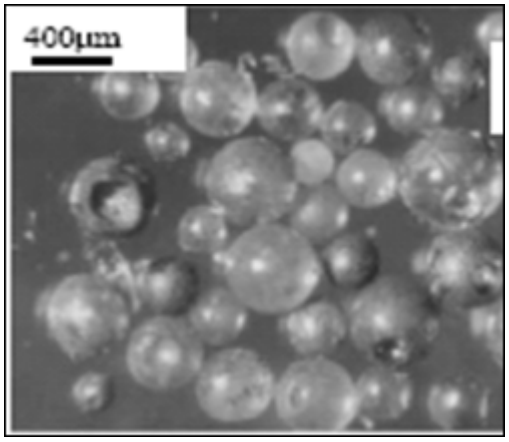

Figure 2-4. Exogenous inclusion: slag entrapment with Al_2O_3-MgO-SiO_2-CaO-FeO (Zhang & Thomas, 2003)

Indigenous inclusions are studied in this thesis; they depend on the nature and quantity of deoxidizer used in the treatment of the steel and the operational practices to decrease them.

Non-metallic inclusions are harmful to mechanical properties of steel (decreasing the toughness and increasing the risk for mechanical or corrosive failure of the final product) and require a removal treatment. During the refining of steel, the inclusions can be modified to decrease their quantity.

Lange (1988) explains the effect of each kind of inclusion on the mechanical properties in the rolled product. During rolling, the fragile inclusions or non-deformable inclusions are broken mainly on the grain edges. This produces surface defects as slivers or blisters. They can act as sites where the cracks starts and produce seams which decrease the mechanical properties such as ductility, Charpy impact value and anisotropy, formability (elongation, reduction area and bendability), cold forgeability and drawability, low temperature toughness and fatigue strength, and affect the corrosion resistance and welding properties.

2.3 Inclusion Morphology

The decrease in the mechanical properties depends of the amount, composition and morphology of inclusions and their distribution. It is necessary to control the inclusion content in the steel to avoid inclusions larger than the critical size harmful to the product. The critical size depends of the final thickness required and application. Zhang & Thomas (2003) summarized the maximum size for inclusions according to the different product characteristics (Table 2-1).

Table 2-1. Maximum inclusion size allowed in different products (Zhang&Thomas, 2003).

Steel Product	Maximum Inclusion size
Automotive and deep-drawing Sheet	100 µm
Drawn and Ironed cans	20 µm
Line pipe	100 µm
Ball Bearings	15 µm
Tire cord	10 µm
Wire	20 µm

Robinson, Martin & Pickering (1979) found that the shape of aluminum oxide inclusions is controlled largely by the supersaturation. Mixing of oxygen rich regions and oxygen poor regions result in the formation of alumina dendrites and aggregates. Branched dendrites are formed in oxygen rich and aluminium rich melts. Spheroidised dendrites are in low oxygen contents areas.

Dekkers (2002) studied the inclusion content at the beginning (after nucleation) and the end of treatment. He classified the inclusions in Low Carbon Aluminum Killed Steels (LCAKS) without calcium treatment according to shape, chemical composition and size. The classification according shape and size only for inclusions studied in this work (pure alumina) is summarized in Table 2-2.

Table 2-2. Inclusion classification in LCAK steel by size and shape (Dekkers, 2002).

Kind of inclusion	Shape	Size	Contribution of O_{total} after Al addition	
			5 min.	25 min.
Spherical	Spherical	Small, diameter 0,5 µm	0%	6.1%
Faceted	Large polyhedral	Diameter > 5 µm	0%	13%
Dendrites	With branches	Size 5-20 µm	0%	1.3%
Clusters	Open network	Size 100 µm	100%	52%

It is possible see in Table 2-2 the impact of each kind of inclusion to the total oxygen content. At the beginning of the treatment (5 minutes after aluminum addition), most of the oxygen content is bound in clusters because of they are the largest inclusions. At the end of treatment the most of clusters float up and in a common sample almost 90% of inclusions are spherical, but ones that are very small therefore have little impact on the total oxygen content (6.1 %). Large inclusions are harmful for the steel, and they contribute most to the total oxygen (52%).

2.4 Modification of Inclusions with Calcium

The addition of calcium or calcium alloys, usually in wire form is made in aluminum killed steels to decrease the volume fraction of oxide and sulphide inclusions.

Calcium will convert solid alumina inclusions into lower melting point calcium aluminates (Figure 2-5) that is lower than the melting point of steel.

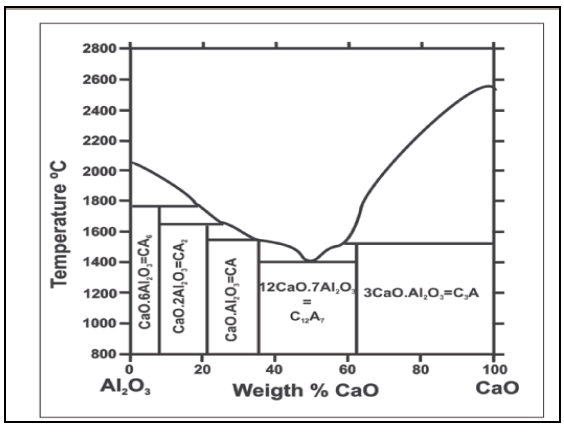

Figure 2-5. Binary system CaO-Al_2O_3

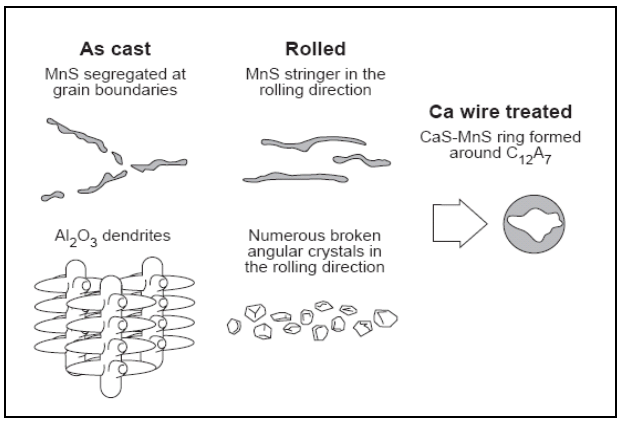

Figure 2-6. Modification of inclusion morphology as a result of calcium treatment (Turkdogan, 1996).

At the beginning of the treatment the inclusions are always pure aluminum oxide, but calcium treatment transforms solid alumina inclusions in liquid calcium aluminates. Calcium treatment is known as inclusion morphology control or modification, because it changes inclusion composition and shape. The changes are schematized in Figure 2-6.

Calcium treatment improves casting because it decreases nozzle clogging and decreases superficial defects in slabs by improving the regularity in casting. Although it is an important point for inclusion engineering it has not been developed in the present work.

2.5 Analysis of Inclusions

There are two kinds of methods to measure the steel cleanliness:

- Direct methods: they are accurate but costly (in time, money and technology)
- Indirect methods: they are fast and inexpensive, but they are not as accurate and only useful as relative indicators.

Direct and indirect techniques can be classified since Table 2-3 by Zhang & Thomas (2003).

Table 2-3. Direct and Indirect methods to analyze inclusions (Zhang & Thomas, 2003)

Method	Evaluation	Characteristics	Techniques
Direct	Inclusion Evaluation of Solid Steel Sections	2-dimensional measurement in solid samples (only amount)	Metallographic Microscope Observation (MMO)
			Image Analysis (IA)
			Sulphur Print
			Scanning Electron Microscopy (SEM)
		2-dimensional measurement in solid samples	Optical Emission Spectrometry with Pulse Discrimination Analysis (OES-PDA)
			Laser Microprobe Mass Spectrometry (LAMMS)

		(amount and composition)	X-ray Photoelectron Spectroscopy (XPS)
			Auger Electron Spectroscopy (AES)
	Inclusions Evaluation of Solid Steel Volumes	3-dimensional measurement in steel matrix	Conventional Ultrasonic Scanning (CUS)
			Mannesmann Inclusion Detection by Analysis Surfboards (MIDAS)
			Scanning Acoustic Microscope (SAM)
			X-ray Detection
		3-dimensional measurement of inclusions separated from steel	Slime (Electrolysis)
			Electron Beam melting (EB)
			Cold Crucible (CC) melting
			Fractional Thermal Decomposition (FTD)
	Inclusions Size Distribution after Inclusion Extraction	3-dimensional measurement (extraction for one of the last 4 techniques)	Coulter Counter Analysis
			Photo Scattering method
			Laser-Diffraction Particle Size Analyzer (LDPSA)
	Inclusions Evaluation of Liquid	Inclusion size and distribution in liquid steel	Ultrasonic Techniques for Liquid System
			Confocal Scanning Laser Microscope
Indirect	By sampler or sensors	Online measurements of inclusion level	Total Oxygen and dissolved oxygen

There is no direct or indirect single method to evaluate steel cleanliness. It is necessary to combine several methods to be able to have a good overall analysis, for problem investigation.

2.6 Inclusion Removal in Ladle Metallurgy

Ladle metallurgy processes are oriented to obtain chemical and thermal homogenization, deep deoxidation and desulphurization, exact alloy composition and also to decrease the non-metallic inclusion content in steel to very low levels. In order to obtain steel cleanliness it is necessary to remove the inclusions and avoid reoxidation. Then the following parameters have to be considered: inclusion properties to improve their removal, stirring and transfer operations, slag control and refractory.

The inclusion size and its properties are important to improve the inclusion removal. Stirring enhances cluster formation and the shape of particles in the clusters depends on the initial oxygen and aluminum activities and holding time (Braun, Elliot & Flemings, 1979). After the aluminum addition, the inclusions evolve; Figure 2-7 shows that larger inclusions are present immediately after aluminum is added and after 10 minutes they disappear.

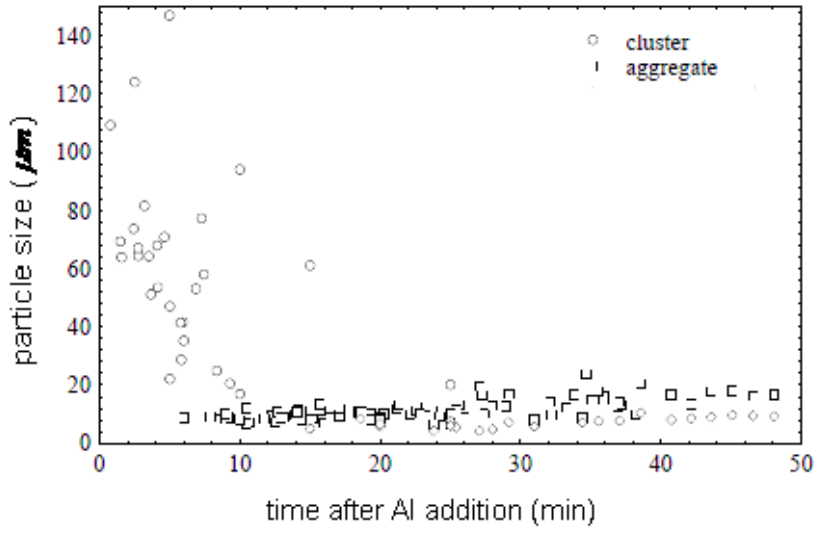

Figure 2-7. Evolution of clusters with the time (Braun, Elliot & Flemings, 1979).

Reoxidation occurs if the oxygen activity in the steel melt is less than the one in the layer in contact with it (slag, refractory or atmosphere).

2.7 Slag Control

Slag has four functions in the metallurgical process: to provide refining of impurities in steel, to avoid steel reoxidation by contact with the atmosphere, to act as thermal insulation and take up the non-metallic inclusions. According to Oertel, Costa and Silva (1999) the effectiveness of the steel refining process is heavily dependent on the characteristics of the slags employed in these process.

2.7.1 Refining of the Impurities in Steel

Secondary metallurgy is the process where the refining of steel is carried out. Chemical composition is adjusted by ferroalloy addition, and the removal of some impurities by the slag (such as sulphur and the non-metallic inclusions, the last one is described in Section 2.7.3).

Except for resulphurized steel, in general sulphur is unwanted in steel, because its presence gives phases of low melting point at grain boundaries which work as crack initiators during rolling and increase the corrosion rate of steel (Bristow et al, 2000). Sulphur is present in the raw material (coke) used for hot metal production. According to the thermodynamic conditions of converter or EAF processes, sulphur cannot removed by primary steelmaking. Wilson and McLean (1980) summarized the process conditions to removal sulphur from the steel:

- Low oxygen potential in the melt; for this condition is necessary that the steel is completely deoxidized.
- Strong stirring at the slag/ metal interface; the slag must be fluid to allow good steel-slag contact.
- High temperature to ensure slag fluidity and lime dissolution.
- Highly basic slag phase to fix the sulphur which is removed from the steel.

Of all the slag-metal reactions, the thermodynamics and kinetics of sulphur transfer have been most rigorously studied (Graham, 2008), and may be represented by the ionic exchange reaction where sulphur is partitioned between the metal and slag phases:

$$\underline{S} + (O^{-2}) \longrightarrow (S^{-2}) + \underline{O} \qquad (2\text{-}8)$$

As the secondary metallurgy process operates under reducing conditions, a simplified approach to desulphurization is to recognize that CaO in slag is the primary desulphurizer:

$$\underline{S} + (CaO) \longrightarrow (CaS) + \underline{O} \qquad (2\text{-}9)$$

The slag composition is fundamental for desulphurization and it is one of the main functions of the slag in the secondary metallurgy process.

2.7.2 Avoiding Steel Reoxidation

Reoxidation (Dekkers, 2002) is produced when the steel is in contact with another phase with a higher oxygen activity.

- Ladle eye; the slag layer is opened by stirring bringing the steel into contact with the atmosphere (21% oxygen).

Intensive stirring causes an emulsification between slag and steel. The slag drops can transport oxygen from the atmosphere, producing oxides (then aluminum and silicon contents decrease in the steel).

- Slag: high FeO content produces reoxidation because the reduction of this by aluminum is thermodynamically favored:

$$3\,FeO + 2\,\underline{Al} \longrightarrow Al_2O_3 + 3\,\underline{Fe} \qquad \Delta G^\circ = -853700 + 240T\ (J/mol) \qquad (2\text{-}10)$$

It is necessary to avoid furnace slag carryover to decrease FeO content. In this way steelmakers work to improve conditions at the end of blowing (less oxidation, high slag viscosity and avoiding reblows). They use devices to minimize or detect vortex formation during tapping with slag balls or darts, as well as infrared and electromagnetic systems. Another way to lower FeO content is by dilution, where synthetic slag additions such as lime, dolomite and calciumaluminate are made.

Iron oxide in the slag is detrimental to the steel cleanliness because it can have higher oxygen activity than in the steel which will cause reoxidation. The relationship between FeO + MnO in ladle slag and total oxygen (TO) is shown in Figure 2-8, and the

alumina inclusion content in the slag is shown as a function of FeO+ MnO in the slag in Figure 2-9.

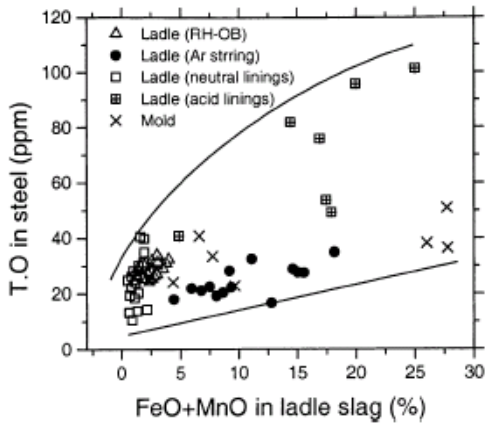

Figure 2-8. Relationship between FeO+MnO in ladle slag and T.O. for different treatments (Zhang & Thomas, 2003).

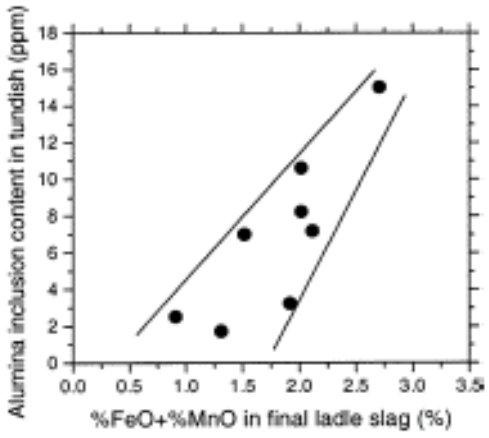

Figure 2-9. Effect of FeO+MnO in ladle slag in inclusion content in tundish (Ahlborg, Bieniosek & Tucci, 1993).

Aluminum is used to deoxidize slag; as FeO content in the slag increases more aluminum is necessary and this decreases the cleanliness level of the steel (Figure 2-10). Some plants use the quantity of aluminum added and the residual aluminum content as an index to control the steel cleanliness. A similar effect can be seen with the phosphorus reversion, BOF or EAF slags contain high phosphorus levels (because it is in equilibrium with high oxygen dissolved in the steel, equation 2-11), if the slag carry over from primary vessel is high, phosphorus reversion is produced when the slag is killed (Figure 2-11).

$$3\,CaO + 2\,\underline{P} + 5\,\underline{O} \longrightarrow Ca_3(PO_4)_2 \qquad K_{1600} = 1.4 \times 10^{-11} \qquad (2\text{-}11)$$

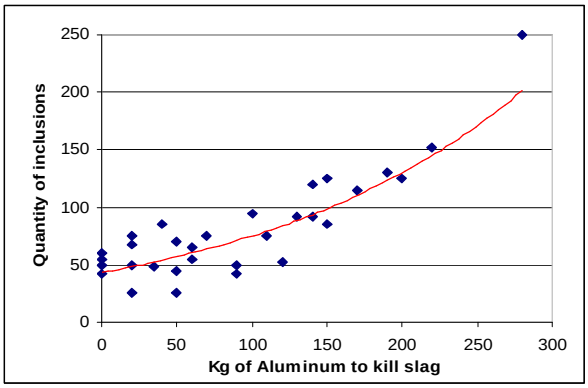

Figure 2-10. Relationship between quantity of inclusions and Kg of aluminum used to kill slag (Brandaleze, Martín, Donayo, Pérez & Gómez, 2007).

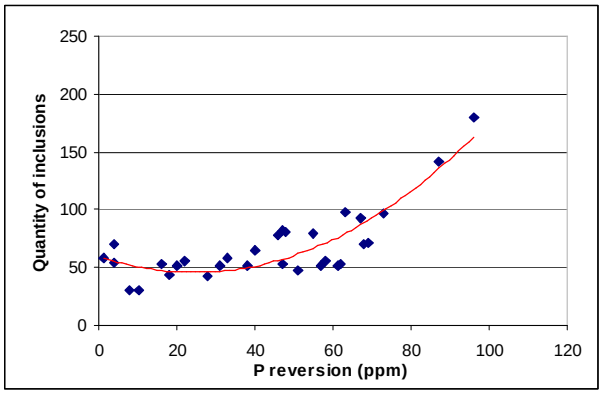

Figure 2-11. Quantity of inclusions in function of phosphorus reversion (Brandaleze, Martín, Donayo, Pérez & Gómez, 2007).

2.7.3 Inclusion Removal to Slag

The process to remove an inclusion by the slag has been modeled (Cramb & Jimbo, 1989; Sridhar & Cramb, 2001; Nakashima & Okamura, 1992) and the following stages must be considered:

- Inclusion approaches the interface
- Rupture of the steel film resulting in inclusion- slag contact
- Dissolution of the inclusion in the slag; for this stage it is very important that the slag is not saturated in alumina.

Taira, Nakashima & Mori (1993) studied Al_2O_3 dissolution in CaO- Al_2O_3- SiO_2 slags and found that boundary layer diffusion was rate controlling.

The particle dissolution rate in slags is a function of temperature and chemistry; the dissolution time decreases when the temperature increases and when the alumina content in the slag decreases for slags with similar MgO and SiO_2 content (Sridhar &

Cramb, 2001). Figure 2-12 shows when temperature increases by 50°C total dissolving time decreases by more than 1/3 (in a CaO- Al_2O_3- SiO_2 slag).

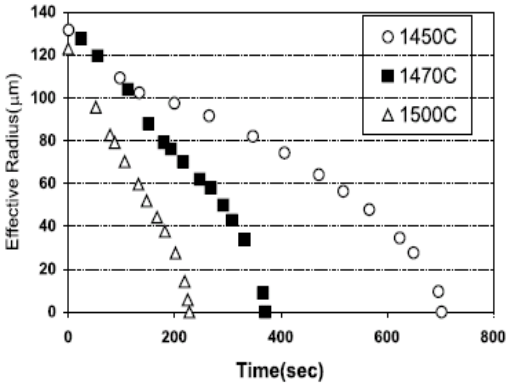

Figure 2-12. Changes in equivalent radius of alumina particles at different temperatures (Slag: 48.9wt% Al_2O_3, 48.4wt% CaO, 0.52wt% MgO and 1.36wt%SiO_2; Sridhar & Cramb, 2001).

Valdez and Cramb (2002) measured the effect of SiO_2 and MgO content in the slag on the Al_2O_3 inclusion dissolution time. Three different slags were analyzed to be able study this effect; two tundish slag where the composition is given by rice shell (used as cover to avoid temperature losses and reoxidation, it is pure silica) and slag carryover from the ladle, and the third slag is from the ladle in equilibrium with an aluminum killed steel. The chemical composition for slags studied is shown in Table 2-4, where CASM and CAS are tundish slags (with and without Mg respectively) and the ladle refers to a common ladle slag. The alumina content is shown by the bulk slag and the oxide content for the saturation slag in alumina by the three slag samples.

Table 2-4. Slag composition (Valdez & Cramb, 2002).

Slag	%SiO_2	%CaO	%MgO	%Al_2O_3 (Bulk Slag)	%Al_2O_3 (Saturation Slag)
CASM	39.5	33.4	7.3	19.5	34.5
CAS	42	36	0.4	21	42
Ladle	5	59	0	36	63

The inclusion removal is a function of the slag viscosity and the driving forces for dissolution. Table 2-4 shows that the ladle slag allows more Al_2O_3 dissolved (in saturation) than the tundish slags; according the effect of the SiO_2 and MgO content on Al_2O_3 dissolution (Valdez and Cramb, 2002). The driving forces for aluminum removal are greater for ladle slag (Δ Al_2O_3 = 27%) than tundish slags (Δ Al_2O_3 = 21% for CAS and 15% for CASM) although ladle slag has higher Al_2O_3 content.

When the SiO_2 content is high the viscosity increases and the driving forces decrease; then the dissolution time increases (Figure 2-13). MgO has a large effect on the driving forces for dissolution; it decreases when MgO increases, but it does not have strong effect on the viscosity. For this reason CASM has lower driving forces than CAS.

This concept is very important because if the kinetics of dissolution is not enough fast, inclusions remain near the interface and increase the risk of reintrainment.

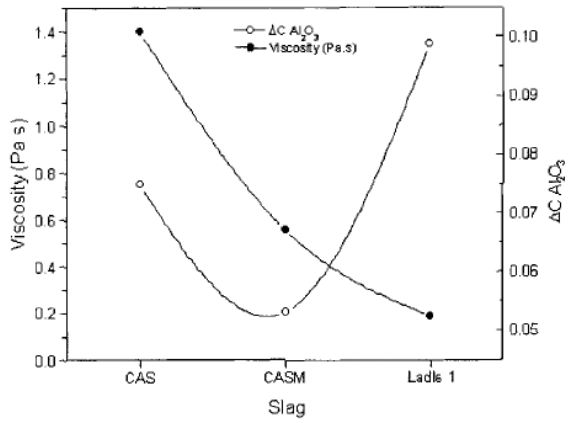

Figure 2-13. Comparison slag viscosity and driving force for dissolution of Al_2O_3 in different slags (Valdez & Cramb, 2002).

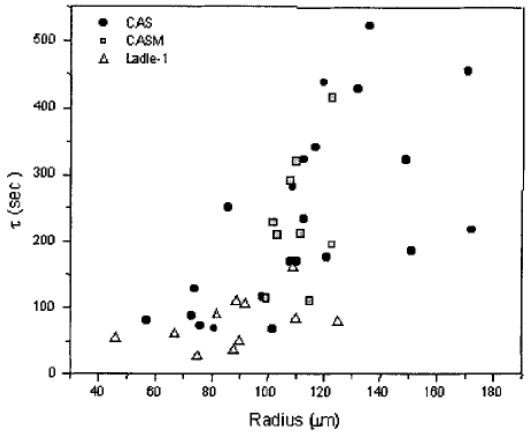

Figure 2-14. Total dissolution time for different Al_2O_3 inclusion size in ladle and tundish slags (Valdez & Cramb, 2002).

The dissolution time of inclusions is inversely proportional to a ratio between super-saturation and slag viscosity (Figure 2-14). Dissolution is faster for small inclusions or slag with low viscosities.

2.8 Stirring

The steel melt is stirred by inert gas (argon in general) bubbling through porous plug(s) positioned at the ladle bottom or by electric induction stirring. In this study, inert gas injected by bottom directional plugs is considered. Gas stirring is produced by injecting gas through a porous or directional refractory plug or a tuyere in the bottom of the ladle (Figure 2-15).

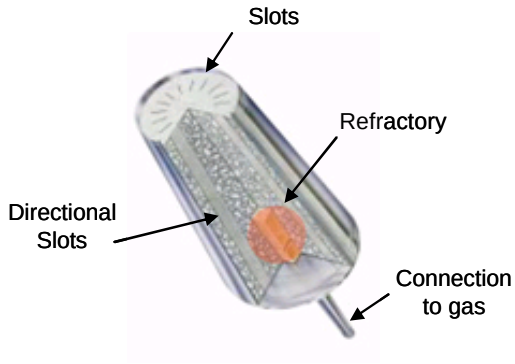

Figure 2-15. Schematic drawing of a directional plug to stir. Website: //km.siderar.ot/mkm/siderar/mkm.asp

Krishnapisharody and Irons (2007) have studied the spouts formation on bath surface due to gas stirring. Figure 2-16 shows the plume region lifts the top surface because of the upward momentum of the flow ("spout"), the slag present there is pushed to the periphery leaving a bare metal surface ("slag eye"). The exposed eye is the only region where liquid metal is in contact with atmosphere and nitrogen and oxygen can be adsorbed there. On the other hand, the refining reactions with slag are limited to the slag-metal contact area (this is the total ladle area less eye area).

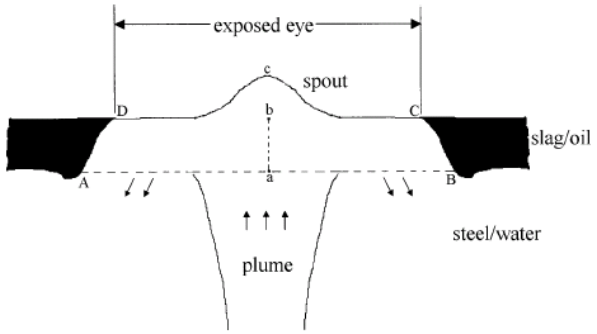

Figure 2-16. Schematic representation of the spout and slag eye formation (Krishnapisharody & Irons, 2007)

Gas bubbling is effective in removing inclusions by two mechanisms: firstly, the bubbles collide with the inclusions and float up with them with higher velocity than an inclusion alone. Secondly, the buoyant plume created by the stirring transports the inclusions to the top surface and produces turbulent mixing with the slag layer.

Stirring the steel bath improves the collisions between inclusions. The inclusions attach to the gas bubbles and rise with them. There are many studies about the stirring effect on steel cleanliness. Cold modeling (Pan, Uemura & Koyama, 1992) has demonstrated that if the particles are not wetted by the liquid phase, they can be caught by gas bubbles and removed by them. Solid inclusions like alumina or silica are not-wetted by liquid steel, so they can attach to the inert gas bubbles and float up with them.

It has been considered (Wang, Lee & Hayes, 1996) that smaller bubbles are better to remove inclusions, so the metallurgical industry has worked to produce finer bubbles (to replace tuyeres and injection lances by porous or directional refractory plugs). Because of it they assume that smaller bubbles have a high probably of collision with inclusions, but they have lower velocity to float up than larger inclusions (larger bubbles have lower probability to catch inclusions than smaller ones).

2.8.1 Bubble Diameter and Terminal Velocity

Anagbo & Brimacombe (1990) have reported that the formation of bubbles at the surface of a porous plug depends on the superficial velocity, gas flow rate per unit surface area of the plug. Fine bubbles are formed when this velocity is less than 0.14 m/s; beyond this, coalescence occurs.

The relationship between bubble and inclusion is described in models by different parameters like bubble size, physical properties (viscosity, density and surface tension) and the velocities.

The terminal velocity and the shape of the bubble depend of the bubble size. In Figure 2-17, all models show a maximum velocity in the transition zone. Bubbles smaller than this value (in the range of 5 mm), are spherical; bubbles bigger than this are ellipsoidal.

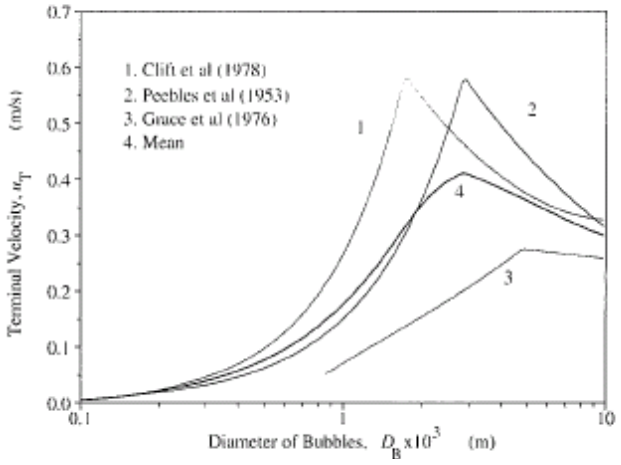

Figure 2-17. Terminal velocities of gas bubbles in liquid steel as a function of the bubble size (Wang, Lee & Hayes, 1996)

2.8.2 Inclusion Removal to Bubbles:

Wang, Lee & Hayes (1996) developed a model to predict the optimum bubble size for inclusion removal by flotation. They assumed that each bubble has: a probability of collision with an inclusion (Pc), a probability of catching an inclusion by adhesion (Pa), and a probability to detachment of it (Pd). Then, the overall probability of a inclusion can be removed to bubble is P (P= Pc*Pa*(1- Pd)).

The mechanism for an inclusion flotation by a gas bubble is described by different authors (Schulze, 1989 and 1992; Weber & Paddock, 1983; Yoon & Luttrell, 1989; Zhang & Taniguchi, 2000), it can be divided in several sub-processes:

a. Approach of a particle to a bubble.
b. Formation of a thin liquid film between the particle and the bubble.
c. Oscillation and/ or sliding of the particle on the bubble surface.
d. Drainage and rupture of the film with the formation of a dynamic three-phase contact (TPC).
e. Stabilization of bubble/ particle aggregates against external stresses
f. Flotation of the bubble/ inclusion aggregates

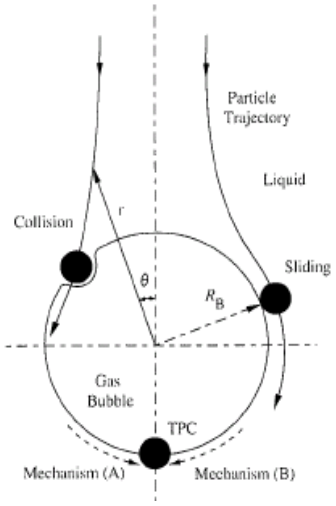

Figure 2-18. Schematic representation of mechanisms of particle attachment to a gas bubble (Miki, Thomas, Denissov & Shimada, 1997)

Pc has a relationship with the inclusion size and the bubble diameter (Figure 2-19), the probability of a bubble of collision with a particle increases when the bubble diameter decreases or inclusion size increases (the latter has a large impact on Pc).

When the bubble size is less than 0.5 μm the bubbles are entrapped by steel convection and they cannot be removed. The adhesion probability (Figure 2-20) increases with a decrease in inclusion size, but it is independent of the bubble diameter. Adhesion depends the sliding rate of inclusion along the bubble (smaller inclusions are easily captured by the gas bubble during sliding), and the rate of steel film drainage and rupture. Smaller inclusions have a higher Pa then the larger inclusions. Wang, Lee & Hayes (1996) proved the optimum efficiency of flotation of inclusions with diameter between 5 to 50 μm, it was obtained using bubble diameters between 0.5 to 2 mm; it was obtained by the calculation of stability of bubble- particle aggregates, the rising time of the gas bubbles and the efficiency for the inclusion removal.

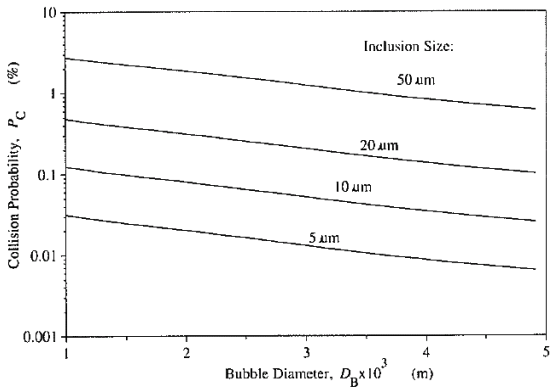

Figure 2-19. Probability by collision inclusion- bubble in a function of bubble and inclusion size (Wang, Lee & Hayer, 1996).

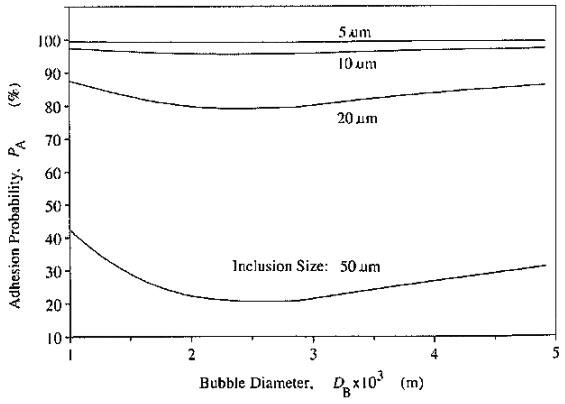

Figure 2-20. Probability by adhesion of inclusion on the surface of bubbles as a function of bubble and inclusion size (Wang, Lee & Hayer, 1996).

Dekkers (2002) studied the impact of the stirring effect on the cleanliness of steel (by a total oxygen measurement). His results are different from values achieved in other plants, they show:

- There is no relationship between total oxygen (T.O.) at the end of the ladle metallurgy versus the gas stirring time in the Sidmar plant (Figure 2-21). Apparently when stirring time increases (without vacuum treatment) it may cause reoxidation (it could be measured by nitrogen pick up).
- Total oxygen at the end of the ladle metallurgy is independent of the volume of stirring gas.
- There is no relationship between total oxygen and flux of gas stirring. (Figure 2-22)

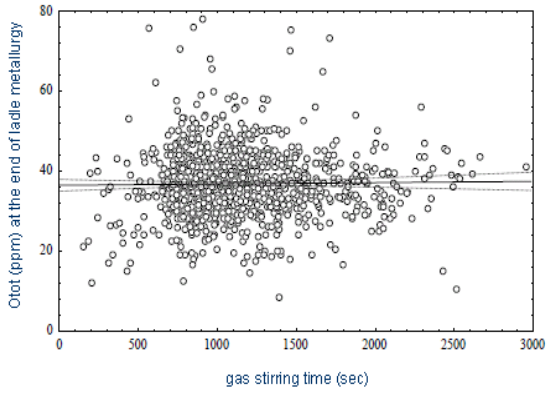

Figure 2-21. T.O. at the end of ladle metallurgy vs stirring time (Dekkers 2002, Chap. 10).

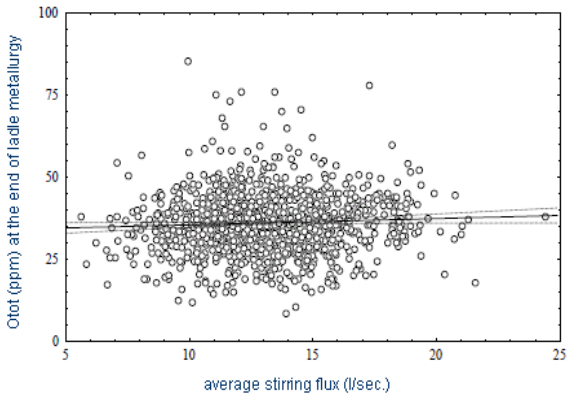

Figure 2-22. T.O. in the ladle vs average flux of gas stirring (Dekkers 2002, Chap. 10).

Miki, Thomas, Denissov and Shimada (1997) and Zhang and Thomas (2002) suggest to first stir vigorously to mix and promote collision of small inclusions into large

ones, and a final stir to recirculate the steel slowly to allow the inclusion removal by the slag and prevent the formation of inclusions.

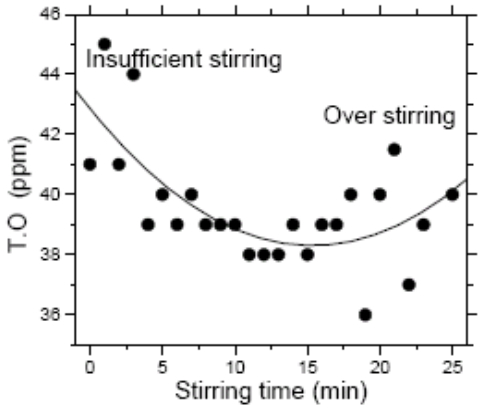

Figure 2-23. T.O. in ladle versus ladle stirring time (Bonilla, 1995).

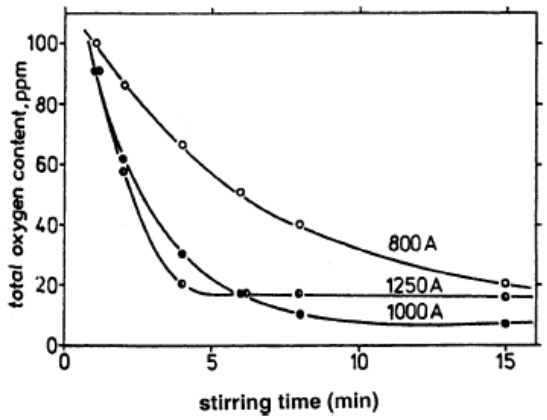

Figure 2-24. Relationship between T.O., stirring power and stirring time (Zhang and Thomas, 2003).

According to Figure 2-23, stirring times about 10- 15 minutes are necessary to remove inclusions (they go to the slag and they are removed to it). Larger stirring flow or longer time is detrimental because:

1- The eye can be opened and reoxidation is produced.

2- Increases the danger of slag entrainment

3- Produces particle collisions into large inclusions

And also it affects other operation conditions as:

4- Ladle lining erosion is produced (increased operation cost).

5- Increases the heat losses (increase operation cost).

Engh and Lindskog (1975) presented a fluid mechanical model for inclusion removal from liquid steel, where the total oxygen content after stirring time (t) is given by:

$$C_t / C_i \approx e^{-\varepsilon t / 27}$$

Where C_i and C_t are initial total oxygen content and after stirring respectively, t is stirring time and ε is stirring power.

In trials made in Ternium Siderar it is possible to see that 15 minutes is enough to remove inclusions; Figure 2-25 shows the inclusion evolution in 5 mm^2 surface area measured by EDS.

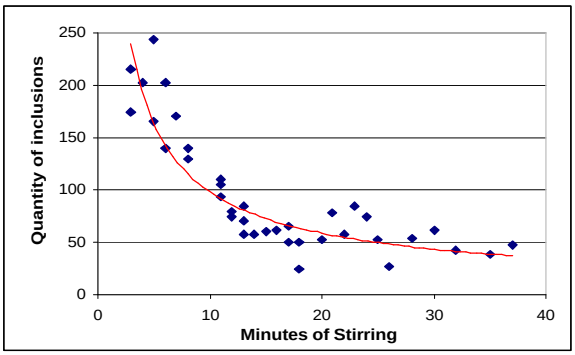

Figure 2-25. Relationship between inclusion content and gas bubbling time in Ternium Siderar (Brandaleze, Martin, Donayo, Pérez & Gomez, 2007).

2.9 Refractory

There are two main kinds of refractories, acid and basic ones; they are in contact with the steel and can affect the cleanliness of it. Bannenberg (1995) studied the relationship between oxygen activity and aluminum content in the steel with acid and basic ladle refractories (Figure 2-26). The oxygen activity is close to the equilibrium in

basic refractory, but is larger than in the acid refractory, because the oxygen activity is higher in these ones.

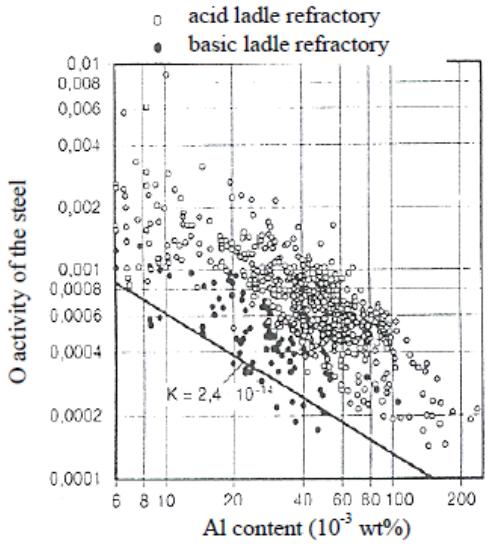

Figure 2-26. Oxygen activity in relationship to aluminum for basic and acid refractory materials (Bannenberg, 1995).

For this reason and life of ladle refractory, nowadays only basic refractory is used in aluminum killed steel. They do not affect the steel cleanliness considerably, but they are very important in inclusion removal. The refractory wall acts as a capture site for inclusions.

Chapter 3

MATHEMATICAL MODEL

3.1 General Aspects

The current thesis describe a mathematical model to estimate the inclusion distribution (in quantity and size) during a secondary metallurgy process in a ladle furnace; transformation and modification of inclusion during steel casting or calcium treatment are not considered. Only aluminum oxide inclusions are considered; in low carbon, aluminum killed steel, this approximation is good, because Al_2O_3 is the main inclusion.

The model is based on the work of several authors to describe inclusion removal to slag, refractory and bubbles, and reoxidation from slag and atmosphere (Wang, Lee and Hayer (1996), Söder (2004), Hallberg, Jönsson, Jonsson and Eriksson (2005), Zhang and Thomas (2002)).

Inclusion nucleation is not modeled; initial alumina inclusion particle size distributions are taken from plant measurements.

3.1.1. Assumptions and Second Order Effects which Have Been Neglected

3.1.1.1 Eye Area:

- This parameter is defined as the steel surface that is free of slag, where the steel is in contact with the atmosphere and reoxidation is produced.

- Eye area is calculated as a function of gas flow rate, ladle height and slag thickness.

3.1.1.2 Inclusions Removed by Slag, Bubbles and Refractory:

- Stirring power and temperature are kept constant in each step.
- Calculations are made for only one type of inclusion (alumina).
- The bubbles are of identical size and uniformly distributed in the two phase plume.
- After each time step the melt is considered homogeneous and the distribution of inclusions is uniform in the melt.
- Inclusions in the size range of radius 1- 10 um are considered in calculations, and they are assumed to be spherical.
- Inclusion formation from slag and refractory is neglected.
- The time of each step is one second.

3.1.1.3 Reoxidation:

- Reoxidation may occur by oxygen transfer from the slag to steel.
- Reoxidation in the eye is considered.

3.1.1. 4 Second Order Effects Neglected:

- Inclusion of other compositions besides alumina.
- Initial inclusion sizes are kept during the process, inclusion growth is not calculated. Inclusion growth calculations increase the complexity of the model with little effect on the results; this is further justified in Section 3.2.7.

- Slag entrainment or other exogenous inclusions are neglected.
- No inclusion transformation is considered.

3.2 Description: Framework of Model

3.2.1 Initial Inclusion Number (N_{Ro}):

The number of inclusions at the beginning of treatment depends of the oxidation level in the tapping and the size distribution of inclusions.

The model considers a size distribution with three different groups (small, medium and large), where R_i is the inclusion radius for each one, the inclusion radius and portion of it in the total content are taken from the plant data immediately after aluminum addition.

The inclusions are produced by deoxidation of steel with aluminum according Equation 2-2 (where alumina activity is equal to 1).

$$2\,\underline{Al} + 3\,\underline{O} \rightarrow Al_2O_{3(s)} \qquad K = a_{[Al]}^{2}\, a_{[O]}^{3} \qquad \text{Log } K = -62680/T + 31.85 \qquad (2\text{-}2)$$

The quantity of particles formed depends of the dissolved oxygen content at the end of blowing (O_{Ini}) and the dissolved oxygen level after deoxidation (O_{Eq}). The last oxygen content is not measured; it can be estimated by a correlation with the aluminum level after tapping, where from Equation 2-2:

$$a_O = [\frac{10^{-\frac{62680}{T}+31.85}}{[a_{Al}]^2}]^{1/3} \quad (3\text{-}1)$$

Considering the activity of any component to be a function of its concentration and according Equation 3-1 (Turkdogan, 2001), where f_O=antilog-3.9[%Al] and f_{Al}=1.

$$\%O_{Eq} = \frac{1}{f_O}[\frac{10^{-\frac{62680}{T}+31.85}}{\{[\%Al)]f_{Al}\}^2}]^{1/3} \quad (3\text{-}2)$$

This is a oxygen in equilibrium with aluminum (free oxygen and oxygen contained in the alumina particles).

The number of total Al_2O_3 molecules (N) produced is defined in Equation 3-3, where 48 is molecular weight of oxygen (g/ mol; considering 3 atoms of oxygen in each molecule of alumina), ρ_{Fe} is the steel density (kg/m^3), 1000 is a conversion factor (density) and N_A is Avogadro's number (1/mol). The aluminum weight is not necessary, because the Al_2O_3 particles produced can be described by each one of its reagents (Equation 2-2).

$$N = \frac{1000(\%O_{Ini} - \%O_{Eq})N_A}{48\rho_{Fe}} \quad (3\text{-}3)$$

Zhang, Pluschkell and Thomas (2002) developed a theory to explain the quantity of alumina molecules which can be found in an inclusion of any radius (for example of

radius i, R_I). The number of molecules (I) included in an inclusion of radius i (R_I) is shown in Equation 3-4, where $R_M = 2.719\ 10^{-10}$ m for an alumina molecule:

$$I = (R_I / R_M)^3 \tag{3-4}$$

The alumina molecules coalesce as inclusions of several sizes. The quantity of particles of each radius (N_{Roi}) at tapping depends of the inclusion radius (R_I), the portion of inclusion of each size ("Z", this value is taken from plant data) and the Al_2O_3 molecular radius (R_M). It is calculated as Equation 3-5:

$$NR_{OI} = \frac{Z(O_{Ini} - O_{Eq})N_A}{0.048\rho_{Fe}I} \tag{3-5}$$

"Z" value is taken from 4 heats sampled and evaluated according to Section 4.4 and 4.5. The alumina inclusion distribution for the first sample of each one of these heats after the deoxidation are drawn in Figure 3.1.

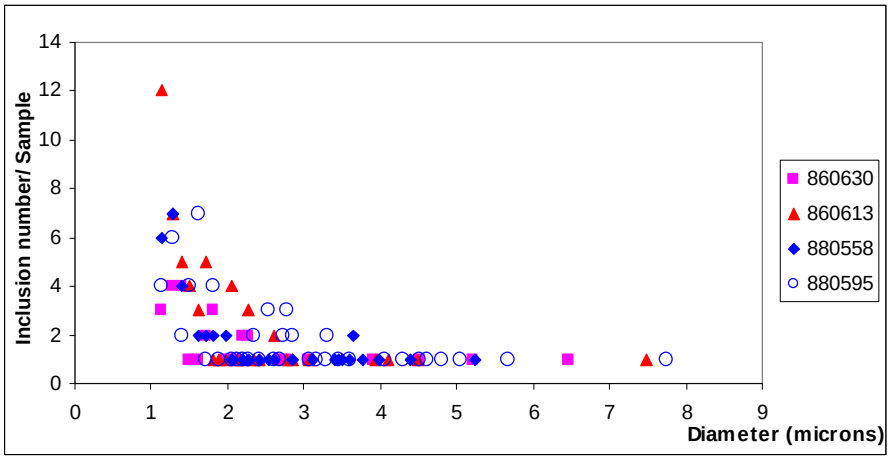

Figure 3-1. Distribution of alumina inclusion in heats analyzed after deoxidation.

Most of the inclusions are between 1 and 5 microns, considering three different groups: inclusions with diameter below 2 microns (54% of total), between 2 and 5 (38%) and between 5 and 10 microns (8%) according to Figure 3-2.

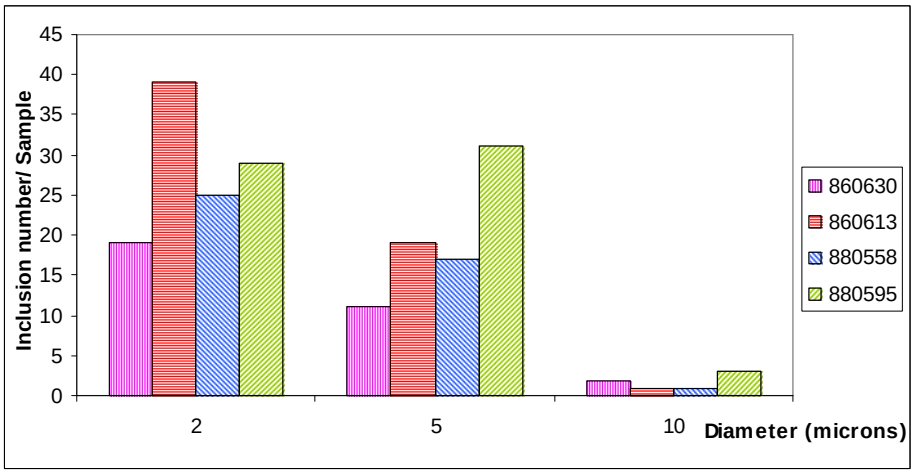

Figure 3-2. Quantity of alumina inclusions in each group for the heats evaluated.

The model calculates this initial inclusion number by each size; the inclusion evolution is calculated for the equations group described below for each inclusion size.

3.2.2 Inclusion Removed by Bubbles Model (from Wang, Lee and Hayer, 1996):

The model uses the Wang, Lee and Hayer (1996) concept. The inclusion can be removed by the bubble only if it is attached to it. The attachment probability P is $P = P_C * P_A * (1 - P_D)$, where P_C is the collision probability and P_A is the probability of catching an inclusion by adhesion. The model considers which all inclusions attached to the bubbles are removed from the steel and there is non detachment ($P_D = 0$).

To explain the collision probability (P_C), an isolated bubble rising through a group of inclusions must be considered. Figure 3-3 shows a flow pattern formed by a series of streamlines around the bubble.

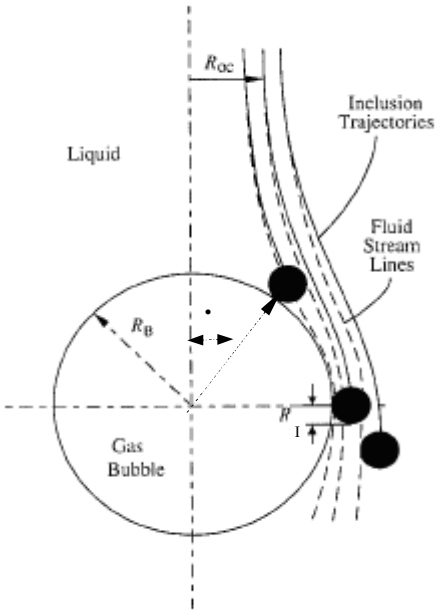

Figure 3-3. Schematic representation of collision of inclusion with a bubble (Wang, Lee & Hayer, 1996).

The inclusion trajectory is defined by the streamline which passes through its centre. Inclusions collide with the bubble when they have a grazing streamline at R_{OC} distance from the centre of bubble; inclusions with streamline distance longer than R_{OC} cannot be attached to the bubble. The collision probability (P_C) is defined as the ratio of the area $A_{OC} = (\pi R_{OC}^2)$ and $A_{BP} = (\pi (R_B + R_I)^2)$, for a particle diameter (D_I) smaller than bubble diameter (D_B) which is the normal condition in steelmaking:

$$P_C = \frac{A_{OC}}{A_{BP}} = \frac{R_{OC}^{\ 2}}{(R_B + R_I)^2} \tag{3-6}$$

R_{OC} is unknown and must be determined from the mathematical description of the grazing streamline. Several models have been developed with different complexities in the mathematical expressions, but with similar results for the collision probability (Wang, Lee & Hayer, 1996) for a range of Reynolds Number from 1 to 500.

Yoon and Luttrell (1989) developed a relatively simple model; it involves the Stokes and potential flow equations to obtain an empirical stream function (Ψ) for 1 < Re < 100. The authors consider that this equation can be applied for Reynolds number larger than 100 but below 500.

$$\Psi = V_B R_B \sin^2\theta \left[\frac{B^2}{2} - \frac{3B}{4} + \frac{1}{4B} + \frac{\mathrm{Re}^{0.72}}{15}\left(\frac{1}{B^2} - \frac{1}{B} + B + 1 \right) \right] \tag{3-7}$$

Where $B = (R_i + R_B)/ R_B$. When Reynolds number is close 0, the equation shows the results for Stokes Law only.

According to Figure 3-3, the maximal distance so that $R_{OC} = R_B + R_I$ along the particle path trajectory when θ = 90°. For smaller distance of far ahead of the bubble:

$$\sin\theta = \frac{R_{OC}}{R_I + R_B} \tag{3-8}$$

Which can be substituted in Equation 3-7 to yield:

$$R_{OC}^{\,2} = \frac{2\Psi}{V_B} \tag{3-9}$$

Heindel and Bloom (1999) defined a system of equations in polar coordinates (spherical coordinates projected onto the x-y plane) for bubble and particle velocities. These equations combined with Equations 3-6, 3-7 and 3-9 give the collision probability as a function of K_1, K_2 and Reynolds number, according Equation 3-10:

$$P_C = \frac{1}{1-K_1}\left[\frac{3}{2} + K_2 + \frac{2\,\mathrm{Re}^{0.72}(2+K_2)}{15(1+K_2)}\right] - \frac{K_2^{\,2}}{(1+K_2)^3} \tag{3-10}$$

Where K_1 and K_2 are the dimensionless relation by velocity and diameter for inclusion and bubble; they are summarized in Equations 3-11 and 3-12:

$$K_1 = \frac{V_Z}{V_B} \tag{3-11}$$

$$K_2 = \frac{D_I}{D_B} \tag{3-12}$$

Some inclusions which have low probability to be attached by collision may be removed from the steel by adhesion. In the adhesion process, the liquid film thinning between a bubble and a particle is controlled by the molecular forces at the interface. If the particle is not wetted, the liquid film will be unstable and will rupture at a critical film thickness (H_{Cr}). Schulze and Birzer (1987) obtained two empirical relationships (Equations 3-13 and 3-14) for critical film thickness, surface tension (σ), contact angle (θ) and Hamaker constant (A_{13B}). Equation 3-13 is used to calculate the critical film thickness.

$$H_{Cr} = 2.33*10^{-8}\left[1000\sigma\left(1-\cos\theta\right)\right]^{0.16} \tag{3-13}$$

$$H_{Cr} = 3.79*10^{-8} A_{13B}{}^{0.16} \tag{3-14}$$

The Hamaker constant (A) is the measure of the Van der Waals force between particles (in a particle- liquid- bubble system), it is described by the number of molecules in a unit volume (q_1), and the constant in London's equation for interaction between two atoms (β_1).

$$A = \pi^2 q_1{}^2 \beta_1 \tag{3-15}$$

Osborne-Lee (1988) showed that the Van der Waals force has very weak temperature dependence, so London's constant does not change with temperature and only q_1 is a function of it. Taniguchi, Kikuchi & Ise (1996) resolved Equation 3-12 for Al_2O_3 in liquid steel, where Hamaker constant (A_{13B}) is $2.3*10^{-20}$, and 1 denotes particle (alumina), 3 liquid (steel) and B gas bubble.

There is a time for the drainage of the liquid film between the gas and the inclusion until the time film rupture occurs, T_F. T_F was verified by Schulze (1989) in his experiments using a pendant water drop and a high speed camera. The inclusion approaches the gas bubble and a thin liquid steel film develops between the inclusion and the bubble; the film gradually drains until the film rupture occurs and the inclusion is attached.

If the collision time is longer than the film drainage time the inclusion will be attached by collision, but if this time is shorter than T_F, the inclusion will rebound away from the bubble or slide on the bubble surface. If the sliding time is longer than T_F the attachment will occur during sliding, but if this time is shorter than T_F the inclusion will slide away.

$$T_F = \frac{2100\mu_{Fe}\left[32(V_Z - V_B)\alpha\right]^{1.2} R_I^{\,3}}{8\sigma G H_{Cr}^{\,2}}\left[\frac{\pi}{180}\right]^2 \qquad (3\text{-}16)$$

The inclusions can float up in a calm bath by density difference (Stokes law). In a gas-stirred liquid metal, the rising velocity in z direction (V_z) is a function of the gas flow rate. In a stirred bath, it is difficult to calculate the relative velocity ($V_r = V_b - V_z$) of a bubble and an inclusion (V_z). Oeters (1994) defined terminal inclusion velocity (V_z) for

different particle Reynolds Number (Re) as a modification Stokes law, in Equation 3-17 the inclusion velocity in the z direction is calculated for 0.5 < Re < 1000.

$$V_Z = \left[\frac{g(\rho_{Fe} - \rho_P)}{9\mu_{Fe}^{0.5}\rho_{Fe}^{0.5}} \right]^{2/3} D_I \tag{3-17}$$

The V_B for bubble diameter > 10 mm is 0.1 m/s and V_z for a inclusion of 2 μm is 0.00012 m/s, 0.0003 m/s for a 5 μm particle and 0.0006 m/s for one of 10 μm; then $V_R \approx V_B$.

α is the semiangle of contact between inclusion and bubble, this is determinated by Equation 3-18, (Schulze, 1989).

$$\alpha = \left[\frac{\pi(\rho_P + 1.5\rho_{Fe})D_I^3}{24\sigma} \right]^{1/2} \tag{3-18}$$

The adhesion probability (P_A) of the inclusion to the bubble by sliding is defined as the ratio of the area $A_{OA} = (\pi R_{OA}^2)$ and $A_{BP} = (\pi (R_B + R_I)^2)$, for a particle diameter (D_I) smaller than bubble diameter (D_B) which is the normal condition in steelmaking:

$$P_C = \frac{R_{OC}^2}{(R_B + R_I)^2} = \sin^2 \theta_{OA} \tag{3-19}$$

It has been found by Yoon and Luttrell (1989, 1992) that P_A can be calculated according Equation 3-20, as a function of bubble and inclusion diameter and velocity :

$$PA = \sin^2\left[2\arctan\exp\left(\frac{-2T_F}{D_B+D_I}\left\{\left[1-\frac{3}{4X}-\frac{1}{4X^3}+\frac{\mathrm{Re}^{0.72}}{15}\left(-\frac{2}{4X^4}+\frac{1}{X^3}+\frac{1}{X}\right)\right].V_B - V_Z\right\}\right)\right] \quad (3\text{-}20)$$

Considering K_2 from Equation 3-12:

$$X = 1 + K_2 \quad (3\text{-}21)$$

It is assumed that the inclusions are removed by stirring only if the particle is attached to the bubble, then the quantity of inclusions of radius *i* removed by stirring (NR_{Bi}) is function of the P_C, P_A, gas flow rate, the distance which have to run (bath height, H), the quantity of particles of each size (NR_I) and the bubble size.

$$\frac{\partial NR_{BI}}{\partial t} = \frac{3QHNR_I TP_C P_A W_{Steel}}{2D_B T_O V} \quad (3\text{-}22)$$

3.2.3 Eye Area (Krishnapisharody and Irons, 2007):

Several authors (Anagbo and Brimacombe (1990), Sahajwalla, Castillejos and Brimacombe (1990), Yonezawa and Schwerdtfeger (2000), Guo and Irons (2002), Krishnapisharody and Irons (2007)) have worked to explain the effect of different variables such as gas flow rate, nozzle size, ladle height, and so on over the eye area.

Krishnapisharody and Irons (2007) developed mathematical models to relate the eye area with the gas flow rate and bath height. They found that the surface area of the exposed eye (A_{Eye}) has a non linear relation with the gas flow rate (Q, in cubic meter per second), ladle height (H, in meter) and also slag thickness, according Equation 3-23.

$$A_{Eye} = 0.414Q^{-0.22}H^{3.78}\left|\left(1+11.6Q^{0.74}H^{-2.46}\right)^{1.5}-1\right| \quad (3\text{-}23)$$

The eye area is important because affects the number of inclusions produce by reoxidation (Equation 3-41 and 3-43) and it gives the useful area to remove inclusions by slag (Equation 3-24).

3.2.4 Inclusion Removal according to Slag Model (by Hallberg, Jönsson, Jonsson and Eriksson, 2005):

Inclusions float up through the liquid metal into the slag where they are removed. The inclusions float up in a calm bath by density difference (Stokes law). In a gas-stirred liquid metal, the rising velocity in z direction (V_z) is a function of the gas flow rate (Equation 3-17).

The model assumes that all the inclusions which reach the slag are removed by it. The number of particles of i radius per unit volume, which are removed to slag (N_{Slag_i}) per unit time is:

$$\frac{\partial N_{Slag}}{\partial t} = \frac{A_{Slag}V_Z NR_I}{V} \quad (3\text{-}24)$$

where the slag area (A_{Slag}) is the difference between the ladle area (A_{Ladle}) and the A_{Eye} calculated in Equation 3-23.

$$A_{Slag} = A_{Ladle} - A_{Eye} \quad (3\text{-}25)$$

3.2.5 Inclusion Removal to Refractory Model (by Zhang and Cai, 2001):

This model considers that the inclusion which arrives at the refractory surface is attached in it and removed from the steel. It is assumed that the inclusions move with the molten steel and the transport of them to the wall and bottom is a diffusion process.

Zhang and Cai (2001) found an empirical equation for the fluid flow near the wall to estimate the variation in inclusion concentration (Equation 3-26). The number of particles of i radius removal to refractory per second is function of turbulent energy dissipation (ε), wall and bottom refractory area (A_{Ref}), inclusion radius and number of inclusion of this size, volume of steel (V) and kinematic viscosity (η_{Fe}).

$$\frac{\partial\left[NR_{\mathrm{Re}\,f}\right]}{\partial t} = -\frac{0.062\varepsilon^{3/4}}{\eta_{Fe}^{5/4}}\frac{A_{\mathrm{Re}\,f}R_I^{\,2}}{V}NR_I \tag{3-26}$$

The turbulent energy dissipation (ε) is calculated according to Zhang, Taniguchi and Matsumoto (2002), considering the gas flow rate (Q), ladle geometry (R_{Ladle} and H), steel density and atmosphere pressure (P).

$$\varepsilon = \frac{2PQ}{\pi R_{Ladle}H\rho_{Fe}}\ln\left(1+\frac{\rho gH}{P}\right) \tag{3-27}$$

3.2.6 Model for Inclusions Produced by Reoxidation (by Hallberg, Jönsson, Jonsson and Eriksson, 2005):

The model calculates the amount of reoxidation products in steel from the other phases in contact with it (slag or atmosphere). From slag, it considers the area in contact with the steel and the chemical composition of this phase, and from the atmosphere the contact area is evaluated (as function of the stirring power, Equation 3-23).

Slag oxidation is quantified by the oxygen content in steel ($[\%O]_{Slag}$) with respect of equilibrium with the reducible oxide in the slag (Equation 3-28), where the oxygen content in the slag is function of the equilibrium constant (K), the molar fraction (X) and the activity coefficient for oxide (γ). Iron activity in steel is considered equal to unity.

The flux of oxygen from the slag to the metal phase due to iron oxide reduction is assumed to be controlled by mass transport of oxygen on the metal side. The driving force for the dissolution is the difference in the oxygen activity in equilibrium with the reducible oxide in the slag and oxygen activity in the metal. The oxygen activity in equilibrium in the slag is assumed to be the oxygen activity in equilibrium with the iron oxide in the slag. The oxygen activity in the steel is assumed to be in equilibrium with dissolved aluminum content in the steel.

$$[\%O]_{Slag} = K_{FeO} X_{FeO} \gamma_{FeO} \quad (3\text{-}28)$$

Iron (Fe) oxide is in equilibrium with its reactants according Equations 3-29 (Turkdogan, 2001).

FeO_s à $\underline{Fe} + \underline{O}$ $K = \gamma_{[Fe]}\ \gamma_{[O]}$ $LogK_{FeO} = -5730/T + 6937$ (3-29)

The activity of iron oxide is calculated as a function of all oxides content in a multicomponent slag (CaO- SiO_2- MgO- MnO- FeO- Al_2O_3 slag) according to the Ohta and Suito (1998) model:

$$Loga_{FeO} = \frac{0.676\%MgO + 0.267\%Al_2O_3 - 19.07}{\%SiO_2} + 0.0214\%CaO - 0.047 \quad (3\text{-}30)$$

And the molar fraction for each oxide (X) is calculated as:

$$X_{FeO} = \frac{\%FeO / PM_{FeO}}{\sum Oxides} \quad (3\text{-}31)$$

Where the oxide addition ($\sum Oxides$) is summarized in Equation 3-32:

$$\sum Oxides = \frac{\%FeO}{PM_{FeO}} + \frac{\%MgO}{PM_{MgO}} + \frac{\%MnO}{PM_{MnO}} + \frac{\%CaO}{PM_{CaO}} + \frac{\%Al_2O_3}{PM_{Al_2O_3}} + \frac{\%SiO_2}{PM_{SiO_2}} \quad (3\text{-}32)$$

The oxygen content in the steel ($[\%O]_{Eq}$) represents the dissolved oxygen in the steel in equilibrium with the aluminum content is summarized in Equation 3-1.

The reoxidation rate is calculated from the difference between the oxygen content in the slag (Equation 3.28) and present in the steel (Equation 3.1), affected by the slag area and the oxygen mass transfer coefficient (Ko,i). The oxygen content in the slag and

in the steel is calculated with each time step and the area of the slag is calculated which each change in the gas flow rate.

$$\frac{\partial[\%O]_{Tot}}{\partial t} = \frac{1}{W_{Steel}}\left([\%O]_{Slag} - [\%O]_{Eq}\right)K_{O,I}A_{Slag} \tag{3-33}$$

The oxygen mass transfer coefficient is a function of the diffusion coefficient of oxygen in steel (Do) and transfer time (t_E) according Higbie's surface theory (Equation 3-34). This theory is applicable for mass transfer between two liquids. Transport is assumed to be controlled in the metal side.

$$K_{O,I} = 2\left(\frac{D_O}{\pi t_E}\right)^{0.5} \tag{3-34}$$

Considering that t_E is described in Equation (3-35) by eye and (3-36) by slag:

$$t_E = \frac{R_{eye}}{v_{eye}} \tag{3-35}$$

$$t_E = \frac{R_{Slag}}{v_{Slag}} \tag{3-36}$$

And $v_{Slag} \langle v_{eye}$, slag phase control diffusion. The v_{Slag} can be defined as a function of gas flow rate (Q) and the slag area (A_{Slag}):

$$v_{Slag} = \frac{Q}{A_{Slag}} \tag{3-37}$$

Higbie's theory for this model is summarized in the Equation 3-38

$$K_{O,I} = 2\left(\frac{D_O Q}{\pi R_{Ladle} A_{Slag}}\right)^{0.5} \tag{3-38}$$

Changing the slag area to eye area in Equation 3-33 and 3-38, the slag oxidation to atmospheric oxygen in Equation 3-33, reoxidation by the atmosphere is obtained (3-39).

$$\frac{\partial [\%O]_{Tot}}{\partial t} = \frac{1}{W_{Steel}} \left([\%O]_{Air} - [\%O]_{Eq}\right) \sum_{I=1} K_{O,I} A_{Eye} \tag{3-39}$$

$$K_{O,I} = 2\left(\frac{D_O Q}{\pi R_{Ladle} A_{Eye}}\right)^{0.5} \tag{3-40}$$

In this thesis inclusion growth mechanisms are not considered the alumina particles produced by reoxidation are new particles and are assumed to have only one

size (it is impossible to validate the inclusion size distribution produced only by reoxidation). Three different inclusion diameters have been studied in this project 2, 5 and 10 μm; when the model is running for a given total oxygen value with the three different sizes in separate ways, there are more smaller inclusions (2 μm) than larger ones (10 μm). The latter ones are more harmful for steel cleanliness (according to Section 2.3); and reoxidation is undesirable in the secondary metallurgy process (Section 2.7.1). Therefore, the model considers that reoxidation produces inclusions with a diameter of 10 μm.

The number of particles of radius R_I produced by reoxidation is calculated as the variation of total oxygen with respect to time and other properties of the particle and the gas (molecular relation ratio, density and molar weight):

$$\frac{\partial N(R_I)}{\partial t} = 9\frac{\frac{\partial [\%O]_{Tot}}{\partial t}}{4\pi}\frac{\rho_{Fe} M_P \eta_P 10^{-6}}{R_I^{\,3} \rho_P M_O \eta_O} \tag{3-41}$$

3.2.7 Inclusion Distribution and Total Oxygen:

In this thesis inclusion growth mechanisms are not considered; the initial size distribution of inclusions is taken after deoxidation according Equation 3-5 using plant data. The agglomeration effect of smaller inclusions by bubbling to form bigger ones (which float up easier) is neglected as well as the growth of inclusions by reoxidation, in which case it is considered which one inclusion size (10 μm) is produced (Section 3.2.6). The assumption that the inclusions do not grow simplifies the model; this

simplification is justified because from a process or practical standpoint there is not much difference between a number of inclusions that are a little bit bigger in diameter and a number of inclusions that is a little bigger of the same diameter, within the narrow bounds of plant data.

Starting from the assumption that the inclusions do not grow, they are removed from the steel by bubbles, slag or refractory or they can be added by reoxidation. Then the total number of inclusions of each size per second is calculated as the initial inclusion number (and addition of inclusions produced by reoxidation in case of bigger inclusion) less the addition of the inclusions removed by bubbling, refractory and slag.

$$\frac{\partial N(R_I)_{Tot}}{\partial t} = \frac{\partial N(R_I)_{Initial}}{\partial t} + \frac{\partial N(R_I)_{\mathrm{Re}\,ox}}{\partial t} - \frac{\partial N(R_I)_{Bubbling}}{\partial t} - \frac{\partial N(R_I)_{\mathrm{Re}\,frac}}{\partial t} - \frac{\partial N(R_I)_{Slag}}{\partial t} \qquad (3\text{-}42)$$

The total change in oxygen per second can be estimated as the increase in the final number of inclusions of radius *i* in time *t*, considering the fraction of each inclusion (X_i) and the volume and weight of steel, atomic weight and Avogadro's Number (Na), according to Equation 3-43.

$$\frac{\partial [\%O]Total}{\partial t} = \sum_{i=1}^{I} \frac{\partial N(R_I)_{Final}}{\partial t} \frac{16000 X_I R_I^{\,2} V}{W_{Steel} N_A} \qquad (3\text{-}43)$$

Chapter 4

EXPERIMENTAL METHODS AND RESULTS

4.1 Description of Ternium Siderar Plant

The samples to validate the model were taken in Ternium Siderar Argentina. The integrated steelmaking plant produces 2.8 million tons per year of tin plate, cold and hot rolled steel.

90% of its production is low carbon aluminum killed steel and the rest of it is aluminum-silicon-manganese killed steel. They are used in automotive, domestic and building industries.

Hot metal supplied by two blast furnaces arrives at the steelmaking shop by torpedo cars (Figure 4-1, a). It is charged into a hot metal ladle and is carried to a modern desulphurization station to remove the sulfur by lime and magnesium coinjection (Figure 4-1, b). The desuphurized hot metal and metallic scrap are charged in the BOF to produce steel by oxidation by oxygen injected at 2.2 Mach velocity. There are three basic oxygen furnaces (BOF) of 200 T of liquid steel (Figure 4-1, C); two of them are in operation and the third is in maintenance at any time. Steel is tapped from the BOF to a 200 T ladle with two bottom porous plugs for bubbling.

All secondary metallurgy processes are made in the ladle furnace and a trimming station (Figure 4-1, d). All production is treated with calcium to modify the inclusions,

then these calciumaluminate inclusions have lower melting point than steel and they are not clog the nozzle during casting (Section 2.4).

Casting is made in a two line continuous caster, and slabs of 200 mm thickness are produced with width between 790- 1650 mm (Figure 4-1, e).

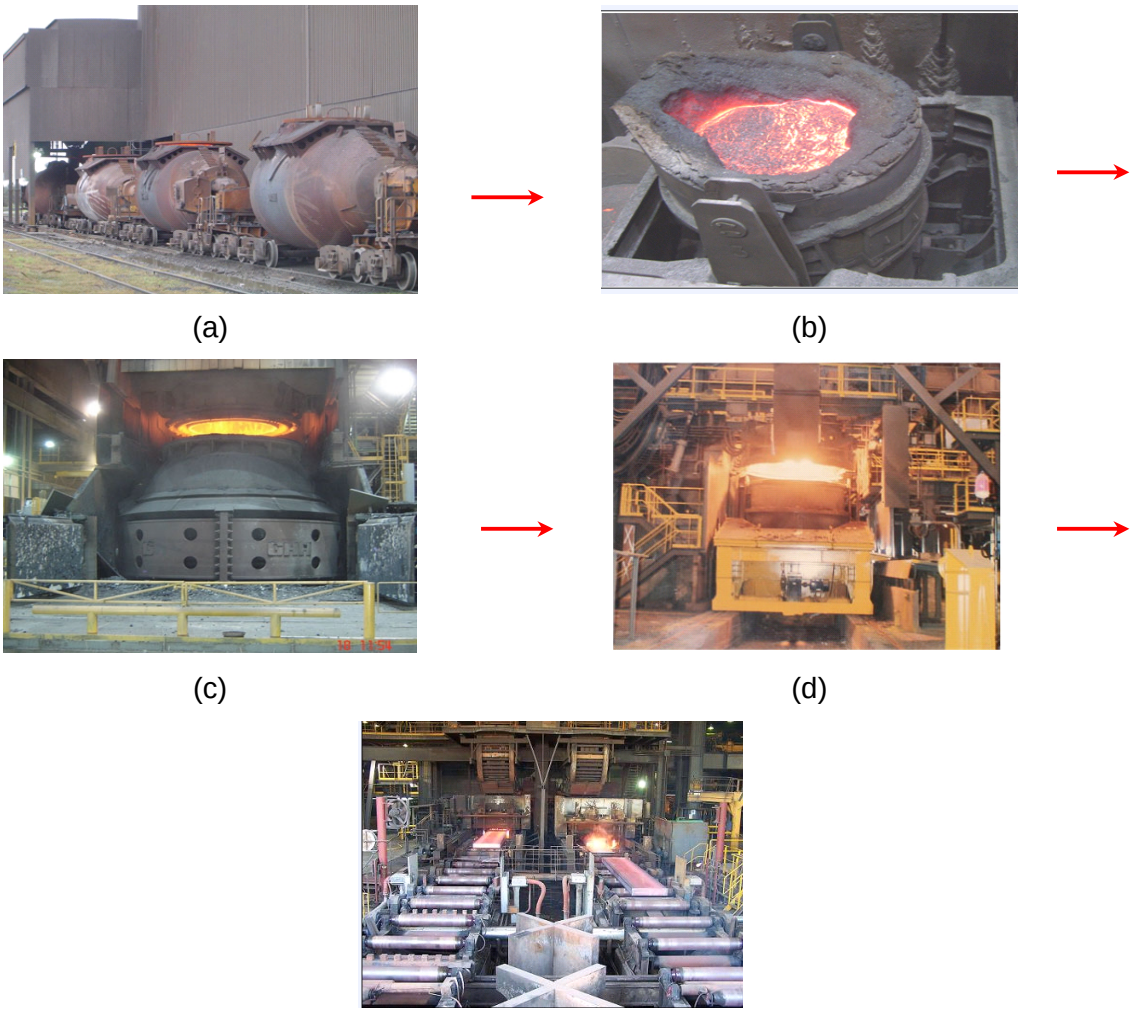

Figure 4-1. Steelmaking process in Ternium Siderar: (a) Torpedo cars from the blast furnace, (b) Hot metal ladle in desulphurization station, (c) Basic oxygen furnace, (d) Ladle furnace, (e) Continuous casting exit. Property of Ternium Siderar company.

4.2 Ternium Siderar Steel Ladle

Ternium Siderar works with 200 T steel ladles oblong in shape and with two bottom porous plugs.

A ladle cross section is shown in Figure 4-2 (a), where it is possible to see the taper from top to bottom; the average diameter is 3.64 m and the height is 3.5 m. In part (b) of the same figure, the internal bottom of a hot steel ladle is shown, where in the picture left corner is the nozzle and the other two holes are the porous plugs.

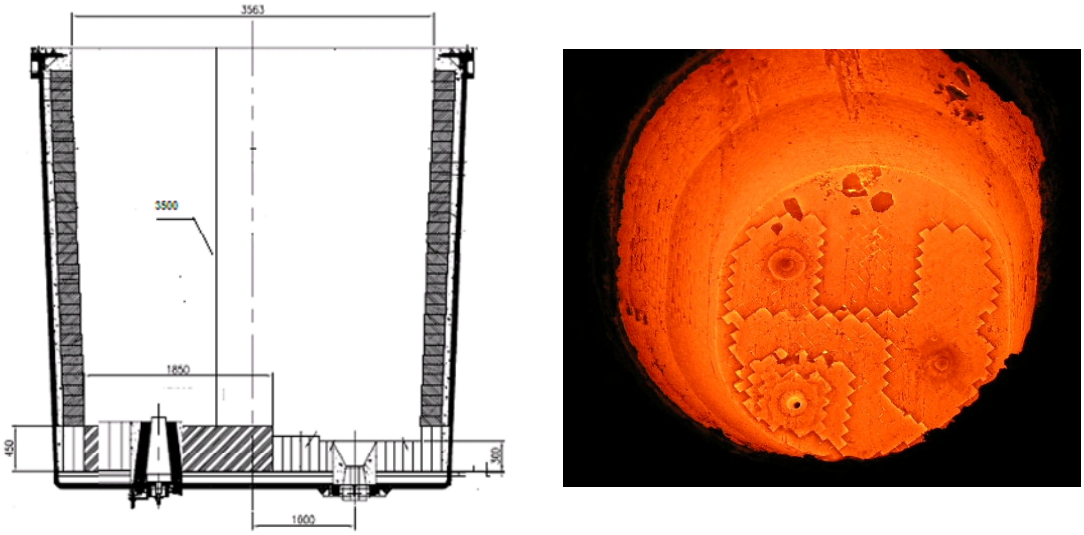

(a) (b)

Figure 4-2. Ternium Siderar steel ladle: (a) Ladle plan, (b) Picture of internal bottom.

4.3 Secondary Metallurgy Process

In the ladle furnace the alloying adjustment is made by wire (aluminum, carbon, titanium, nitrogen, and boron) and by hopper (lime, bauxite, dolomite, vanadium, niobium, manganese and silicon). The thermal adjustment is made by electrical

reheating through three graphite electrodes with a reheating rate of 3.5- 4 °C/minute. The reheat is made normally in two steps, the first to reach 1600°C (a good temperature to produce desulphurization) and the second step to obtain the necessary temperature to send the ladle to continuous casting.

During the secondary metallurgy process (in ladle furnace and trimming station), argon gas is bubbled through two porous plugs from the ladle bottom. If the plugs are blocked for any reason a top lance to bubble argon is used in the two stations. The flow rate used to stir the liquid steel is from 100 (soft bubbling) to 1200 liters/ minute (strong stirring) in each plug.

The ladle arrives at the LF from the BOF tapping with the steel killed (2-4 ppm of dissolved oxygen in equilibrium with 0.03- 0.04% Aluminum), and with a semikilled slag (3- 5% of FeO and 0.5- 2% MnO). The general process consists in five steps (Figure 4-3):

1- Soft stirring is used for homogenization and temperature and slag samples are taken. The operator deoxidizes the slag with small aluminum pieces and decides the lime-bauxite and dolomite additions which are necessary to obtain the aim slag composition.

2- First electrical heating is used to reach desulphurization temperature; the time depends of the initial temperature. Additions of ferroalloys are made by wire injection and from hoppers.

3- Temperature, steel and slag samples are taken to conclude the chemical and thermal adjustment. If it is necessary, a new addition is made and hard stirring for homogenization and removal of inclusions is made.

4- Second electrical heating is used; the time depends of the last temperature and the aim temperature for the continuous casting process.

5- Soft stirring to float out inclusions is used; temperature and steel samples are taken.

6- In this process the temperature increases by electrical heating and decreases by stirring.

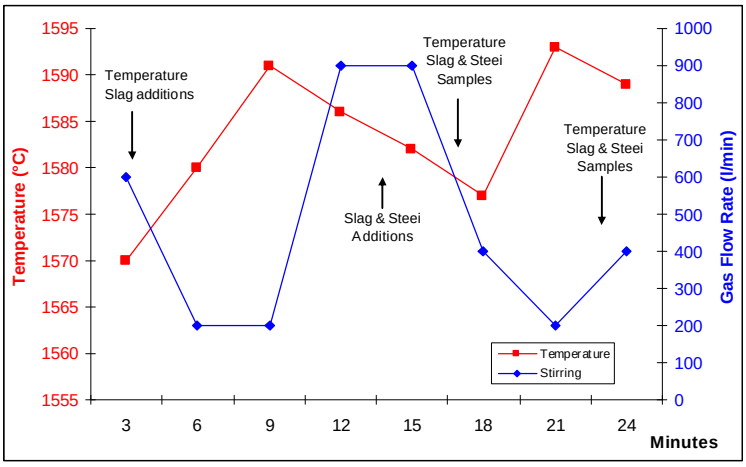

Figure 4-3. Steps of the ladle furnace process

The last part of the secondary metallurgy process is in the trimming station (TS); it is a new station which was built in Ternium Siderar in 1997 to increase the productivity of the ladle furnace (because it decreased the LF process time from 40 to 25 minutes plus 15 minutes in the TS). Here only soft stirring and calcium treatment are performed. This process consists in 3 steps (Figure 4-4):

1- Soft stirring is used to float out inclusions; this time can be longer if it is a very low carbon steel or a clean steel where more flotation time is required.

2- Calcium treatment is made with injection of SiCa, AlCaSi or AlCaFe wire, depending of the maximum silicon level allowed in the steel. Calcium is added to form globular inclusions; these new inclusions are liquid at casting temperature and do not clog the nozzle.

3- Final soft stirring to float up inclusions. Temperature, steel and slag samples are taken to control the process. During this process the temperature decreases by stirring.

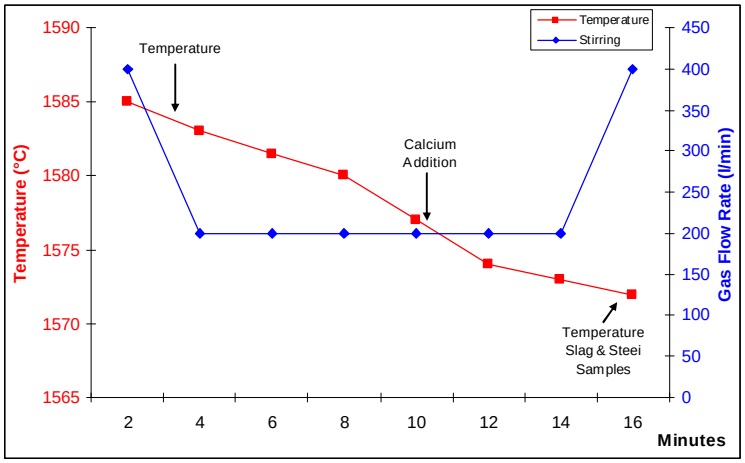

Figure 4-4. Steps of the trimming station process

4.4 Sampling

Four different heats were sampled and analyzed to validate the model. Samples were taken in low carbon aluminum killed steels during Secondary Metallurgy process. In Figure 4-5 the gas flow rate during the process, power on (to reheat) and temperature evolution are plotted to show the point of process where each sample was taken. Time zero is when tapping is finished.

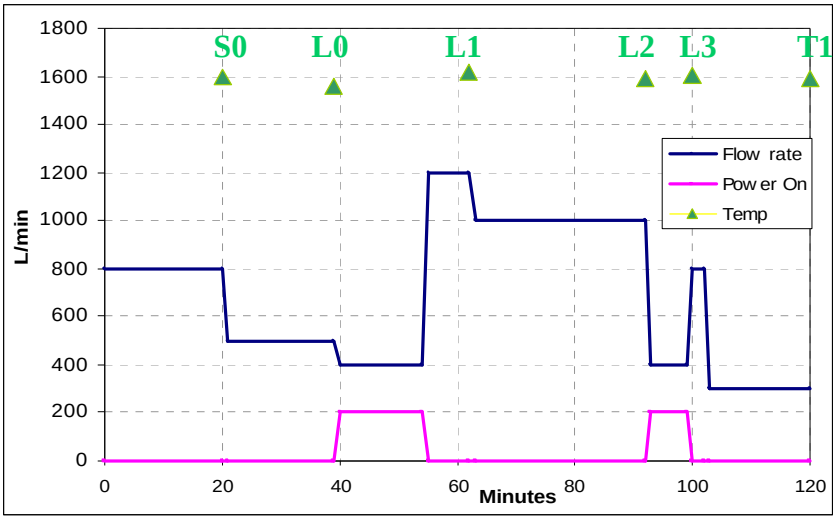

Figure 4-5. Schematic secondary metallurgy process to show the time of samples.

The samples are described below; in all these points temperature, slag and steel were sampled:

- S0: Sample 0 is the sample after tapping when deoxidation is finished.
- L0: It is the first sample when the ladle arrives in the Ladle Furnace, before the slag deoxidation and adjustment.
- L1: It is the sample after the first heating and slag adjustment.
- L2: It is the sample after the strong stirring, in general all the additions were made before it.
- L3: It is after the second electric heating and when the aim steel composition is obtained.
- T1: It is in the trimming station after the soft stirring and before the calcium injection.

Samples after calcium treatment are not taken because this process is not included in the current model.

The steel sampler is the lollipop kind without any killing agent (zirconium is not used, because it modifies the inclusion content and morphology). It is taken to analyze the chemical composition and then must be prepared for the SEM to investigate the inclusion content.

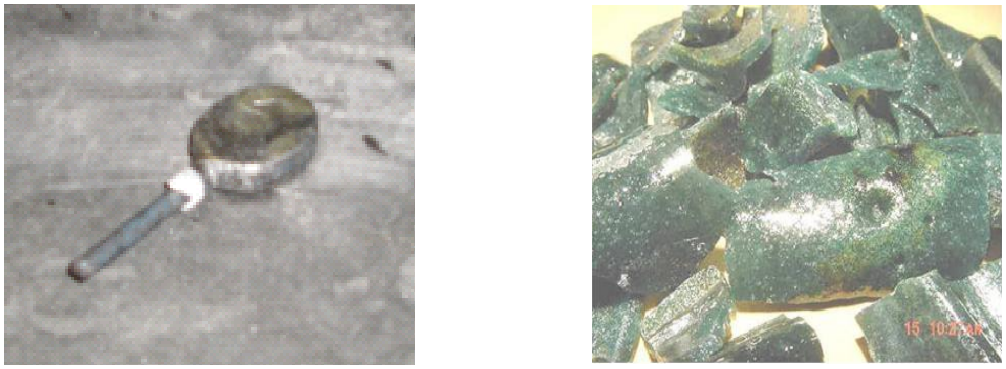

(a) (b)

Figure 4-6 Samples: (a) Lollipop steel sample, (b) Slag sample.

4.5 Analysis

Slag composition is determined by X-ray fluorescence in a compacted pellet of milled slag, Figure 4.7. The X- ray equipment is an ARL 9800 XP SIM-SEQ XRF (analysis by sequential in fixed channels and calibration by UniQuantâ®, a special software package). The slag is crushed, a magnet is passed to remove the metallic iron, and then a pellet is formed by pressure. The compositions of Ca, Mg, Mn, Si, Fe, S, Al, P, Ti are taken as pure elements and after they are expressed as %weight of oxide. (Appendix B).

Figure 4-7. Slag analysis: compact pellet of mill slag.

The quantity of each element in the liquid steel core is determined by spectrometry as %weight. (Appendix B).

The same samples were polished to be analyzed by a Philips SEM 515 with microanalysis EDAX system. It does quick chemical analysis for elements with atomic number greater than 6 and weight concentration greater than 0.5%. Then it is possible to obtain inclusion size and composition. This analysis was made in the IAS (Argentinian Iron and Steel Institute).

SEM (Scanning Electron Microscopy) scans 5 mm^2 areas to give inclusion distribution. It looks for small field, and this field is considered in the final area only when there is at least one inclusion, Figure 4.8.

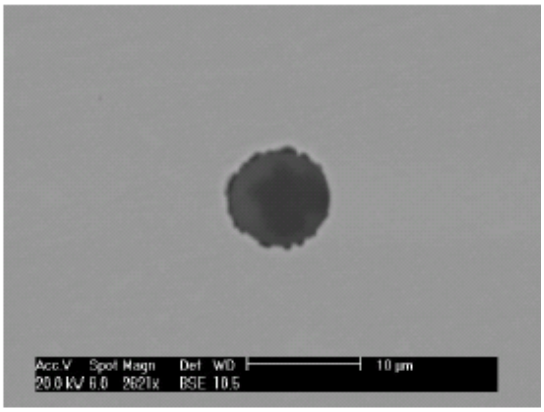

Figure 4-8. Inclusion analysis: inclusion seen in SEM (Espinosa, 2005).

SEM- EDAX (Winkler, Angeli & Mayr) allows analysis of morphology (size and shape) and chemistry of nonmetallic inclusions, with EDAX microanalysis system. It consists of a conventional scanning microscope (SEM) and chemical microanalysis for each inclusion is conducted by use of a lithium drifted energy dispersive silicon X-ray detector (EDAX). The equipment analyzes representative peaks for each element and gives an Excel file with the number of inclusions, size and chemical composition in each field. This data must be filtered to separate the real inclusions from porosity (high iron content), and abrasive incrustations (SiC presence), etc. The data base from each sample was analyzed manually to determinate the quantity and composition of inclusion distribution.

4.6 Results

4.6.1 Steel and Slag Composition for Heats

The complete composition of the steel is summarized in Appendix B. Manganese (Mn) and Aluminum (Al) are the only elements considered by the model. The evolution of

these metals during secondary metallurgy is shown in Figures 4.9 and 4.10 for the four heats, where each line corresponds to a different heat.

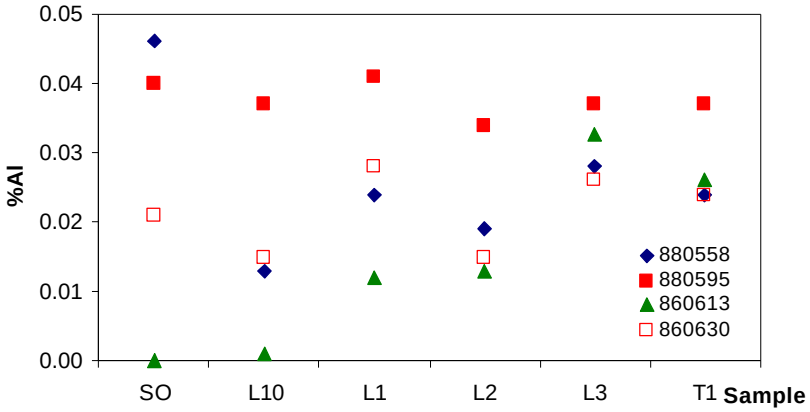

Figure 4-9. Aluminum analysis of the steel during secondary metallurgy

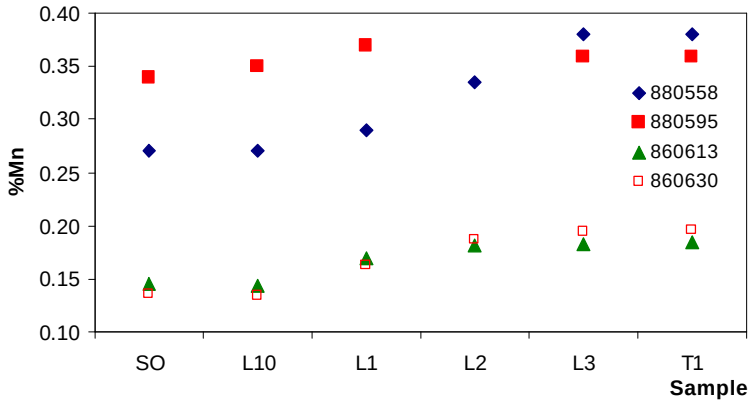

Figure 4-10. Manganese analysis of the steel during secondary metallurgy

All the slag's oxides are used to calculate slag oxidation in the model. FeO is plotted because it is a direct indicator of slag oxidation; other oxides are plotted in Appendix B.

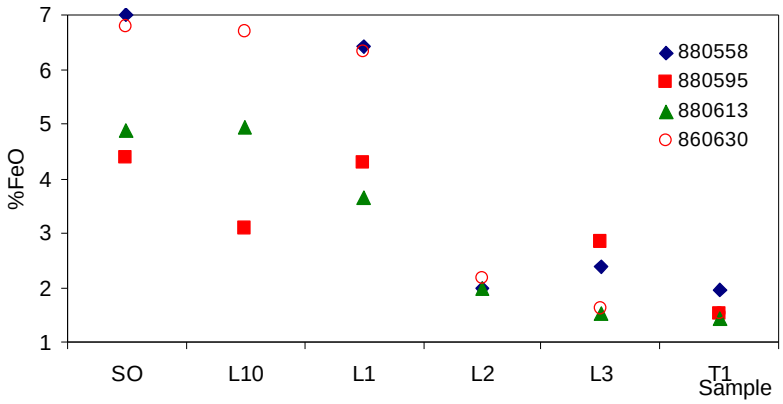

Figure 4-11. Iron oxide trend during secondary metallurgy

The values of sulfur and phosphorous oxide are always lower than 0.8%, and for this reason are not considered by the model.

The complete analysis of each heat (steel, slag and temperature) and the process conditions (oxygen activity, stirring, aluminum addition, etc) are summarized in the Appendix B.

4.6.2 Inclusion Composition

The inclusion composition is summarized in the ternary diagrams of Figure 4-12 for one heat (880558); the diagrams for all heats are plotted in Appendix C (quite similar results, for heats 880595 and 860630). The CaO- MgO and Al_2O_3 composition plotted in the ternary diagrams are weight percent, they are adjusted at 100% as if they were the only oxides in the slag. All these samples are before the calcium treatment and the composition is affected by deoxidation (Al_2O_3), and oxides from slag (CaO and MgO). In this particular heat the quantity of pure Al_2O_3 inclusions increases during the process; this is the opposite observation to Graham (Graham 2008). The inclusions Al_2O_3-MgO or

Al_2O_3- CaO in general are larger than pure Al_2O_3 inclusions, and for this reason they can float up easier than smaller ones. In a good secondary metallurgy process, most of the inclusions are Al_2O_3 inclusions (Figure 4-12 (e)).

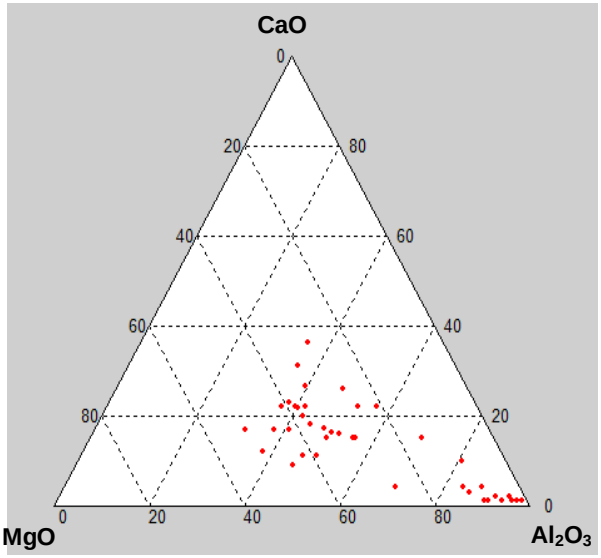

(a) Inclusions composition in So

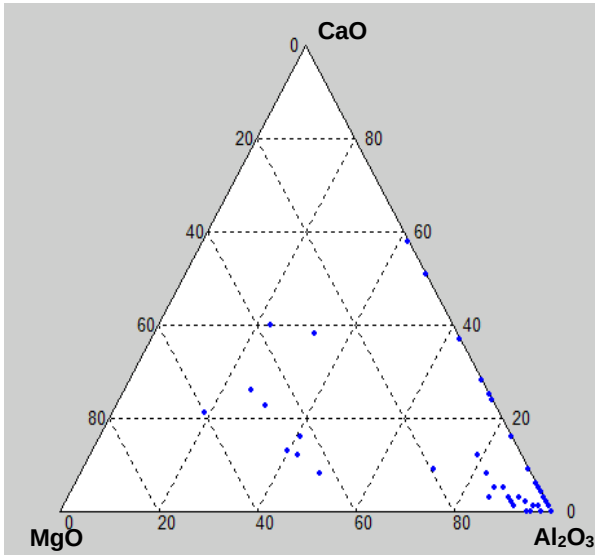

(b) Inclusions composition in L0

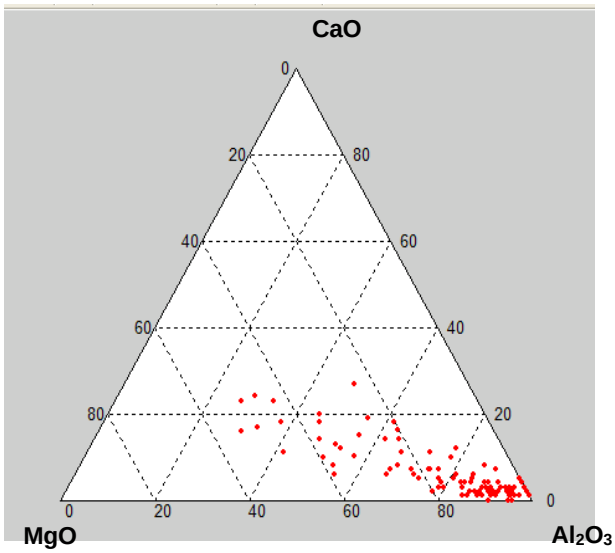

(c) Inclusions composition in L1

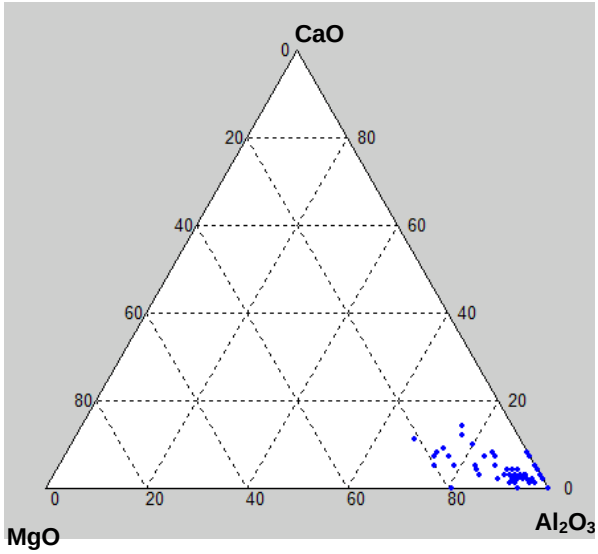

(d) Inclusions composition in L2

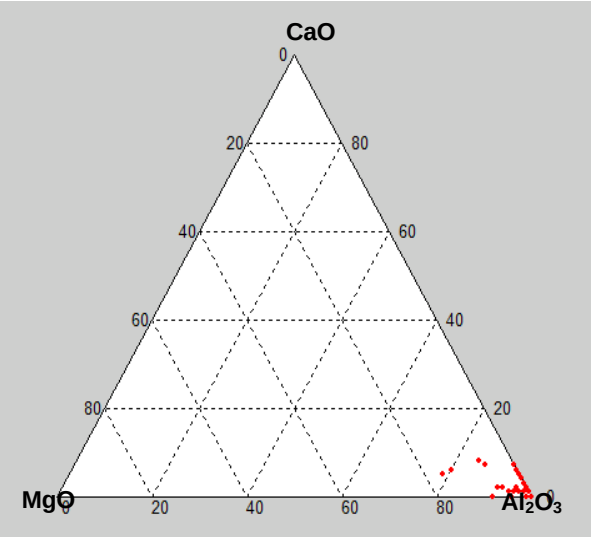

(e) Inclusions composition in L3

Figure 4-12. Ternary diagram with the inclusion composition during process of heat 880558.

The fourth heat (860613) shows similar tendency but the chemical composition of the final inclusions has Al_2O_3 and CaO (Figure 4-13). It may be explained by the high CaO content in the slag of this heat.

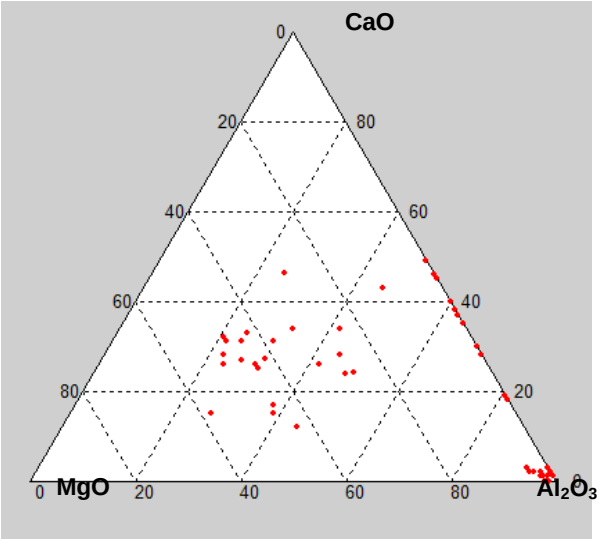

(a) Inclusions composition in So

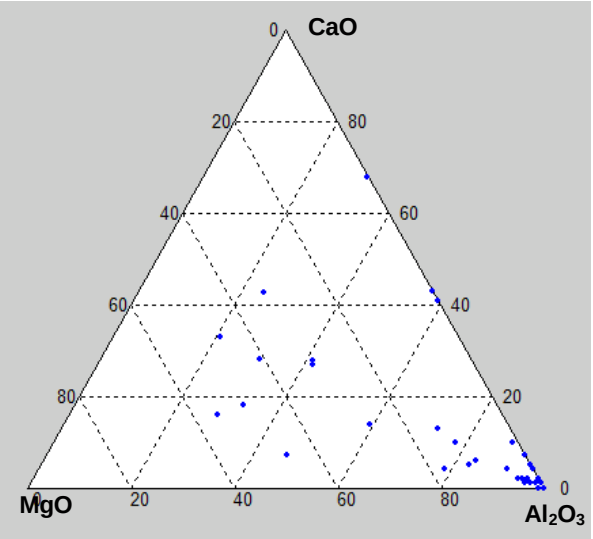

(b) Inclusions composition in Lo

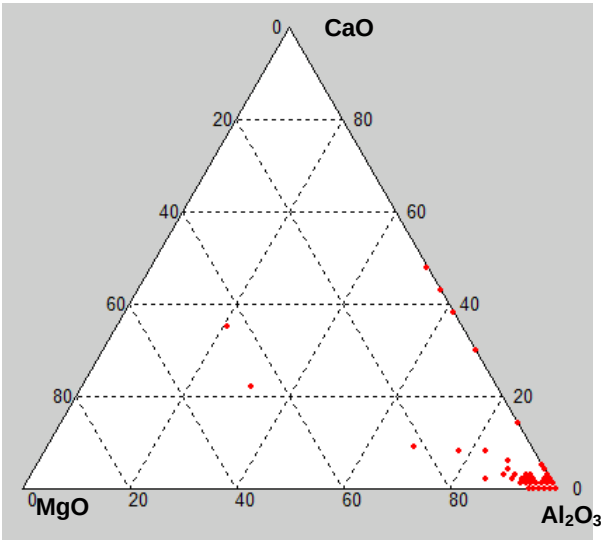

(c) Inclusions composition in L1

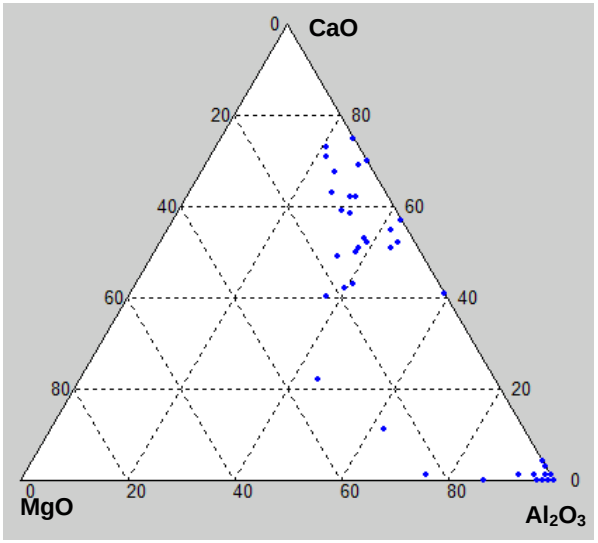

(d) Inclusions composition in L2

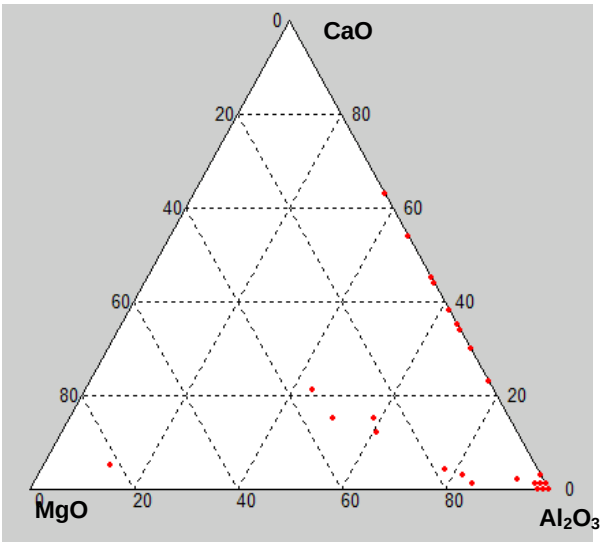

(e) Inclusions composition in L3

Figure 4-13. Ternary diagram with the inclusion composition during process of heat 860613.

4.7 Model Results Compared with Experimental Data

The quantity, size and composition of the inclusions were analyzed for each sample. In the examination of all samples the inclusions were divided in four size groups, diameter below 2 µm, below 5 µm, below 10 µm and below 20 µm. In the last group only

a few inclusions in some samples were found; for this reason the model was run with size distribution up to 10 µm. The values of each heat are shown in the Figures 4-14 to 4-17 and the comparison between real and calculated values are graphed in logarithmic scale.

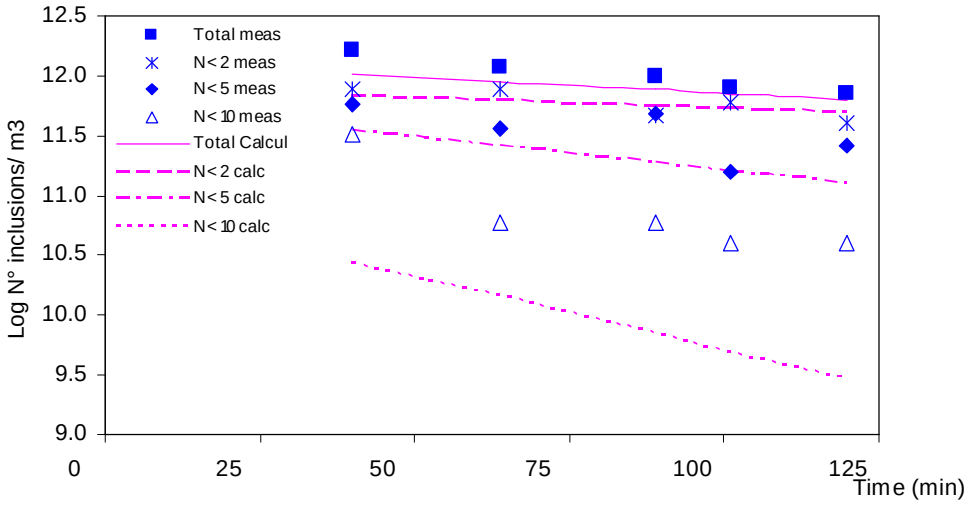

Figure 4-14. Comparison of measured and modeled inclusion distribution for heat 860613

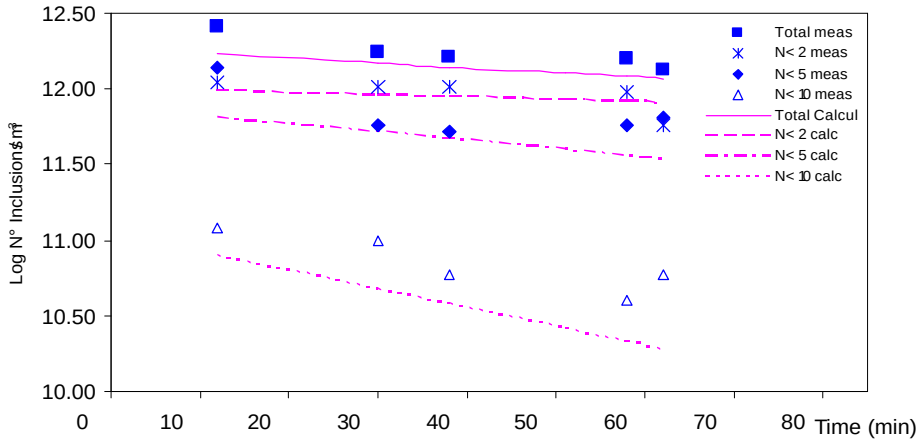

Figure 4-15. Comparison of measured and modeled inclusion distribution for heat 880595

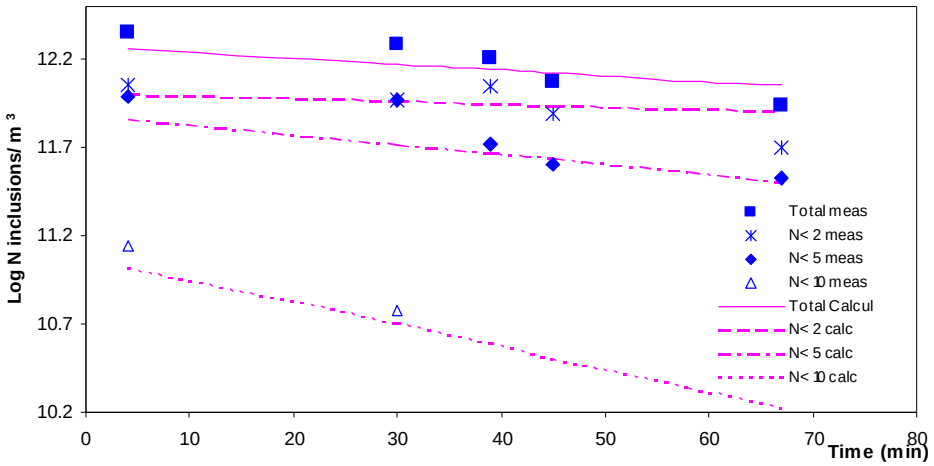

Figure 4-16. Comparison of measured and modeled inclusion distribution for heat 860588

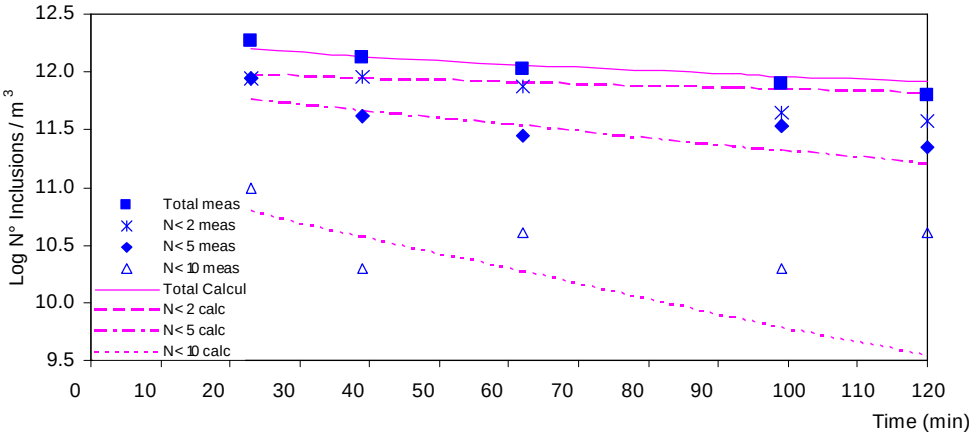

Figure 4-17. Comparison of measured and modeled inclusion distribution for heat 860630

Generally, there is very good agreement between the model and the data. The reasons for this are examined in the Discussion.

Chapter 5

DISCUSSION

In the previous Chapter, very good agreement between the model and experimental results was presented. In the following sections, the reasons for the good agreement will be examined and the sensitivity to assumptions will be explored.

5.1 Bubble Diameter and Terminal Velocity

Different authors (Oeters, 1994; Hoefele & Brimacombe, 1979) studied bubble diameter as a function of gas flow rate; these models use density, surface tension, gas flow rate and the inner nozzle diameter as variables. They were set for the conditions used in this work and the results are shown in Figure 5-1; the gas flow rate is considered in the plant data range (200 to 1400 l/min of inert gas) and the inner nozzle or pore diameter of the porous plug is 0.020 m.

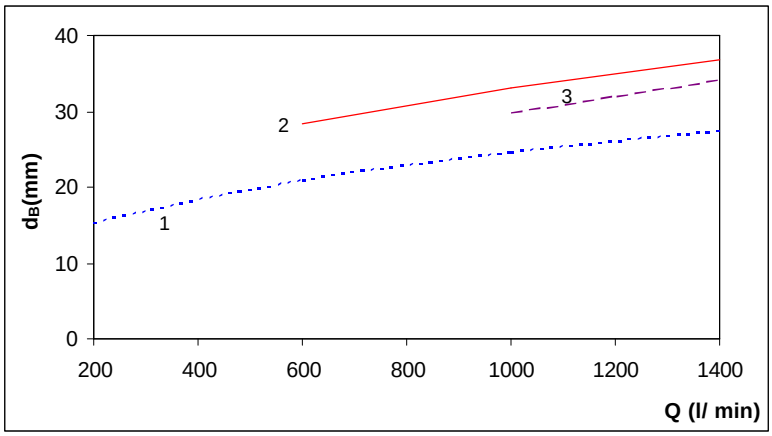

Figure 5-1. Correlation between the bubble diameter (d_B) and the gas flow rate (Q). 1: Meersmann (Oeters, 1994), 2: Davidson (Oeters, 1994), (Qg = (40- 1000)*10^{-6} m^3/s), 3: Hoefele&Brimacombe, (1979), (Qg > 200*10^{-6} m^3/s).

The correlation for bubble diameter by different authors gives diameters between 15 and 35 mm respect to flow rate. Irons and Guthrie (1981) demonstrated that bubbles in liquid metal are larger than in water models because of the bubble volume is proportional to surface tension and bubbles spread across the nozzle. Their studies with different nozzles show that the normal bubble gas diameter in steel is larger than 30 mm. The bubble size is unknown in the present study, so this value is assumed.

The terminal velocity of the bubble depends of bubble diameter; velocity increases when the bubble is larger, and the velocity is function of the gas flow rate because it determines the size of the bubble. Since the bubble diameter is around 30 mm for metal bubbling, a sensitivity analysis on the effect of different bubble diameter on the terminal velocity is shown in Figure 5-2 for velocity correlations from different authors (Levich, 1962; Peebles & Garber, 1953; Davis & Taylor, 1950). There is a variation of 40 % for this bubble size.

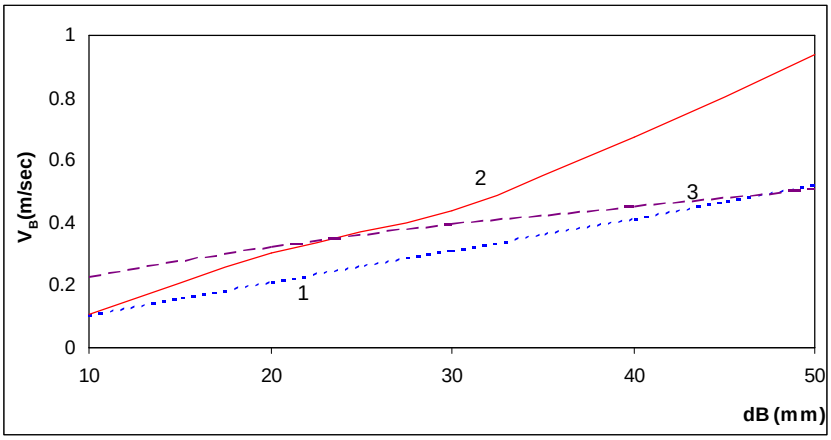

Figure 5-2. Correlation between the terminal bubble velocity (v_B) and the bubble diameter (d_B). 1: Levich, 1962 (Re = 500- 1200); 2: Peebles and Garber, 1953 (Re = 500- 1200); 3: Davies & Taylor, 1950.

In Figure 5-3 the number of inclusions removed from the steel calculated by the model is plotted for three different bubble diameters (10, 30 and 50 mm), although 30 mm is the expected value for steelmaking other values were used to determine the impact of bubble size.

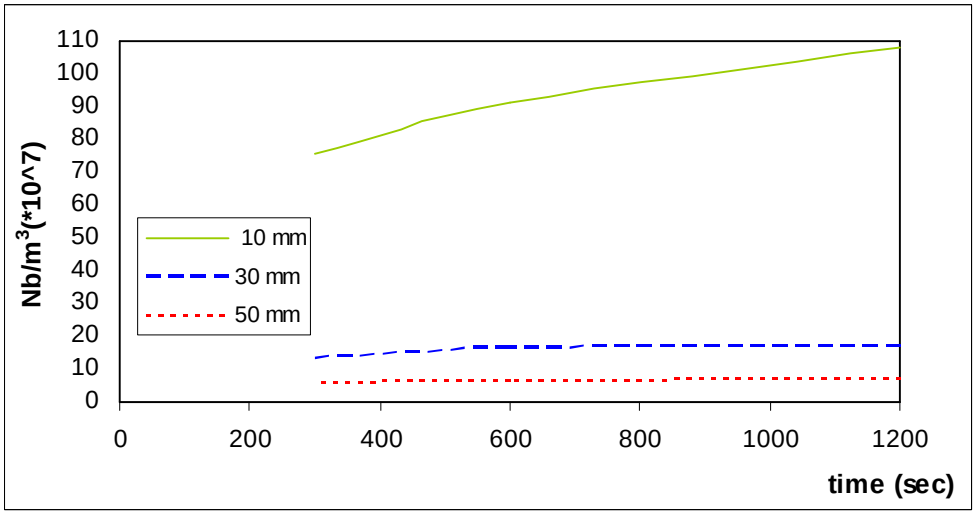

Figure 5-3. Variation of number of inclusions per cubic meter removed by bubbling (Nb/m^3) during process for different bubble diameter.

The number of inclusions removed by bubbling increases when the bubble diameter is smaller, bubbles with diameter between 30 to 50 mm have similar behavior to remove inclusions respect to the time of bubbling. Smaller bubbles achieve a better cleanliness according this model, but the production of bubbles with diameter smaller than 30 mm requires a change in the gas injection technology for metal stirring.

The current model contemplates three inclusion removal mechanisms: removal by refractory, slag and bubbling, and the reoxidation mechanism which increase the number of inclusion. Removal by bubbling is the mechanism affected by bubble size. Figure 5-3 shows that there is some difference in the rate of inclusion removal between a bubble with 30 or 50 mm diameter (Equation 3.22), but the other factors such as reoxidation and removal by slag balance this effect to achieve a similar cleanliness value where the final inclusion numbers are quite similar (Figure 5-4).

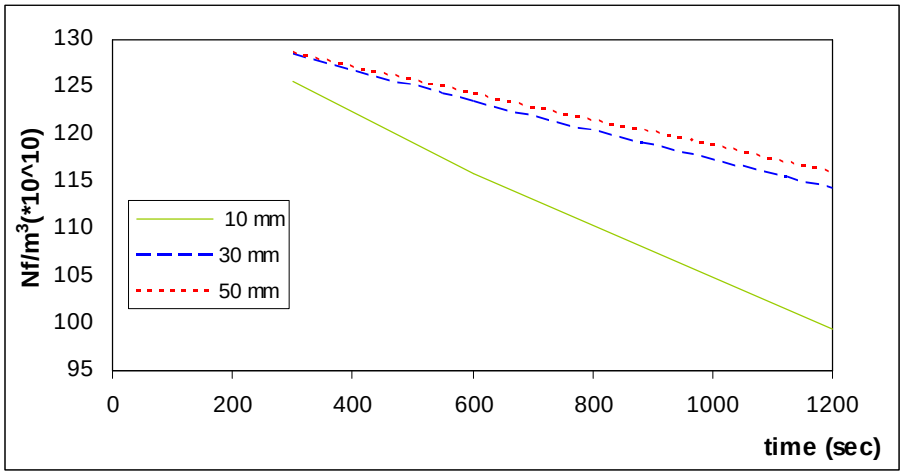

Figure 5-4. Variation of final remaining number of inclusion per cubic meter (Nf/m^3) after removal by bubbling during processing for different bubble diameters.

The impact of qualitative bubbles (smaller than 30 mm diameter) in this removal mechanism is quantitative greater than a 30 mm bubble . This concept comes from the Wang, Lee and Hayes theory (Section 2.8 of this thesis), where the probability of smaller bubbles colliding with an inclusion is very high. Although the effect of velocity is the opposite (smaller bubbles float up lower than larger ones), finally smaller bubbles collide easily with an inclusion and more inclusions are removed attached by these bubbles.

5.2 Effect of Each Mechanism on Inclusion Removal

Different mechanisms are described to model the inclusion removal (bubbling, slag and refractory) and inclusion increment (reoxidation) during the secondary metallurgy process. The initial number of inclusions (produced according to the deoxidation practice at the end of primary metallurgy process), is increased by reoxidation during the process, by reoxidation from the atmosphere and by the slag if it is oxidized. Figure 5-5 shows the number of inclusions produced by reoxidation depending on initial conditions of 500 ppm of oxygen dissolved before deoxidation practice and after deoxidation the steel contains 0.02% Al and 0.3% Mn. These are in equilibrium with a ladle slag with 4% FeO, 1%MnO, 8% MgO, 55% CaO, 4% SiO_2 and 28% Al_2O_3, steel temperature of 1600 °C, and stirring rate of 600 l/min.

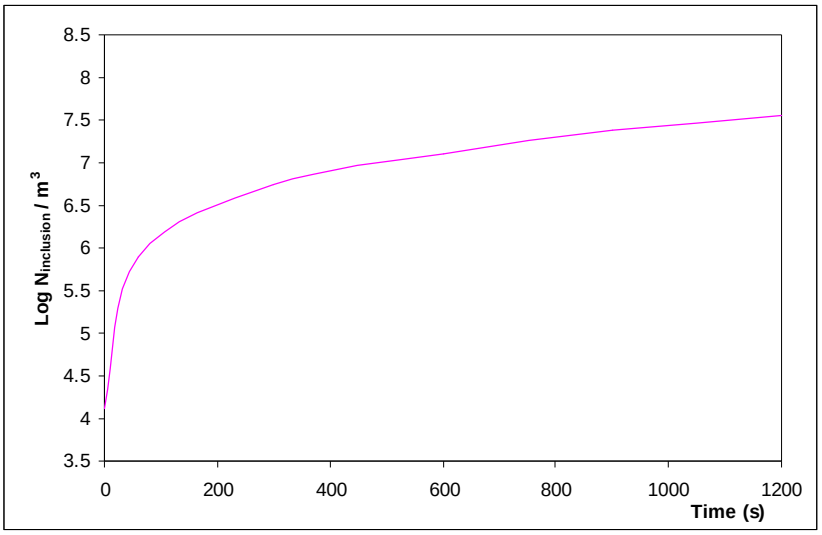

Figure 5-5. Effect of inclusion number increment produced by reoxidation

The start of in Figure 5-5 is one second after nucleation occurs (this is the minimum time to run this model), and reoxidation is low. During the process the number of inclusions increases by reoxidation and its impact depends of slag oxidation and the exposed eye to atmosphere (which is a function of gas flow rate). The individual effects of slag and stirring on reoxidation will be developed in section 5.3.

The other three mechanisms developed in the model work opposite to reoxidation; they remove inclusions during the process reducing the final number of them. Figure 5-6 shows the quantity of inclusions removed by each mechanism from the steel bath over the process. Figure 5-6 was based on the same initial conditions as Figure 5-5.

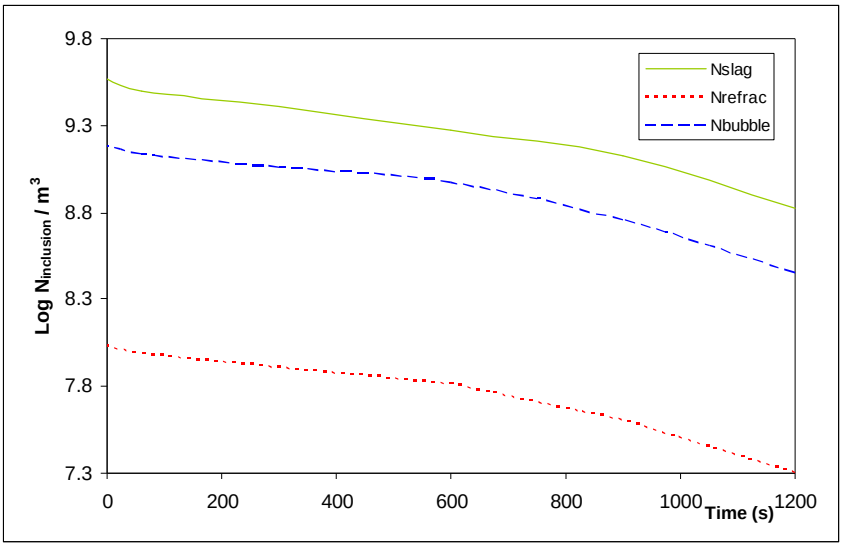

Figure 5-6. Quantity inclusions remaining by removal effect of each mechanism during the process

Removal by refractory is directly proportional to refractory area and initial number of inclusions, and a function of gas flow rate through the turbulent energy dissipation (ε) according to Equation 3-26. This can be simplified for each inclusion size as:

$$\frac{\partial\left[NR_{\mathrm{Re}\,f}\right]}{\partial t} \propto \frac{\varepsilon^{3/4} A_{\mathrm{Re}\,f}}{V} \tag{5-1}$$

Equation 5-1 it shows that this mechanism is important in comparing different ladle sizes because the refractory area has more impact than the gas flow rate according to Equation 3.27. Starting from the relationship refractory area over steel volume (A_{Ref}/ V), it is possible to see that tall and narrow ladles have more surface area and residence

time to remove inclusions than short and wide ones. For a fixed ladle size the variable is the stirring but this mechanism has less impact than removal by bubbling and slag.

Inclusion removed by bubbling and slag have a similar effect. Although removal by slag is greater than by bubbling (Figure 5-6); their curves have the same shape. It can be explained through the equations which regulate each mechanism. Removal by bubbling calculated by Equation 3-22, depends of some constants related to the ladle (height and steel volume), to the bubbles (diameter and velocity) and particles (inclusion diameter and velocity) which explain the probability of an inclusion to be removed by a bubble according to collision and adhesion probability. The main variables are summarized in Equation 5-2 for the rate of inclusion removal for particles of different radius.

$$\frac{\partial[NR_{Bi}]}{\partial t} \propto QTP_C P_A \tag{5-2}$$

Inclusion removal by bubbling is directly proportional to gas flow rate, when the bubble diameter is fixed (as explained Section 5.1). The other important factor is the relationship between inclusion size and bubble collision and adhesion (calculated by P_C and P_A).

When inclusion removal by slag is reviewed, Equation 3-24 shows that gas flow rate is not considered and the mechanism depends of inclusion velocity in z direction and the slag area. But the slag area is function of flow rate, because it is the ladle area less the eye area and this latter variable depends on gas flow rate according Equation 3-23.

Removal by slag is the most important mechanism to remove inclusions according this model, but really this is not the fundamental mechanism; it is the result of flotation of inclusions. In this mechanism a major simplification was considered; the model considers that all inclusions which arrive at the slag are caught by it. This simplification implies that inclusion dissolution in the slag is instantaneous and it does not depend of the slag composition as Sridhar and Cramb and Valdez and Cramb explained (Section 2.7.2). For slags that are far from Al_2O_3 saturated this simplification is good, but this assumption may not be appropriate when the slag viscosity is high or it is saturated with MgO.

An important assumption must be done as regards the inclusion dissolution in the slag. There is dissolution only there is a mixing between the slag and the steel, therefore the inclusions are removed by the slag only during the bubbling process.

5.3 Reoxidation Effect (by Slag and Atmosphere)

The effect of slag oxidation state on the inclusion numbers produced by reoxidation is shown in Figure 5-7. The model was run for two different slag oxidation levels, for both cases the initial oxygen content before deoxidation practice was 600 ppm, and the gas flow rate for both processes was 500 l/min. The steel was deoxidized with aluminum, when the deoxidation practice finished the steel bath contained 0.3% of manganese in both cases and the aluminum registered as in Table 5-1. Since the steel and slag are in equilibrium, for low aluminum content in equilibrium with high oxygen content in the metal bath (according to Equation 3.1) a high oxidation state in the slag is expected; all these values are summarized in Table 5-1 as High Slag Oxidation. On the other hand Low Slag oxidation is considered when the residual aluminum content is high,

because the oxygen in equilibrium with it must be low and the same condition for the slag. All the steps (different times) have been run with the same values; there are no other changes in steel and slag compositions or flow rate.

Table 5-1. Steel and slag composition for reoxidation mechanism tests.

Slag Oxidation	%Al	%FeO	%MnO	%CaO	%MgO	$\%Al_2O_3$	$\%SiO_2$	NR_O ($1/m^3$)	NR_F ($1/m^3$)
Low	0.03	2	0.5	56	8	29.5	4	$1.66*10^{12}$	$1.46*10^{12}$
High	0.01	8	3	52	7	27	4	$1.64*10^{12}$	$1.45*10^{12}$

Table 5-1 shows also the number of the inclusions produced by deoxidation practice (NR_O) and after 900 sec (NR_F) of treatment for both situations. When deoxidation is poor, the initial number of inclusions is lower than for a strong deoxidation because part of the oxygen remains dissolved in the steel bath. When the model runs with these parameters, lower inclusion content at the end of treatments is obtained with high oxidation in the slag and low aluminum content in the steel. Although high oxidation in the slag in equilibrium with low aluminum dissolved would appear to be a better situation, it is not possible in practice where low oxygen content is necessary to cast the steel and for other refining processes as desulphurization. Considering that the oxygen dissolved in the steel must be lower than 5 ppm to be able to cast the steel in continuous casting, if Equation 3-1 is applied the oxygen dissolved is 5 ppm in equilibrium with 0.03% of aluminum, when this equation is applied by the high oxidation in the slag condition where the aluminum in the steel is 0.01% the oxygen dissolved is 12 ppm.

The inclusion removal mechanisms (bubbling, refractory and slag) are independent of the slag oxidation, but this parameter has a major impact on reoxidation; it is the only variable plotted (Figure 5-7).

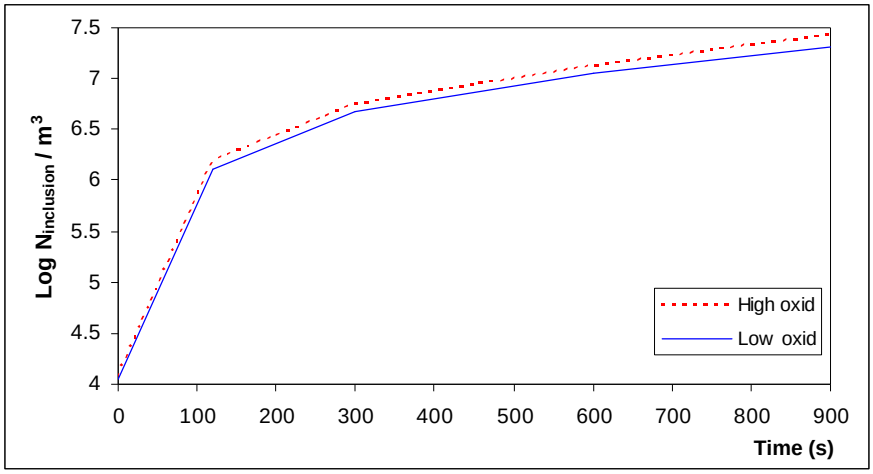

Figure 5-7. Effect of slag oxidation level on the inclusion number produced by reoxidation.

Slag oxidation level has a small effect on the inclusion formation by reoxidation in the model because it considers only the oxygen free to produce oxide according to Equations 3-35 and 3-36; the effect on inclusion removal by slag composition is not considered. The oxygen content in the steel in equilibrium with the slag is calculated by Equation 3-2. The variation in the oxygen content in the steel and the slag-metal interface according to Equation 3-28 varies between $2.3*10^{-3}$ % and $1.89*10^{-3}$ %, for the slag composition shown in Table 5-1 where FeO plus MnO contents change from 2.5 to 11% which are wide ranges of values for a ladle slag.

In the real process the slag oxidation level must be decreased during secondary metallurgy to allow for desulphurization and assure there is no alumina by reoxidation

which can clog the nozzles during casting. Considering these process conditions, it can be concluded that slag oxidation level effect on reoxidation can be neglected in comparison to other effects in this model. It is a limitation of the model because the effects of oxides on the cleanliness (according to Figure 2-8) cannot be modeled at the present time.

The effect of stirring on the inclusion number produced by reoxidation is shown in Figure 5-8. The data used to run the model for different stirring intensities is 600 ppm of oxygen dissolved in the steel before deoxidation practice, after the aluminum was added to kill the steel the residual values are 0.03% of aluminum and 0.3% of manganese in the steel, and slag composition used is 3% of FeO, 1% of MnO, 56% of CaO, 8% of MgO, 28% of Al_2O_3 and 3% of SiO_2. The gas flow rate is 400 l/min and 1200 l/min for each test; these conditions and the composition do not change during different steps.

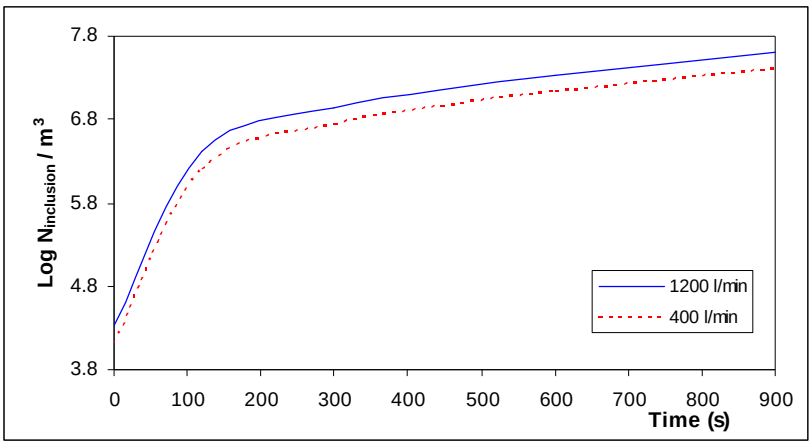

Figure 5-8. Effect of gas flow rate on the inclusion number produced by reoxidation.

Figure 5-8 shows that the inclusions produced by reoxidation at 400 l/min are the same that values calculated earlier (Figure 5-7). Reoxidation by slag cannot be isolated

from gas stirring because it provides the liquid stirring for the reoxidation reactions which are controlled by transport on the metal side. The driving force is the difference in the oxygen potential between the phases. According to Equation 3-36 oxygen produced by reoxidation is a function of the oxygen potential difference between steel and slag ($[\%O]_{Steel}$ - $[\%O]_{Slag}$), the oxygen mass transfer coefficient ($\kappa_{O,I}$) and the contact surface area ($A_{contact}$), summarized in Equation 5-3:

$$\frac{\partial[\%O]_{Tot}}{\partial t} \propto ([\%O]_{Tot} - [\%O]_{Phase}), \kappa_{O,I}, A_{Contact} \quad (5\text{-}3)$$

It is important to note in Figure 5-8 the reoxidation varies with the gas flow rate, basically by the impact over the contact surface (the eye area). The eye area varies from 3.34 m^2 for 400 l/min of gas flow rate to 5.92 m^2 for 1200 l/min (calculated by Equation 3-23). The gas flow rate influences oxygen mass transfer coefficient too because of it is function of gas flow rate and contact area (Equation 3-38).

5.4 Effect of Stirring Power on the Inclusion Removal by Bubbling and Slag

Although the stirring power affects reoxidation, it is important for removal of inclusions by other mechanisms such as bubbling and slag capture.

The final number of inclusions after removal by slag during the process is plotted in Figure 5-9 for the same conditions that Figure 5-8, considering normal stirring for mixing and homogenization (400 l/min) and a strong flow rate (1200 l/min).

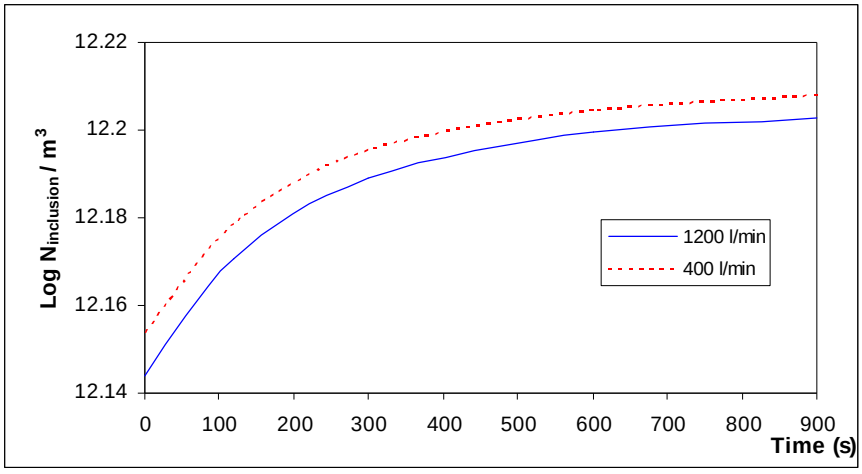

Figure 5-9. Effect of gas flow rate on the number of inclusion removal by slag.

According to Figure 5-9 softer stirring is better for inclusion removal by slag than a stronger one (the final number of inclusions at 900 seconds is lower when the stirring is softer). This is because the mechanism of removal by slag developed in the current model, considers that all the inclusions which arrive at the slag are removed from the steel; with this concept the most important variable for the mechanism is the contact area for slag- steel. Slag area is calculated as the difference between the ladle area (a constant for each plant) and the eye area (according Equation 3.23); in this case the slag area varies from 7.07 m^2 by 400 l/min of argon flow rate to 4.48 m^2 by 1200 l/min. This variation in slag area according to gas flow rate explains the difference in the inclusion removal shown in Figure 5-8.

The effect of stirring on inclusion flotation (i.e., attachment to bubbles) is not considered here, but rather in inclusion removal by bubbling; by slag removal mechanism (Equation 3-24) particles float up by velocity in z direction (Equation 3-17) where the inclusion diameter is important.

The effect of stirring on inclusion removal by bubbling is plotted in Figure 5-10 for the same process conditions as Figure 5-8.

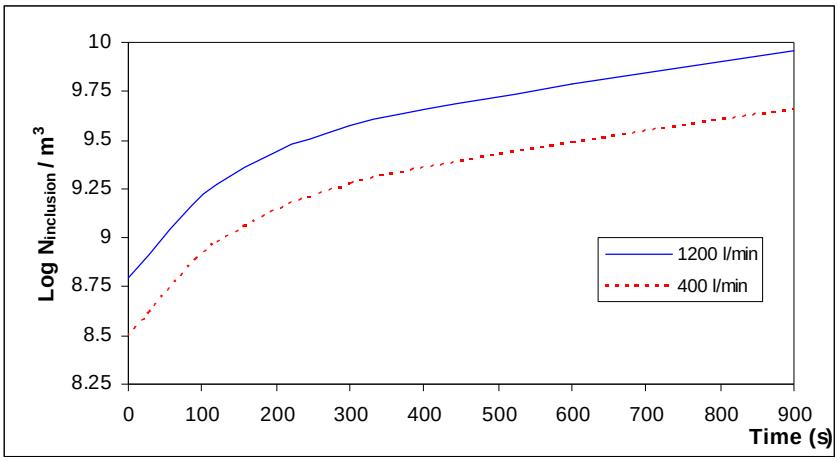

Figure 5-10. Effect of gas flow rate on the number of inclusion removal by bubbling.

An increase in gas flow rate improves the inclusion removal by bubbling; this effect is shown in Figure 5-10, where stronger stirring is more efficient to removal inclusion than a softer one (where the final inclusion number at the end of treatment is lower by strong stirring). This is because removal by bubbling mechanism developed in the current model is directly proportional to gas flow rate (Equation 3-22).

The other factors considered in removal by bubbling mechanism are independent of the gas flow rate (as probability of collision and adhesion) but they are very affected by inclusion size. This effect will be developed in Section 5.5.

5.5 Effect of Inclusion Size on Efficiency by Different Removal Mechanisms

The model considers three different inclusion sizes according to the experimental ranges (2, 5 and 10 µm). All the Al_2O_3 produced starting from the initial oxygen content is divided in inclusions of different sizes, 54% of oxygen forms inclusion of 2 µm, 38% produces 5 µm inclusions and the last 8% is contained in the 10 µm ones according to Figure 3-2.

Although, during reoxidation, inclusions of different sizes can be produced, the model considers all the alumina produced by reoxidation forms particles of only one size. It is not possible to validate the inclusion size distribution only by reoxidation, Section 3.2.6.

Figure 5-11 shows the impact of inclusion size in the slag removal mechanisms, where the 5 µm inclusions are removed easier than the 2 µm ones. This is because the larger inclusions have faster flotation velocity (according Equation 3-17, velocity in direction "z" is function of the inclusion diameter) than smaller particles.

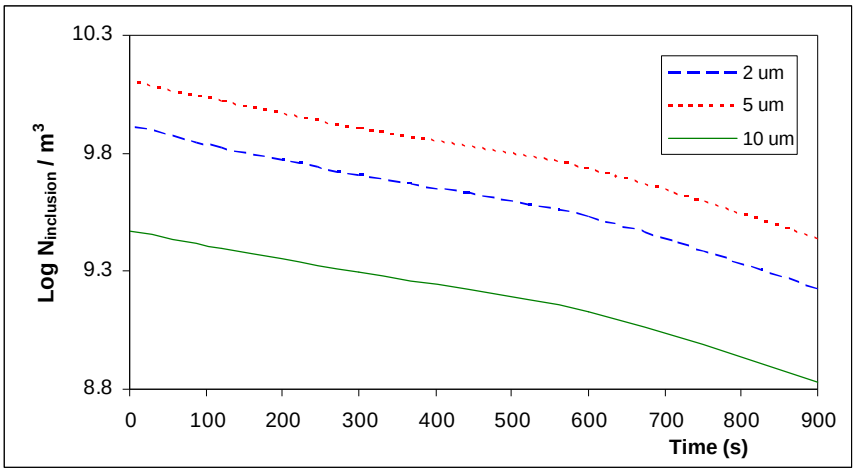

Figure 5-11. Impact of inclusion size on the particle remaining number after slag removal mechanism.

The contradiction presented in Figure 5-11 with the largest inclusions (10 µm particles) is explained by the initial inclusion number. The number of inclusions removed by slag depends of the initial inclusion number for each time (Equation 3.24). The initial particle number for 10 µm inclusions is very low with respect the other ones; for this reason their removal looks lower than for smaller inclusion sizes.

Similar behavior regulates the bubbling removal mechanism. The collision probability is proportional to inclusion diameter (Figure 2-19) while adhesion probability increases with a decrease in the inclusion size (Figure 2-20). Although both effects are opposite the overall inclusion removal by bubbling is increased for larger particle sizes, as the effect shown in Figure 5-12 to 2 and 5 µm inclusion diameters, where the number of particles remaining in the steel are drawn (considering a cumulative number of inclusion removed).

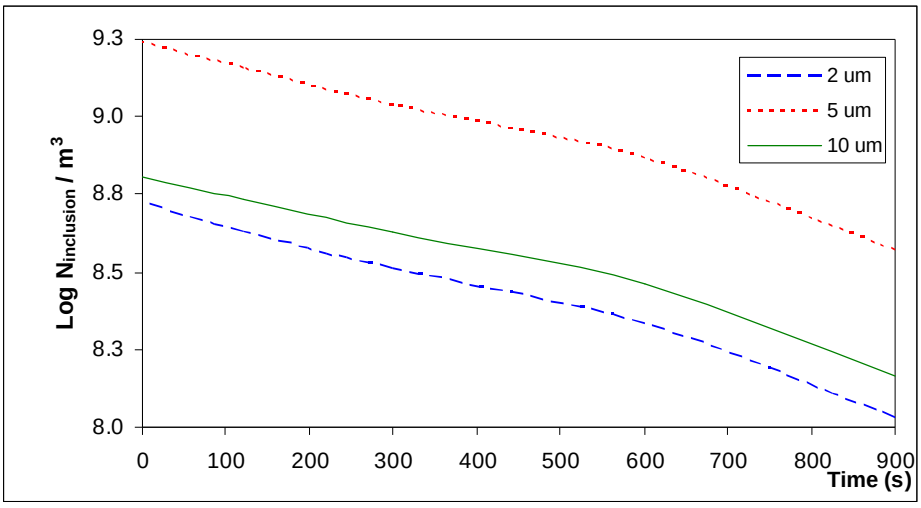

Figure 5-12. Impact of inclusion size on the number of particles remaining after bubbling removal mechanism.

Inclusion removal by bubbling for 10 µm particle diameter in Figure 5-12 shows similar results as in Figure 5-11, this is because it is function of the inclusion initial number (Equation 3.22). The difference between the positions of the curve of 10 µm inclusion with respect to the other inclusion sizes in both figures can be explained by Table 5-2, where the inclusions removal by bubbling and slag were calculated with the same conditions of Figure 5-8 over 10 seconds of processing without considering the initial inclusion number.

Table 5-2. Effect of inclusion size on the bubbling and slag removal mechanism without consideration of the initial inclusion number for each particle size.

Inclusion Diameter	**Number of inclusions removed by Slag/m^3 over 10 seconds**	**Number of inclusions removed by Bubbling/m^3 over 10 seconds**
2 µm	$20.23 * 10^6$	$62.88 * 10^4$
5 µm	$216.13 * 10^6$	$292.03 * 10^4$
10 µm	$598.10 * 10^6$	$747.43 * 10^4$

Removal of the largest inclusions compared to particles of 5 µm diameter has a similar relationship for both mechanisms (2.8 times by slag compared with 2.6 times by the bubbling mechanism). A large difference is shown in Table 5-2 between the removal of 10 µm inclusions compared to that of 2 µm particles. The larger inclusions are removed by slag 29.6 times faster than the smaller ones and this relationship is 11.9 for removal by bubbling.

5.6 Results of Model for Different Process Conditions

One of the most important variables in the secondary metallurgy process is the gas bubbling flow rate; because stirring is necessary to homogenize the steel chemically and thermally, to dissolve the ferroalloys and to desulphurize; but it impacts inclusion removal and generation as was presented in Sections 5.3 and 5.4.

Three different stirring levels were run in the model to study the impact of this variable on steel cleanliness: optimal stirring (with initial strong stirring (800 l/min) followed by soft stirring to promote inclusion flotation (200 l/min)), low stirring which is insufficient to float up inclusions (100 l/min during the whole process) and over stirring (strong stirring during the process, 1200 l/min). The final inclusion number is plotted in Figure 5-13; the other conditions used are: 0.03% Al and 0.3% Mn, 1.5% FeO, 0.5% Mn, 57% CaO, 8% MgO, 30% Al_2O_3 and 3% SiO_2.

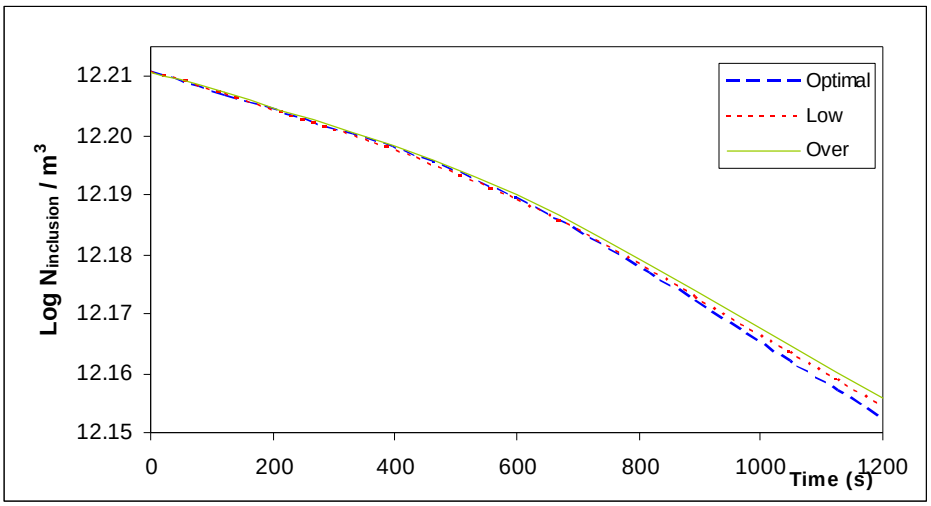

Figure 5-13. Impact of stirring level during process on the total inclusion number.

The model was run in four steps: 1, 120, 600 and 1200 seconds. Starting from 600 seconds there are differences among the stirring levels. Over stirring is always poorer to remove inclusions than the others, because of the reoxidation is high. Low stirring has a smaller final inclusion number in step of 600 seconds, but the final value is higher this is because stirring to flotation is insufficient with respect to the optimal bubbling.

The optimal stirring process should present a better inclusion removal rate than the value shown in Figure 5-13, because the strong stirring is produced at the beginning to coalesce inclusions and to form bigger ones which float up easier than smaller particles (Miki, Thomas, Denissov & Shimada 1997 and Zhang & Thomas 2003, developed in section 2.8.2). But the model does not consider inclusion growth and for this reason the beneficial effect is lower than expected.

An interesting point is the effect of stirring level on small and large inclusions. Most of the total inclusion number is formed by the 2 µm inclusions; Figure 5-14 plotted the stirring impact over the smallest particles.

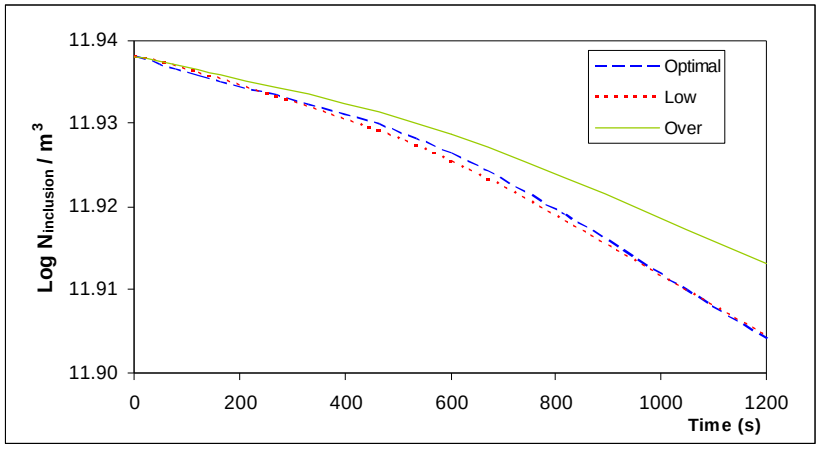

Figure 5-14. Impact of stirring level during process on the inclusion number of diameter 2 µm.

The smallest inclusions are more easily removed by soft stirring than by stronger stirring. As was explained in Section 5.2, reoxidation affects small inclusions more than large ones and small particles are removed less by bubbling and slag than large particles (Section 5.4).

Removal of inclusion of 10 µm is studied in Figure 5-15, where for this inclusion size the removal is directly proportional to the gas flow rate. Because the reoxidation has a low impact on large inclusions, and particles removal by bubbling and slag both of which increase with stronger stirring.

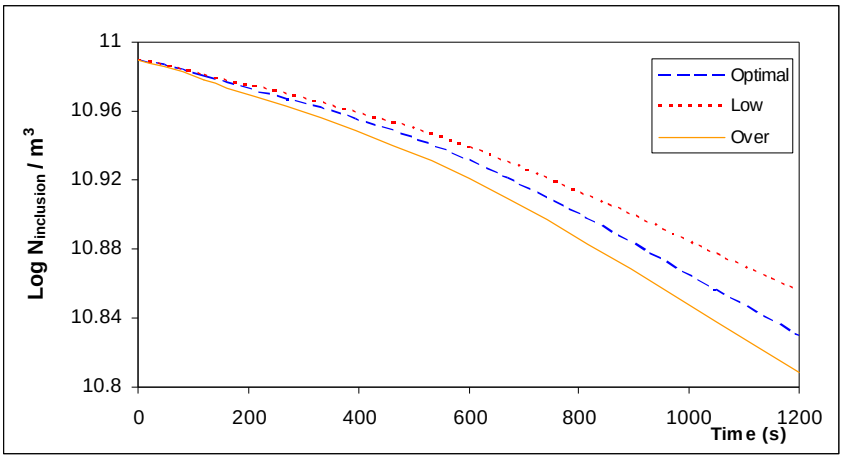

Figure 5-15. Impact of stirring level during process on the inclusion number of diameter 10 µm.

Using Figures 5-13 to 5-15 it can be concluded that if the optimal stirring is not possible, it is preferable an over stirring than understir, because the strong stirring easily removes the largest inclusions which can produce defects (Section 2.3).

The current model cannot explain an important impact of the strong stirring over the steel cleanliness, the slag entrapment. Strong stirring produces a steel- slag emulsion and slag can be entrapped producing macroinclusions (exogenous inclusions), but this effect has not been modelled yet.

Another factor that is important in the secondary metallurgy process is the initial oxidation level before aluminum deoxidation. This model was run for two different situations: high initial oxidation (1200 ppm O) and low oxidation (500 ppm O), the other variables used were: 0.03% Al and 0.3% Mn, 1.5% FeO, 0.5% Mn, 57% CaO, 8% MgO, 30% Al_2O_3 and 3% SiO_4 and 400 l/min of gas flow rate. The results are summarized in Figure 5-16.

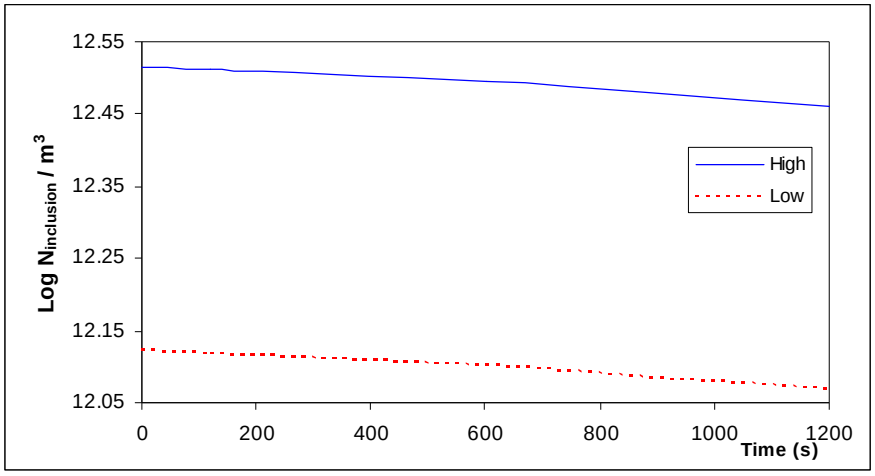

Figure 5-16. Impact of the initial oxidation level over the total final inclusion number.

Figure 5-16 shows that the steel cleanliness achieved depends directly of the initial oxygen level (when the steel is killed only with aluminum). As the quantity of inclusions depends of the initial oxygen is not necessary to see the effect of this factor on the different inclusion sizes.

From this figure it can be concluded that to obtain the same quantity of inclusions at the end of treatment flotation time must increase when the initial oxygen level is higher. Another option to achieve low inclusion content with high initial oxidation is

making a predeoxidation with carbon and then continues with aluminum; this is a very common practice used by steelmakers.

Chapter 6

CONCLUSIONS

6.1 Summary and Conclusions

The thesis presents a mathematical model for the ladle metallurgy furnace that may be used by process engineers to analyze the impact of bubbling, slag and initial oxidation level on inclusion distribution control (quantity and size of them). The sampling practice employed in Ternium Siderar for this study, allowed obtaining samples of aluminum killed steel with different level of the main variables analyzed.

The primary findings of this investigation are the following:

1. The number of inclusion remaining after the process according the initial inclusion number and removal mechanism is calculated according to Equation 3.42 and the total oxygen content by Equation 3.43.

2. The initial inclusion size distribution considers three different groups whose initial number is determined according to the samples analyzed. They are: inclusions with diameter below 2 microns (54% of total), below 5 (38%) and 10 microns (8%).

3. Immediately after aluminum is added deoxidation is produced, it generates an initial number of inclusions that decreases during the process and it may increase only by reoxidation. The increment by reoxidation depends of slag oxidation and the exposed area to atmosphere (“eye”, which is a function of gas flow rate). When oxidation level is

greater at the beginning of process more inclusions are formed and more time of bubbling is necessary to achieve a good cleanliness level.

4. Refractory area provides a site for inclusion removal; it is function of refractory surface and of the gas flow rate. With similar stirring power, tall and narrow ladles are better to remove inclusions than short and wide ones. This mechanism has less impact than removal by bubbling and slag.

5. Removal by bubbling mechanism is directly proportional to gas flow rate, and function of the relationship between inclusion size and bubble collision and adhesion probabilities. The probability of an inclusion to be attached to a bubble is independent of the gas flow rate but it is affected by inclusion size.

6. Inclusion removal by slag is the most important mechanism to remove inclusions according this model; its effect is similar to the bubbling one because it depends of inclusion velocity in z direction and the slag area (function of gas flow rate). This is not the fundamental mechanism; it is the result of the flotation of inclusions. A major simplification was considered; all inclusions which arrive at the slag are caught by it, it implies that inclusions dissolve in the slag instantaneously without depending of the slag composition (effect important according to Sridhar & Cramb and Valdez & Cramb). For slags that are far from Al_2O_3 saturated this simplification is good, but it is not appropriated when the slag viscosity is high or it is saturated with MgO. According to the model the slag composition only impacts on the reoxidation mechanism.

7. The driving force for reoxidation is the difference in the oxygen potential between the phases. Reoxidation reactions are controlled by transport on the metal side; so reoxidation by slag cannot be isolated from gas stirring. It increases with the gas flow rate basically because enlarges the eye area (Krishnapisharody & Irons) and the oxygen

mass transfer coefficient. The model presents a limitation with respect to the effect of the slag oxidation on the steel cleanliness; it calculates lower inclusion content at the end of treatment in a steel with an initial poor deoxidation (in equilibrium with high slag oxidation) which in other one with strong deoxidation. It would appear to be a better situation, it is not possible in the practice where low oxygen content is necessary to cast the steel and for refining processes such as desulphurization. The model considers all the particles produced by reoxidation are only one size, because it is not possible to validate the inclusion size distribution produced only by this mechanism.

8. Softer stirring is better for removal inclusion by slag than stronger one, because according this model the most important variable for this mechanism is the contact area for slag- steel. Slag area is calculated as the difference between the ladle area and the eye area. By slag removal mechanism particles float up by velocity in z direction where the inclusion diameter is important. The current model cannot explain the slag entrapment (exogenous inclusions); a steel- slag emulsion can be produced where slag is entrapped by strong stirring.

9. The number of inclusions removed by bubbling increases when the bubble diameter is smaller. Bubbles smaller than 30 mm diameter remove four times as many inclusions as one of 30 mm; they have a high probability of collision with inclusion and may remove more inclusions although their velocity is lower than larger ones (Wang, Lee and Hayes theory). The production of bubbles with diameter smaller than 30 mm is not possible with current gas injection technology for metal stirring (Irons and Guthrie, 1981). Considering removal by bubbling for bubbles with diameter between 30 to 50 mm the difference is slight; but this effect is balanced by reoxidation and removal by slag balance to achieve a quite similar inclusion numbers.

10. Larger inclusions are removed by slag easier than smaller ones, due to their higher flotation velocity. Similar behavior regulates the bubbling removal mechanism, the collision probability is proportional to inclusion diameter while adhesion probability increases with a decrease in the inclusion size, and although both effects are opposite the overall inclusion removal by bubbling is increased for larger particle sizes.

11. Stirring is fundamental in the secondary metallurgy process. Over stirring produces a poor inclusion removal because the reoxidation is high. Low stirring does not produce reoxidation, but the final particle value is high due to insufficient stirring for flotation. The optimal stirring process (strong stirring at the beginning to coalesce inclusions and to form bigger ones; Miki, Thomas, Denissov & Shimada and Zhang & Thomas) should present a better inclusion removal than value found by the model, because it does not consider inclusion growth and for this reason the beneficial effect is lower than expected.

12. An interesting point is the effect of stirring level on small and large inclusions. The smallest inclusions are more easily removed by soft stirring than by a stronger one. Reoxidation produces more small inclusions than larger ones (considering a fixed oxygen increment) and small particles are removed less by bubbling and slag than large particles. Removal of large inclusions is directly proportional to the gas flow rate; reoxidation has a low impact on large inclusions, and particles removal by bubbling and slag increase with stronger stirring. It can be concluded that if the optimal stirring is not possible, it is preferable an over stirring than understir, because the strong stirring easily removes the largest inclusions which can produce defects.

13. The inclusions found are pure alumina (product of deoxidation) and with oxides from slag (CaO and MgO). The data analyzed shows that the quantity of pure Al_2O_3 inclusions increases during the process; this is the opposite observation to Graham (Graham

2008). The inclusions Al_2O_3-MgO or Al_2O_3- CaO in general are larger than pure Al_2O_3 inclusions, for this reason they can float up easier than smaller ones.

6.2 Future Work

This project gives tools to model the effect the some of most important variables to affect the inclusion control in ladle metallurgy furnace. Points identified requiring further researching are:

1. The effect of slag composition in the inclusion removal by slag with low basicity (high viscosity) or MgO saturated.

The current assumption that the inclusions are dissolved instantly, if the chemical and physical properties of slag (viscosity and the driving forces) do not allow kinetics of dissolution enoughly fast, inclusions remain near the interface and increases the risk of reentrainment.

2. Inclusion growing by stirring.

Gas bubbling is effective to remove inclusions because bubbles collide with the inclusions and float up them faster than an inclusion alone, it is an important variable used in inclusion control.

3. Removal mechanism by inclusion modified by calcium treatment.

Calcium treatment modified the inclusion morphology and the effect of the mechanisms studied respect to the alumina inclusion. It is a process used in many steelshops.

BIBLIOGRAPHY

Ahlborg K., Bieniosek T. and Tucci J. (1993). Slag Making Practices at the LTV Steel Cleaveland Works. 76th Steelmaking Conference Proc., ISS, Warrendale, 469-473.

Anagbo P.E. and Brimacombe J. K. (1990). Plume Characteristics and Liquid Circulation in Gas Injection through a Porous Plug. Metallurgical Transactions B, vol 21B, pp 637-48.

Aoki J., Zhang L. and Thomas B. (2005). Modelling of Inclusion Removal in Ladle Refining. 3rd International Congress on the Science and Technology of Steelmaking ICS Proceedins, AISTech, 319- 332.

Bannenberg N.. (1995). Interactions between the Refractory Material and the Steel and its Effect on the Clean Steel Production. Stahl und Eisen, 115, 2, 75- 82.

Bonilla C. (1995). Slivers in Continous Casting, 78th Steelmaking Conference Proceedings, Vol 78, ISS, Warredake, 41- 45.

Brandaleze E., Martin A., Donayo R., Pérez J. and Gómez A. (2007). Study of the evolution of microinclusions during ladle furnace refining at Siderar in order to review the downloading criteria. 7th International Conference on Clean Steel.

Braun T.B., Elliot J.F. & Flemings M.C. (1979). The Clustering of Alumina Inclusions. Met. Trans. B, 10B, 171- 184.

Bristow D., Carter R., Frakes H., Lewis D., Mang J. and Sattelberger S. (2000). Ferroalloys and Alloying Additives Handbook: 2nd Edition. New York: Shieldalloy Metallurgical Corporation.

Clift R., Grace J.R. and Weber M.E. (1978). Bubbles, drops and particles. Academic Press, 27, 112, 130, 172.

Cramb A. and Jimbo I. (1989). Calculation of the Interfacial Properties of Liquid Steel-Slag System. ISIJ Int., 16, 157-165.

Davis R.M. and Taylor G. (1950). The Mechanics of Large Bubbles Rising through Liquids in Tubes. Proc. Royal Society, Series A, 200, N° A1062, 375- 390.

Dekkers R. (2002). *Chapter 4.* Ph D Thesis, 25- 41.

Dekkers R. (2002). Chapter 10, Ph D Thesis, 133- 151.

Elliot J. and Gleiser M. (1960). Thermochemistry for Steelmaking (Vol. 1). Reading Mass.: Addison- Wesley Pub. Co.

Engh T.A. and Lindskog N. (1975). A Fluid Mechanical Model of Inclusion Removal. Scandinavian Journal of Metallurgy, 4, 49-54.

Espinosa C. (2005). Chapter 4, Mechanical Engineer Thesis, UBA. 24- 31.

Ghosh A. (2001) Secondary Steelmaking: Principles and Applications. Chapter 4, 79-102.

Graham K. (2008). Chapter 4, Ph D Thesis, 105- 124.

Graham K. (2008). Chapter 5, Ph D Thesis, 207- 251.

Guo D. and Irons G.A. (2002). A Water Model and Numerical Study of the Spout Height in a Gas Stirred Vessel. Metallurgical Transaction B, 33B, 377- 384.

Hallberg M., Jönsson P.G., Jonsson T.L. and Eriksson R. (2005). Process Model of Inclusion Separation in a Stirred Steel Ladle. Scandinaviasn Journal of Metallurgy, 34, 41- 56.

Heindel T. and Bloom F. (1999). Exact and Approximate Expressions for Bubble/ Particle Collision. Submitted to Journal of Colloid and Interface Science, 1- 40.

Hoefele E. O. and Brimacombe J.K. (1979). Flow Regimes in Submerged Gas Injection. Metallurgical Transaction B, 10B, 631- 648.

Irons G.A. and Guthrie R.I.L. (1981). Bubbling behavior in Molten Metals. Canadian Metallurgical Quarterly, Vol 19, N° 4, 381- 387.

Krishnapisharody K. and Irons G. (2007). A Study of Spout on Bath Surfaces from Gas Bubbling: Part I. Experimental Investigation. Metallurgical and Materials Transaction 38B, 367-375.

Kor G.J.W. and Glaws P.C. (1998). Chapter 11: Steelmaking and Refining Volume, The AISE Steel Foundation, 694-713.

Lange K.W. (1988). Thermodynamic and Kinetic Aspects of Secondary Steelmaking Process. *International Materials Review*. Vol 33, 53- 89.

Levich V.G. (1962). Physicochemical hydrodynamics. Englewood Cliffs, 395- 470.

Lu D. (1992). Kinetics Mechanisms and Modeling of Calcium Treatment of Steel. PhD Thesis.

Miki Y., Thomas G., Denissov A. and Shimada Y. (1997). Model of Inclusion Removal during RH Degassing of the Steel. Iron Steelmaker, 24, N°8, 31.

Nakashima K. and Okamura K. (1992). Behavior of Fines in the Blast Furnace. Proc. 4th Conf. Molten Slags and Fluxes, ISIJ, 505- 510.

Oeters F. (1994). Metallurgy of Steelmaking. VSHD, Berlín, 225- 240.

Oertel L.C., Costa E and Silva A. (1999). Application of Thermodynamic Modelling to Slag-Metal Equilibria in Steelmaking. Calphad, v 23, n 3-4, 379- 391.

Ohta H. and Suito H. (1998). Activities of SiO_2 and Al_2O_3 and Activity Coefficients of Fe_tO and MnO in CaO-SiO_2-Al_2O_3-MgO Slags. Metallurgical Materials Transaction B, Vol. 29 B, 119- 129.

Osborne-Lee I.W. (1988). Particles on Surface I. K. L. Mittal Plenum Press, New York and London, 77.

Pan W., Uemura K-I and Koyama S. (1992). Cold Model Experiment on Entrapment of Inclusions in Steel by Inert Gas. Tetsu-to-Hagane, Vol 78, N 8, 87

Peebles F.N. and Garber H.J. (1953). The Motion of Gas Bubbles in Liquids. Chemical Rng. Prog, 49, 88.

Robinson S.W., Martin I.W. & Pickering F.B. (1979). Formation of Alumina in Steel and its Dissemination during Mechanical Working. Met Techn, 157- 169.

Sahajwalla V., Castillejos A.H. and Brimacombe J.K. (1990). The Spout of Air Jets Upwardly Injected into a Water Bath. Metallurgical Transaction B, 21B, 71- 80.

Sano M. and Mori K. (1976). Bubble Formation from Single Nozzles in Liquid Metals. Trans. Japan Institute of Metals 17, 344- 352.

Schulze H.J. (1989). Hydrodynamics of Bubble-Mineral Particle Collisions. Mineral Process and Extractive Metallurgy Rev 5, 43-76.

Schulze H.J. (1992). Probability of Particle Attachment on Gas Bubbles by Sliding. Advances Colloid Interface Science. Vol 40, 283.

Schulze H.J. and Birzer J.O. (1987). Stability on Thin Liquid Film on Langmuir-Blodgett Layers on Silica Surfaces. Colloids Surface, 24, 209- 224.

Söder M. (2004). PhD Thesis, Growth and Removal of Inclusions during Ladle Refining.

Sridhar S., Cramb A.W., Lee S.H., Tse C., Yi K.W., Chevrier V. and Orrling C. (2001). Separation and Dissolution of Al_2O_3 Inclusions at Slag/ Metal Interfaces. Journal of Non-Cristalline Solids, 282, 41- 48.

Taira S., Nakashima K. and Mori K. (1993). Kinetic Behavior of Dissolution of Sintered Alumina into CaO-SiO_2-Al_2O_3 Slags. ISIJ Int. 33(1) , 116-123.

Taniguchi S., Kikuchi A., Ise T. and Shoji N. (1996). Model Experiment on the Coagulation of Inclusion Particles in Liquid Steel. ISIJ International, 36, S117.

Turkdogan E. T. (1996), Fundamentals of Steelmaking. The Institute of Materials (London, England), Chapter 9.

Turkdogan E. T. (2001), Retrospect on Technology Innovations in Ferrous Pyrometallurgy. Canadian Metallurgical Quarterly, Vol. 40, N° 3, 255- 308.

Valdez M., Prapakorn K., Cramb A.W. and Sridhar S. (2002). Dissolution of Alumina Particles in CaO- Al_2O_3- SiO_2- MgO Slags. Iron and Steelmaking, Vol 29, 47- 52.

Van der Eijk C., Grong O. and Walmsley J. (2000). Effect of Deoxidation Practice on the Inclusion Formation in Low Alloy Structural Steels. *6^{Th} International Conference on Molten Slags, Fluxes and Salts*.

Wang L., Lee H-G and Hayer P. (1996). Prediction of the Optimum Bubble Size for Inclusion Removal from Molten Steel by Flotation. ISIJ Int., 36, N° 1, 7- 16.

Weber M. E. and Paddock D. (1983). Interceptional and Gravitational Collision Efficiencies for Single Collectors at Intermediate Reynolds Number. Journal Colloid Interface Science, 94, N° 2, 328.

Wijk O. (1995). Inclusion Engineering. Scaninject VII. 7th International Conference on Refining Process. Part I, 35-67.

Wilson W. and McLean A. (1980): Desulphurization of Iron and Steel and Sulphide Shape Control. Warrendale, PA: Iron and Steel Society of AIME.

Winkler W., Angeli J. and Mayr M. (2006). Automated SEM-EDX Cleanness Analysis and its Application in Metallurgy. 7th International Worshop Progress in Analytical Chemistry in the Steel and Metal Industries. Luxemburg. 16- 18.

Yonezawa K. and Schwerdtfeger K. (2000). Dynamics of the Spout of the Gas Plumes Descharging from a Melt: Experimental Investigation with a Large-Scale Water Models. Metallurgical Transaction B, 31B, 461- 468.

Yoon R.H. and Luttrell G.H. (1989). The Effect of Bubble Size on Fine Particle Flotation. Mineral Process and Extractive Metallurgy Rev 5, 101-122.

Yoon R.H. and Luttrell G.H. (1992). A Hydrodynamic Model for Bubble-Particle Attachment. Journal Colloid Interface Science, 154, 129-137.

Zhang L. and Cai K. (2001). Experimental and Theoretical Study on the Cleanliness of Steel. 84Th Steelmaking Conference Proceedings. ISS/AIME, Vol 84, 275-291.

Zhang L. and Taniguchi S. (2000). Fundamentals of Inclusion Removal from Liquid Steel by Bubble Flotation. International Materials Reviews, Vol 45, N° 2, 59- 82.

Zhang L., Pluschkell W. and Thomas B. (2002). Nucleation and Growth of Alumina Inclusion during Deoxidation. 85th Steelmaking Conference (Nashville), Vol 85, 463- 476.

Zhang L. and Thomas B.G. (2002). Alumina Inclusion Behaviour During Steel Deoxidation. 7th European Electric Steelmaking Conf., Vol. II, Associazione Italiana di Metallurgia, 2.77.

Zhang L. and Thomas B. (2003). State of the Art in Evaluation and Control of Steel Cleanliness. *ISIJ*, Vol 43, 3, 271- 291.

Zhang L. and Thomas B. (2003). Inclusions in Continuous Casting of Steel. XXIV National Steelmaking Symposium Mexico, 138- 183.

Zhang L., Taniguchi S. and Matsumoto K. (2002). Water Model Study on Inclusion Removal from Liquid Steel by Bubble Flotation under Turbulent Conditions. Iron and Steelmaking, Vol 29, N° 5, 326- 336.

APPENDIX

Appendix A: Model

% Define Variables:

% n -- Number of input samples

% a -- Collision efficiency

% A_{13b} -- Hamaker constant of inclusion- liq steel-bubble system

% a_{FeO} -- FeO activity coefficient in the slag

% alfa -- Semiangle of contact between inclusion and bubble

% A_{eye} -- Eye area without slag (m^2)

% Al -- Aluminium content in the steel (%)

% Al_O -- Alumina content in slag (%)

% A_{Ladle} -- Ladle are (m^2)

% A_{Slag} -- Slag area (m^2)

% A_{Wall} -- Refractory area (m^2)

% B -- Constant (Miyashita equation)

% Ca -- CaO content in slag (%)

% d_B -- Diameter of the bubble (m)

% d_{Fe} -- Steel density (Kg/ m^3)

% d_g -- Gas density (Kg/ m^3)

% d_i -- Diameter of the inclusion (m)

% dp -- Particle density, Al_2O_3 is consider (Kg/ m^3)

% D_O -- Diffusion coeficient of oxygen in steel (m^2/ s)

% E -- Turbulent energy dissipation (m^2/ s^3)

% Fe -- FeO content in slag (%)

% G -- Dimensionless constant

% g -- Gravity acceleration (m/ s^2)

% H -- Height of ladle (steel height) (m)

% i -- Number of molecules in each particle

% h_{cr} -- Critical film thickness (m)

% k_{oi} -- Mass transfer coefficient (depends of stirring intensity for slag)

% k_{oi1} -- Mass transfer coefficient (depends of stirring intensity for eye)

% K_{FeO} -- FeO equilibrum constant

% K_{MnO} -- MnO equilibrum constant

% m -- Total number of molecules function of total oxygen ($1/m^3$)

% Mg -- MgO content in slag (%)

% Mn -- MnO content in slag (%)

% Mn_s -- Manganese content in the steel (%)

% Mo -- Molar Weigh of Oxygen (Kg)

% M_p -- Molar Weigh of particle, Al_2O_3 is considered (Kg)

% M_{Ca} -- Molar CaO weigth

% M_{Fe} -- Molar FeO weigth

% M_{Mg} -- Molar MgO weigth

% M_{Mn} -- Molar MnO weigth

% M_{Si} -- Molar SiO_2 weigth

% n_O -- Effect oxygen in molar ratio

% n_P -- Effect particle in molar ratio

% Na -- Avogadro's Number (1/ mol)

% N_0 -- Initial number of total inclusions ($1/m^3$)

% N_{rb} -- Total number of "effective adhesions" bubble- inclusion ($1/ m^3$)

% N_{ref} -- Number of iclusion of Ri removal to refractory ($1/ m^3$)

% N_{Slag} -- Number of particles removal to slag

% N_{Ri} -- Number of particles of Ri

% N_{reo} -- Number of particles produced by reoxidation ($1/ m^3$)

% N_{fi} -- Number of total inclusions at the end of treatment ($1/ m^3$)

% O_{atm} -- Oxygen in atmosphere for reoxidation (%)

% O_{dis} -- Total Oxygen for reoxidation, it's dissolve oxygen (%)

% O_{ini} -- Total oxygen befor tapping (ppm)

% O_{int} -- Oxygen in equilibrium with FeO and MnO of slag (%)

% Oeq -- Oxygen in equilibrium with aluminum content (%)

% Otot -- Total oxygen (ppm)
% Pa -- Adhesion probability
% Pc -- Collision posibility
% P -- Atmospheric pressure (bar)
% Q -- Flow caudal per Tn of steel(Nm^3/ s * Tn steel)
% R -- Ideal gas constant (J/ mol K)
% Re -- Reynolds number
% Ri -- Radius of particle (m)
% rl_{adlle} -- Ladle radius (m)
% r_m -- Radius of molecule (m)
% text1 -- Temperature (K)
% text1 -- Time input data (s)
% t_f -- Film drainage and rupture time (s)
% T_0 -- Temperature of the gas before pluges (K)
% totalm -- Total moles of oxides in the slag
% Si -- Silica content in slag (%)
% St -- Surface tension (N/m)
% sum_text1 -- Total time (s)
% u_{Fe} -- Steel viscosity (Kg/ m.s)
% u_g -- Gas viscosity (Kg/ m.s)
% V -- Volume of the steel (m^3)
% v_b -- Velocity of the bubble (m/ s)
% v_{Fe} -- Kinematic viscosity (m^2/ s)
% v_{Stoke} -- Velocity for Stoke's law (m/ s)
% vz -- Velocity for stirring in z direction (m/ s)
% V_{Ri} -- Volume of particles with Ri (m^3)
% W_{steel} -- Weight of steel (Kg)
% x -- Diameter relationship
% X_{FeO} -- FeO molar fraction

% Initialize d_{Fe},d_p,g,R_i,u_{Fe} and v_z
a = 0.3; % Collision efficiency

A_{13b} = 2.3*10^-20; % Hamaker constant to Al_2O_3

B = 0.63; % Constant (Miyashita equation)

d_{Fe} = 6900; % Steel density

d_g = 0.332; % Gas density

d_p = 3960; % Particle density, consider Al_2O_3

Do = 3*10^-9; % Diffusion coefficient of oxygen in steel

g = 9.81; % Gravity acceleration

G = 4; % Dimensionless constant

kemp = 0.35; % Empirical constant to correct removal to slag

M_O = 32; % Molar oxygen weigth

M_P = 102; % Molar particle weigth

M_{Ca} = 56.1; % Molar CaO weigth

M_{Fe} = 71.9; % Molar FeO weigth

M_{Mg} = 40.3; % Molar MgO weigth

M_{Mn} = 70.9; % Molar MnO weigth

M_{Si} = 60.1; % Molar SiO_2 weigth

n_P = 1; % Molar ratio particle- oxygen

n_O = 3; % Molar ratio particle- oxygen

Na = 6.022*10^23; % Number of atoms per mol

N_0 = 10000; % Initial number of inclusions

P = 1.013; % Atmospehric pressure (bar)

R = 8.314; % Ideal gas constant (J/ mol K)

rm = 2.719*10^-10; % Radius of molecule (m)

St = 1.4; % Surface tension (N/m)

u_{Fe} = 0.007; % Steel viscosity

u_g = 0.0000225; % Gas viscosity

v_{Fe} = 0.000001; % Kinematic viscosity (m^2/ s)

% Read in the first value (only in the beginning)

r_{ladle} = 1.82;

H = 3.5;

W_{steel} = 193000;

T_0 = 298;

A_{ladle} = pi * rladle^2;

Oatm = 20.9;

set(handles.textnum,'string',num2str(handles.cont))

T = str2num(get(handles.edit1,'string'));

Q= str2num(get(handles.edit2,'string'));

Q = Q /(60*Wsteel);

O_{ini} = str2num(get(handles.edit3,'string'))/10000;

Al = str2num(get(handles.edit4,'string'));

Mn_s = str2num(get(handles.edit5,'string'));

Fe = str2num(get(handles.edit6,'string'));

Mn = str2num(get(handles.edit7,'string'));

Ca = str2num(get(handles.edit8,'string'));

Mg = str2num(get(handles.edit9,'string'));

Si = str2num(get(handles.edit11,'string'));

Alo = str2num(get(handles.edit10,'string'));

% General calculations

V = W_{steel}/ d_{Fe};

h_{cr} = 3.79*10^-8 * A_{13b}^0.16;

E = 2 * Q * P * logm(1 + d_{Fe} * g * H/P)/ (pi * r_{ladle} * H * d_{Fe});

% Calculate %O in the steel in equilibrium with Al content in it

O_{eq} = [10(-62680/T+31.85]/[Al*(10)-3.9Al];

% Calculate %O in the slag for FeO

K_{FeO} = exp((-116100+48.4*T)/(R*T));

a_{FeO} = 10^((0.676*Mg + 0.267*Alo - 19.07)/ Si + 0.0214*Ca - 0.047);
totalm = (Fe/M_{Fe}) + (Mn/M_{Mn}) + (Al_0/M_p) +(Si/M_{Si}) + (Ca/M_{Ca}) + (Mg/M_{Mg});
X_{FeO} = Fe/M_{Fe} / totalm;
O_{int} = K_{FeO} * X_{FeO} * a_{FeO};
m = (Oini - Oeq) * Wsteel * Na/ (V*16*3);

% Calculate Slag area
A_{eye} = 0.414 * (193 * Q/2)^-0.22 * H^3.78 *[(1 + 11.6 * (193*Q/2)^0.74 * H^-2.46)^1.5 - 1]*2;
A_{Slag} = A_{Ladle} - A_{eye};
A_{wall} = pi * 2 * r_{ladle} * H;

% Calculate k_{oi} with Higbie's surface theory (A. Ghosh book):
k_{oi} = 20 * (D_0 * Q/ (pi * r_{ladle} *A_{slag}))^0.33;
k_{oi1} = 20 * (D_0 * Q/ (pi * r_{ladle} *A_{eye}))^0.33;

%cGet the total time to run:
t = str2num(get(handles.edit12,'string'));

% BUBBLE MODEL
% General Calculation
d_b = 0.03;
v_b = d_b * [g/ 36 * (d_{Fe}/ u_{Fe})^0.5]^(2/3);
Re = v_b * d_g * d_b/ ug;

% REOXIDATION: Calculate Oxygen produce for Reoxidation (%O_{dis}) at time text1
O_{dis} = [((O_{int} - O_{eq}) * k_{oi} * A_{Slag}) + ((O_{atm} - O_{eq}) * k_{oi1} * A_{eye})]/ W_{steel};
V_{Ri} = (O_{dis} * d_{Fe} * M_p * n_p* 0.000001)/ (d_p * M_0 * n_0);

% Initialize sum:

sum_NRi = 0;

```
sum_t = 0;

% CALCULATION Ri = 10^-6 (1.2 is considered, because with 1 there isn't
enough flotation compare with measured values)

R_i = 0.00000116;
d_i = 2 * R_i;

% Calculate particle velocity (v_z)
v_z = [g * (d_Fe - d_p)/(9 * u_Fe^0.5 * d_Fe^0.5)]^(2/3) * d_i;

% Calculate number of particles of each radius
i = (R_i/r_m)^3;
NR_0 = m/ (5.4 * i);

step=10;
for ii = 1:step:t
   if (ii == 1 && handles.cont==1)
      sum_NRi = NRo;
   else
      sum_NRi = handles.Nfi;
   end

sum_t = step;

% BUBBLE MODEL
% Calculation of some variables from the input datas

k1 = v_Z/ v_B;
k2 = d_i/ d_B;
x = 1 + k2;
```

% Calculation particles removal to bubbles

alfa = [pi * (d_p + 1.5*d_{Fe})*d_i^3/ (24 * St)]^0.5;
t_f = 2100 * u_{Fe} * (32 * (v_Z-v_B) * alfa)^1.2 * (pi/ 180)^2 * Ri^3 / (8 * G * St * h_{cr}^2);
y = -2 * t_F * [(1 - 0.75/x - 0.25/x^3 + Re^0.72/ 15 * (-2/ x^4 + 1/ x^3 + 1/ x)) * v_B – v_Z];
Pa = [sin(2*atan(exp(y/(db+di))))]^2;
Pc = k2^2/ (1-k1) * [1.5 + k2 + 2 * Re^0.72 * (2 + k2)/ (15 * x)]/ x^3;
N_{rb} = 3 * Q * H * sum_N_{Ri} * T * Pc * Pa * 193000/ (2 * d_B * T_0 * V);

% Calculation particles removal to refractory (Zhang model)

N_{ref} = 0.062 * A_{wall} * E^0.75 * Ri^2 * sum_NRi * sum_t/ (V * v_{Fe}^1.25);

% Calculate N of particles removal to slag at time text1

N_{slag} = sum_t * A_{slag} * v_Z * sum_NR_i/ V;

% Calculate N of particles with R_i at the end of treatment

N_{Fi} = sum_NRi - N_{rb} - N_{slag} - N_{ref};

% Calculate Total Oxygen at the end of treatment

O_{tot} = 7.4 * N_{Fi} * i * 16000* V/ (W_{steel} * Na);
% CALCULATION R_1 = 2.5 10^-6

R_1 = 0.0000025;
d_1 = 2 * R_1;

$i_1 = (R_1/rm)^3;$
$NRo_1 = m/ (3.8 * i_1);$

% Calculate particle velocity (v_Z)

$v_{Z1} = [g * (d_{Fe} - d_p)/(9 * u_{Fe}^0.5 * d_{Fe}^0.5)]^(2/3) * d_1;$

```
 if (ii == 1 && handles.cont==1)
    sum_NR1 = NRo1;
 else
    sum_NR1 = handles.Nf1;
 end
```

% BUBBLE MODEL
% Calculation of some variables from the input data

$k3 = v_{Z1}/ v_B;$
$k4 = d_1/ d_B;$
$x_1 = 1 + k4;$

% Calculation particles removal to bubbles

$alfa = [pi * (d_P + 1.5*d_{Fe})*d_1^3/ (24 * St)]^0.5;$
$t_f = 2100 * u_{Fe} * (32 * (v_{Z1} – v_B) * alfa)^1.2 * (pi/ 180)^2 * R_1^3 / (8 * G * St * h_{cr}^2);$
$y_1 = -2 * t_f * [(1 - 0.75/x_1 - 0.25/x_1^3 + Re^0.72/ 15 * (-2/ x_1^4 + 1/ x_1^3 + 1/ x_1)) * v_B - v_{Z1}];$
$Pa_1 = [sin(2*atan(exp(y_1/(d_B+d_1))))]^2;$
$Pc_1 = k4^2/ (1-k3) * [1.5 + k4 + 2 * Re^0.72 * (2 + k4)/ (15 * x_1)]/ x_1^3;$
$N_{rb1} = 3 * Q * H * sum\_NR_1 * T * Pc_1 * Pa_1 * 193000/ (2 * d_B * T_0 * V);$

% Calculation particles removal to refractory (Zhang model)

N_{ref1} = 0.062 * A_{wall} * E^0.75 * R_1^2 * sum_NR_1 * sum_t/ (V * v_{Fe}^1.25);

% Calculate N of particles removal to slag at time $text_1$

N_{Slag1} = sum_t * A_{slag} * v_{Z1} * sum_NR_1/ V;

% Calculate N of particles with Ri at the end of treatment

N_{f1} = sum_NR_1 - N_{rb1} – N_{Slag1} - N_{ref1};

% Calculate Total Oxygen at the end of treatment

O_{tot1} = 1 * N_{f1} * i_1 * 16000* V/ (W_{steel} * Na);

% CALCULATION R_2 = 0.000004

R_2 = 0.000004;
d_2 = 2 * R_2;

% Calculate particle velocity (v_Z)
v_{Z2} = [g * (d_{Fe} - d_p)/(9 * u_{Fe}^0.5 * d_{Fe}^0.5)]^(2/3) * d_2;

% Calculate number of particles of each radius

$i_2 = (R_2/r_m)^3;$
$NR_{02} = m/ (0.8 * i_2);$

```
   if (ii == 1 && handles.cont==1)
      sum_NR2 = NR02;
   else
      sum_NR2 = handles.Nf2;
  end
```

% BUBBLE MODEL
% Calculation of some variables from the input datas

$k5 = v_{Z2}/ v_B;$
$k6 = d_2/ d_B;$
$x_2 = 1 + k6;$

% Calculation particles removal to bubbles

$alfa = [pi * (d_p + 1.5*d_{Fe})*d_2^3/ (24 * St)]^0.5;$
$t_F = 2100 * u_{Fe} * (32 * (v_{Z2} – v_B) * alfa)^1.2 * (pi/ 180)^2 * R_2^3 / (8 * G * St * h_{cr}^2);$
$y_2 = -2 * t_F * [(1 - 0.75/x_2 - 0.25/x_2^3 + Re^0.72/ 15 * (-2/ x_2^4 + 1/ x_2^3 + 1/ x_2)) * v_B - v_{Z2}];$
$Pa_2 = [sin(2*atan(exp(y_2/(d_B+d_2))))]^2;$
$Pc_2 = k6^2/ (1-k5) * [1.5 + k6 + 2 * Re^0.72 * (2 + k6)/ (15 * x_2)]/ x_2^3;$
$N_{rb2} = 3 * Q * H * sum\_NR_2 * T * Pc_2 * Pa_2 * 193000/ (2 * d_B * T_0 * V);$

% Calculation particles removal to refractory (Zhang model)

$N_{ref2} = 0.062 * A_{wall} * E^0.75 * R_2^2 * sum\_NR_2 * sum\_t/ (V * v_{Fe}^1.25);$

% Calculate N of particles removal to slag at time $text_1$

N_{Slag2} = sum_t * A_{Slag} * v_{Z2} * sum_NR_2/ V;

% Calculate N of particles with Ri produced by reoxidation at time text1

N_{reo2} = (3 * VR_i * t)/ (4 * pi * R_2^3);

% Calculate N of particles with R_i at the end of treatment

N_{f2} = sum_NR_2 - N_{rb2} - N_{Slag2} - N_{ref2} + N_{reo2};

% Calculate Total Oxygen at the end of treatment

O_{tot2} = 1.6 * N_{f2} * i_2 * 16000* V/ (W_{steel} * Na);
handles.N_{fi}=N_{fi};
handles.N_{f1}=N_{f1};
handles.N_{f2}=N_{f2};
end

% Tell user

fprintf ('The reoxidation for diameter < 10um is: %f\n', N_{reo2});
fprintf ('The total oxygen at the end of treatment is: %f\n', O_{tot}+Ot_{ot1}+ O_{tot2}+O_{eq}*10000);
fprintf ('The number of particles of diameter < 2um at the end of treatment is: %f\n', N_{fi}/10^10);
fprintf ('The number of particles of diameter < 5 um at the end of treatment is: %f\n', N_{f1}/10^10);

fprintf ('The number of particles of diameter < 10 um at the end of treatment is: %f\n', N_{f2}/10^10);

fprintf ('The number of particles removal to bubble is: %f\n', N_{rb});

fprintf ('The number of particles removal to bubble is: %f\n', N_{rb1});

fprintf ('The number of particles removal to bubble is: %f\n', N_{rb2});

fprintf ('The number of particles removal to slag is: %f\n', N_{Slag});

fprintf ('The number of particles removal to slag is: %f\n', N_{Slag1});

fprintf ('The number of particles removal to slag is: %f\n', N_{Slag2});

fprintf ('The time consider in this experiment is: %f\n\n', t);

Appendix B: Heats Process Parameters

B.1 Heat 880558, Initial Oxygen: 581 ppm

Sample	Time (sec)	Temper (°K)	Flow rate (l/ min)	% Al	% Mn	% FeO	% MnO	% CaO	% MgO	% Al2O3	% SiO2
So	240	1853	800	0.032	0.27	7	4.35	53.1	8.09	28.1	5.80
L10	1800	1824	300	0.013	0.27	7	4.35	53.1	8.09	28.1	5.80
L11	2340	1834	600	0.024	0.29	6.4	4.52	53.6	9.04	28.0	5.41
L12	2700	1825	1100	0.019	0.335	2	1.35	55.2	11.90	29.4	5.59
L13	3480	1862	700	0.028	0.38	2.4	1.56	54.3	10.50	29.2	5.12
T1	4020	1856	400	0.024	0.38	1.9	1.62	54.4	10.40	28.9	5.13

Table B-1. Process Parameters for Heat 880558

B.2 Heat 880595, Initial Oxygen: 674 ppm

Sample	Time (sec)	Temper (°K)	Flow rate (l/ min)	% Al	% Mn	% FeO	% MnO	% CaO	% MgO	% Al2O3	% SiO2
So	720	1844	1000	0.040	0.34	4.4	2.95	54.7	12.3	28.3	5.85
L10	1800	1826	300	0.037	0.35	3.1	2.84	54.4	12.0	28.0	5.58
L11	2280	1821	500	0.041	0.37	3.1	0.97	49.7	13.8	29.8	5.08
L12	3060	1870	600	0.034	0.36	2.8	0.97	49.7	12.9	29.8	5.08
L13	3480	1854	600	0.037	0.36	2.8	0.81	50.8	12.9	30.0	5.30
T1	3720	1850	400	0.037	0.36	1.5	0.66	51.2	12.4	30.0	5.20

Table B-2. Process Parameters for Heat 880595

B.3 Heat 860630, Initial Oxygen: 611 ppm

Sample	Time (sec)	Temper (°K)	Flow rate (l/ min)	% Al	% Mn	% FeO	% MnO	% CaO	% MgO	% Al2O3	% SiO2
So	1200	1854	800	0.021	0.136	6.77	3.02	52.9	8.59	28.8	8.24
L10	2340	1830	300	0.015	0.135	6.69	3.12	51.1	8.30	28.4	8.20
L11	3720	1888	500	0.028	0.163	6.32	3.10	50.6	8.56	28.1	8.02
L12	5520	1861	1300	0.015	0.188	2.16	1.37	51.2	9.95	29.8	7.53
L13	5940	1876	500	0.026	0.195	1.63	0.57	51.9	11.24	29.8	7.41
T1	7200	1866	300	0.024	0.196	1.52	0.49	49.8	11.00	29.5	6.82

Table B-3. Process Parameters for Heat 860630

B.4 Heat 880613, Initial Oxygen: 760 ppm

Sample	Time (sec)	Temper (°K)	Flow rate (l/ min)	% Al	% Mn	% FeO	% MnO	% CaO	% MgO	% Al2O3	% SiO2
So	2400	1834	600	0.000	0.145	4.87	2.27	49.0	9.30	29.7	5.48
L10	3840	1820	200	0.001	0.144	4.94	2.46	48.6	9.46	29.6	5.38
L11	5340	1887	500	0.012	0.170	3.66	1.75	48.2	9.69	30.1	5.08
L12	6060	1873	1000	0.013	0.181	1.98	0.93	49.5	11.46	30.7	4.77
L13	6360	1883	500	0.033	0.183	1.51	0.93	50.8	11.35	31.0	4.65
T1	7200	1867	300	0.026	0.185	1.44	0.43	50.3	11.00	30.8	4.47

Table B-4. Process Parameters for Heat 860613

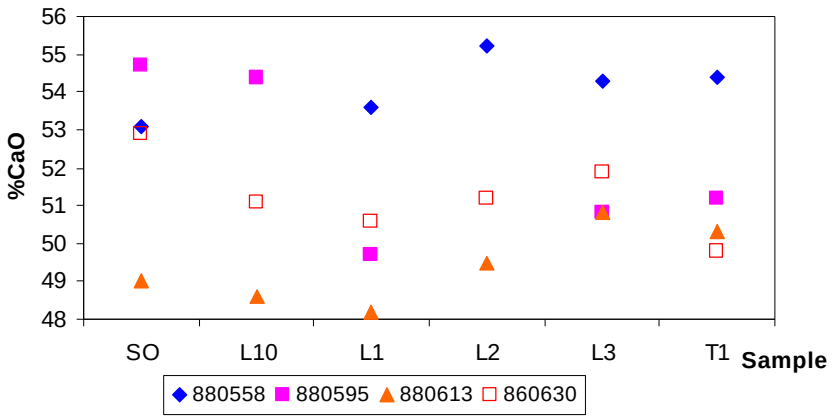

Figure B-1. Calcium oxide evolution during secondary metallurgy

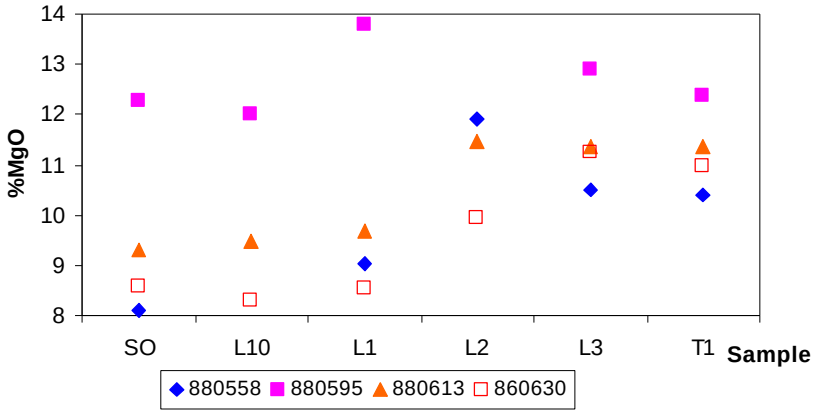

Fig B-2. Magnesium oxide evolution during secondary metallurgy

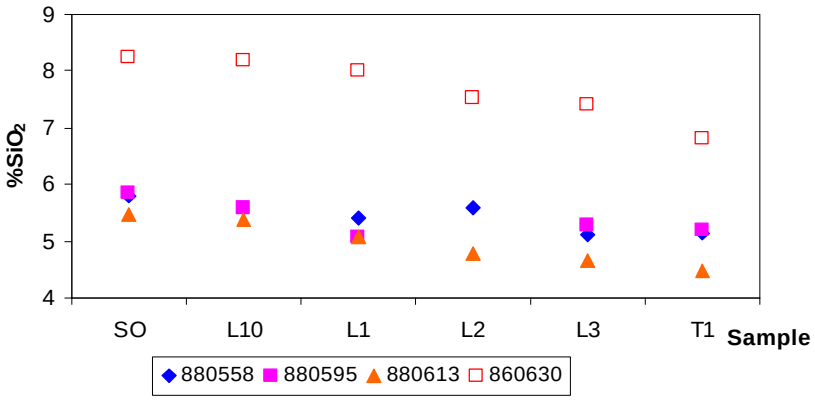

Figure B-3. Silica evolution during secondary metallurgy

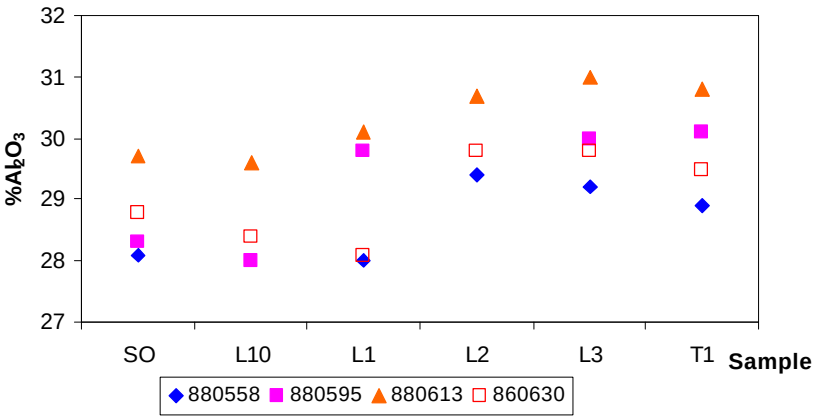

Fig B-4. Alumina evolution during secondary metallurgy

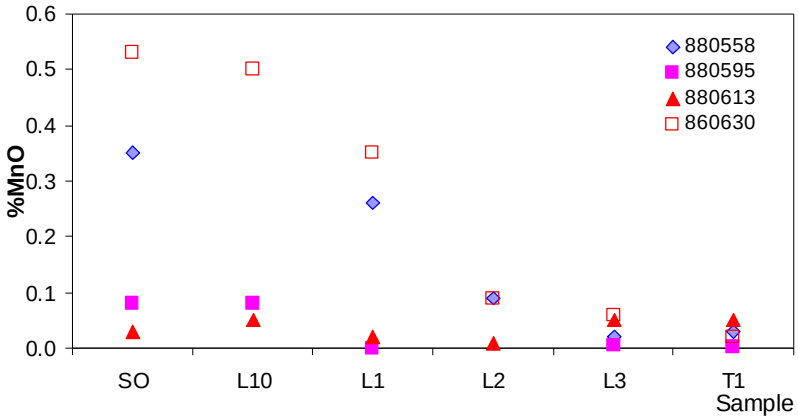

Fig B-5. Manganese oxide evolution during secondary metallurgy

Appendix C: Variation of Inclusion Composition during the Secondary Metallurgy

C.1 Inclusion Composition for Heat 880588

	% Al	%FeO	%MgO	%CaO	%SiO_2
SO	0.046	7.0	8.09	53.1	5.80
L10	0.013				
L1	0.024	6.43	9.04	53.6	5.41
L2	0.019	2.0	11.9	55.2	5.59
L3	0.028	2.38	10.5	54.3	5.12
T1	0.024	1.94	10.4	54.4	5.13

Table C-1 . Steel and slag composition for heat 880588

C.2 Inclusion Composition for Heat 860613

	% Al	%FeO	%MgO	%CaO	%SiO_2
SO	0	4.87	9.30	49.0	5.48
L10	0.001	4.94	9.46	48.6	5.38
L1	0.012	3.66	9.69	48.2	5.08
L2	0.013	1.98	11.46	49.5	4.77
L3	0.033	1.51	11.35	50.8	4.65
T1	0.026	1.44	11.35	50.3	4.47

Table C-2 . Steel and slag composition for heat 860613

C.3 Inclusion Composition for Heat 880595

	% Al	%FeO	%MgO	%CaO	%SiO_2
SO	0.04	4.4	12.3	54.7	5.85
L10	0.037	3.1	12.0	54.4	5.58
L1	0.041	4.3	13.8	49.7	5.08
L2	0.034				
L3	0.037	2.8	12.9	50.8	5.30
T1	0.037	1.52	12.4	51.2	5.20

Table C-3. Steel and slag composition for heat 880595

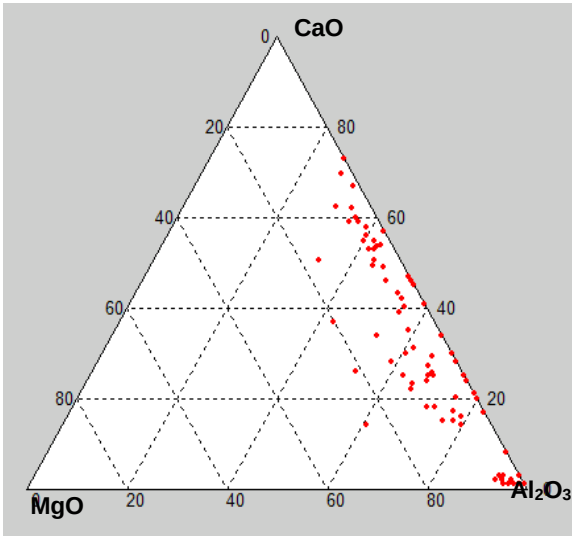

(a)

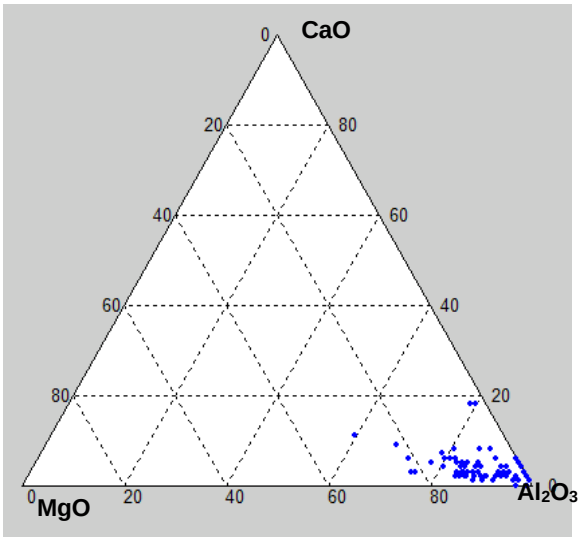

(b)

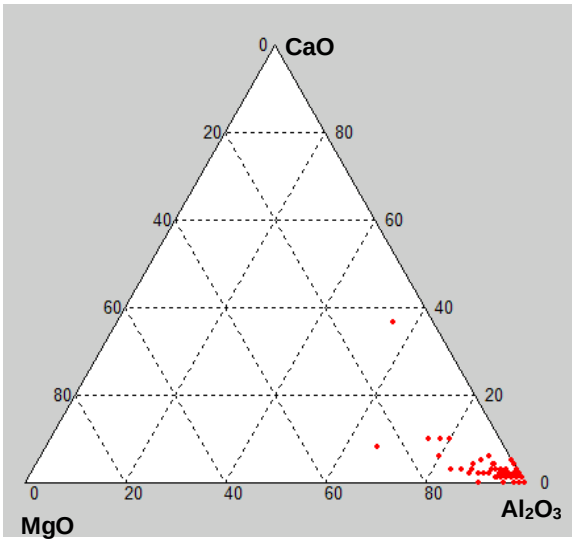

(c)

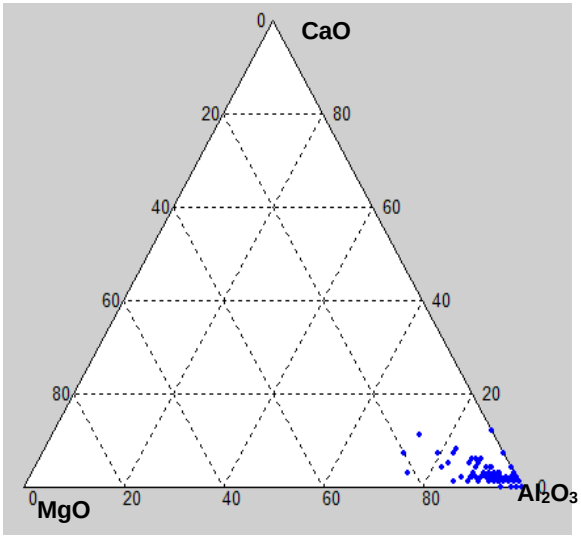

(d)

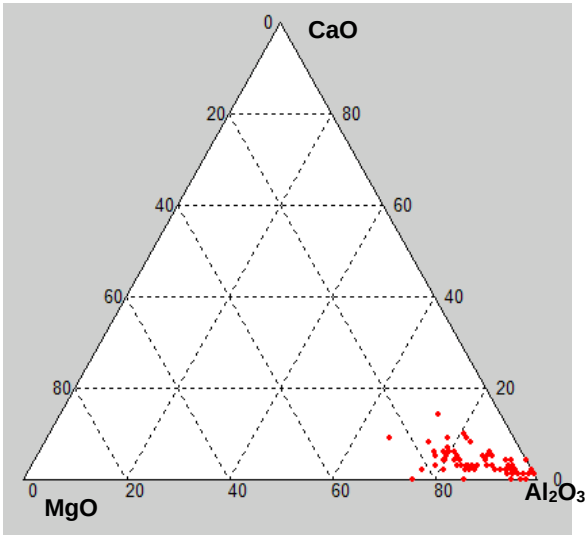

(e)

Figure C-1. Inclusion composition for heat 880595: (a) S0; (b) L0; (c) L1; (d) L2; (e) L3

C.4 Inclusion Composition for Heat 860630

	%Al	%FeO	%MgO	%CaO	%SiO_2
S0	0	4.87	9.30	49.0	5.48
L10	0.001	4.94	9.46	48.6	5.38
L1	0.012	3.66	9.69	48.2	5.08
L2	0.013	1.98	11.46	49.5	4.77
L3	0.033	1.51	11.35	50.8	4.65
T1	0.026	1.44	11.35	50.3	4.47

Table C-4. Steel and slag composition for heat 860630

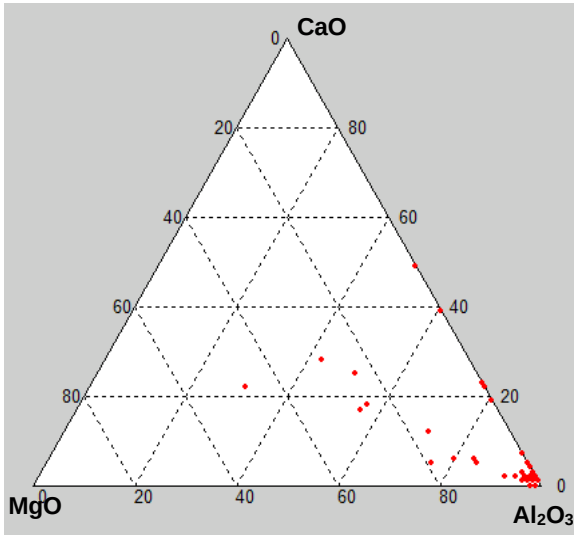

(a)

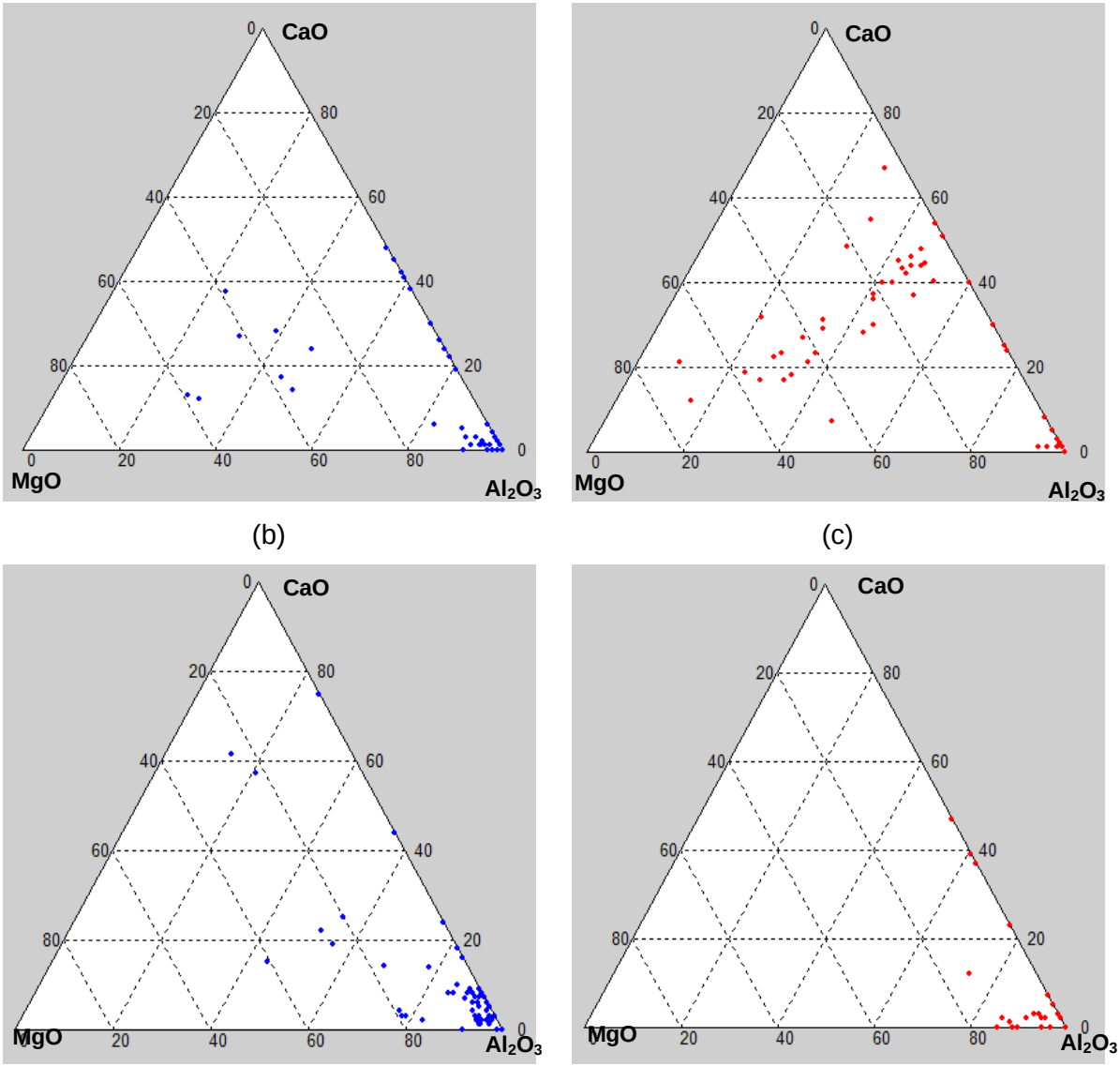

(b) (c)

(d) (e)

Figure C-2. Inclusion composition for heat 860630: (a) S0; (b) L0; (c) L1; (d) L2; (e) L3